TOPICAL REVIEW

Fe-based superconducting thin films—preparation and tuning of superconducting properties

To cite this article: J Hänisch *et al* 2019 *Supercond. Sci. Technol.* **32** 093001

View the article online for updates and enhancements.

IOP ebooks™

Bringing you innovative digital publishing with leading voices to create your essential collection of books in STEM research.

Start exploring the collection - download the first chapter of every title for free.

Topical Review

Fe-based superconducting thin films—preparation and tuning of superconducting properties

J Hänisch[1] ⬤, K Iida[2] ⬤, R Hühne[3] ⬤ and C Tarantini[4] ⬤

[1] Karlsruhe Institute of Technology, Institute for Technical Physics, Hermann-von-Helmholtz-Platz 1, D-76344 Eggenstein-Leopoldshafen, Germany
[2] Department of Materials Physics, Nagoya University, Chikusa-ku, Nagoya 464-8603, Japan
[3] IFW Dresden, Institute for Metallic Materials, Helmholtzstraße 20, D-01069 Dresden, Germany
[4] Applied Superconductivity Center, National High Magnetic Field Laboratory, Florida State University, Tallahassee, FL 32310, United States of America

E-mail: jens.haenisch@kit.edu

CrossMark

Abstract

Thin films of Fe-based superconductors (FBS) have been utilized in a plethora of different experiments for a fundamental understanding of the superconductivity in these materials, as well as for understanding and improving the materials with regard to possible applications. The developments and progress in thin film growth of these materials in the past 10 years are reviewed with a focus on the two main deposition techniques used so far for FBS (pulsed laser deposition, and molecular beam epitaxy). Possible choices of substrates or buffer systems are motivated and explained with regard to misfit, thermal expansion, chemical stability, etc. In the second part of this review, investigations on tuning the superconducting properties, especially critical temperature T_c and critical current density J_c, in FBS thin films are reviewed.

Keywords: Fe-based superconductors, thin films, pulsed laser deposition (PLD), molecular beam epitaxy (MBE), critical temperature, critical current density, strain

(Some figures may appear in colour only in the online journal)

1. Introduction

The discovery of superconductivity in the iron-based layered superconductor LaOFeP by Kamihara *et al* [1] at temperatures around 4 K had been recognized by only a small community interested in exotic new superconductors. This changed dramatically, however, when the same research group led by Hosono reported on an enhancement of T_c to around 26 K by the exchange of P with As, as well as electron doping by the partial substitution of O for F to form LaFeAsO$_{1-x}$F$_x$. [2] That meant 'high-T_c superconductivity' in Fe-based superconductors (FBS), and world-wide theoretical [3] as well as experimental basic research [4] and application oriented efforts [5] started. This led to the discovery of superconductivity also in other material

classes with the same crystallographic feature, i.e. with Fe-pnictide [6] or Fe-chalcogenide layers (tetrahedron), within just half a year. There are four main classes of FBS widely investigated today, which are shortly named by the elemental stoichiometry [7]: 11 (i.e. the iron-chalcogenides, mainly FeSe [8] (together with vacancy, sulphur and oxygen doping) and the system Fe(Se$_{1-x}$Te$_x$) [9, 10]), 111 (mainly LiFeAs [11], the only stoichiometric FBS at ambient pressure, and NaFeAs [12]), 122 (the metallic Fe-pnictides; mainly AEFe$_2$As$_2$, [13, 14] $AE =$ Ba, Sr or Ca with several possible atomic substitutions leading to superconductivity), and 1111 (the Fe-oxypnictides, mainly LnFeAs(O$_{1-x}$F$_x$), Ln: lanthanoid). Besides the above mentioned, there are further classes, e.g. the 112 structures [15], the intercalated 11 structures [16], chalcogenides with 122 structure [17],
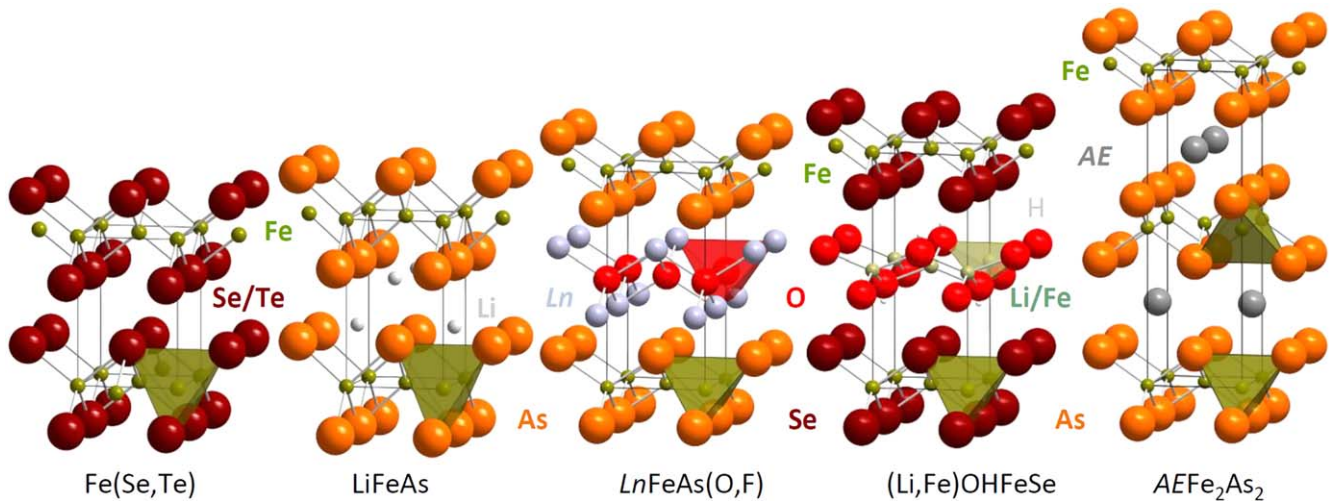
Figure 1. Schematic crystal structure of the five Fe-based superconducting compound classes prepared as thin films so far. *Ln*: lanthanoid (La, Nd, Sm, Gd), *AE*: alkaline earth (Ba, Sr, Ca). For AEFe$_2$As$_2$, the interlayer distance d equals half the c-axis lattice parameter.

structures with thick blocking layers (also belonging to the oxypnictides) [18–20] which may show difficulties in sample preparation, rather low T_c values and/or limited application potential. Two compound classes nevertheless gained some interest recently, the 1144 structures, which show promising high J_c values in high magnetic fields [21], and (Li,Fe)OHFeSe [22, 23], an intercalated structure which can be grown as thin films with excellent structural and superconducting properties [24] (section 4.2.1). The five compound classes of Fe-base superconductors that have been prepared in the form of thin films so far are depicted in figure 1.

In the 1950s, a series of superconducting alloys and compounds containing iron had been found, all with T_c values well below 10 K [25–32]. There are, however, several interesting and exciting differences between these classical compounds and the FBS. First of all, some FBS show much higher T_c values. The maximum T_c of FBS in bulk samples at ambient conditions is found in the iron-oxypnictides at around 56 K in Gd$_{1-x}$Th$_x$FeAsO [33], 55 K in SmFeAsO$_{1-\delta}$ [34], and 58 K in SmFeAsO$_{1-x}$F$_x$ [35], which bridges the temperature range of the classical low-T_c superconductors and the cuprate high-T_c superconductors with T_c values above 90 K. Secondly, in the FBS, the iron plays a crucial role for the superconductivity since the band structure near the Fermi level is dominated by the five 3d orbitals, rendering these compounds to multiband superconductors [36]. Third, the FBS are in close proximity to a magnetic phase, whereas the former Fe-containing superconductors did not show magnetism. This also means, the FBS show unconventional superconductivity mediated by magnetic interactions (spin density waves) [37], with complex phase diagrams [38] around quantum critical points [39] and order parameter symmetries other than pure s-wave [40]. Soon after discovery, it became apparent that some of these compounds do have application potential [5]. Two main application fields are usually discussed: low-T high-field power applications (e.g. magnet coils) and microelectronics (SQUIDs and detectors). However, applications based on Josephson junctions seem not to

be realistic due to the metallic nature of barrier layer. To realize practical SQUIDs, an increase of the junction resistance by an artificial insulating barrier is vital.

In the following, we review the main methods and results for the deposition of Fe-based superconducting films with special focus on ways to tune their properties. In section 2, we discuss the choice of substrates before we review the two main methods pulsed laser deposition (PLD) and molecular beam epitaxy (MBE) as well as some other methods less common for FBS. In sections 3 and 4, respectively, tuning of the critical temperature by strain and gating as well as of the critical current density by the addition of artificial pinning centres (APCs) are reviewed and discussed before the results are summarized in section 5.

2. Thin film preparation

Thin films are good platforms for both fundamental and applied superconductivity research. Whenever new superconducting materials are discovered, much effort is devoted to growing single crystals for exploring physical quantities. Indeed, after the discovery of FBS sizeable single crystals of AEFe$_2$Pn$_2$ (*Pn*: pnictogen) and Fe*Ch* (*Ch*: chalcogen) were grown by several methods (e.g. Sn-flux, self-flux and Bridgeman methods). However, single crystals are not always available due to the difficulty of their growth. For instance, large single crystals of *Ln*FeAs(O,F) are difficult to obtain, whereas high-quality, epitaxial thin films of LaFeAs(O,F), NdFeAs(O,F) and SmFeAs(O,F) on various substrates with a large surface of 10 mm × 10 mm have been fabricated by PLD and MBE. Thanks to the non-equilibrium growth, thermodynamically metastable phases which do not exist in nature can be stabilized [e.g. (Ba$_{1-x}$RE$_x$)Fe$_2$As$_2$ (*RE*: rare earth), FeSe$_x$Te$_{1-x}$ ($0.1 \leqslant x \leqslant 0.4$), and superlattices]. Furthermore, investigating the interplay between dimensionality and superconducting properties is possible with films. Of course, bulk single crystals with layered structure where the

layers are bound by the van der Waals force can be turned into flakes of a few atomic layers by the scotch tape method. Nevertheless, growing ultra-thin films is a more straightforward way. Also electrochemical etching enables thinning of any film to a few atomic layers. Thin films are also useful for investigating the effect of biaxial in-plane strain on the superconducting properties. Usually, mismatch of lattice parameters and/or of the linear thermal expansion coefficients between film and substrate has been implemented for generating strain. For applied superconductivity research, thin films have been investigated regarding possible electronic device applications [41] as well as the 2nd generation superconducting tapes based on cuprates [42, 43].

Due to the acute toxicity of As and Se, especially via inhalation and for water organisms, special care has to be taken when preparing FBS. Typical measures are: separate waste streams, As filters between deposition chamber and pumps, minimizing exposure times (e.g. by keeping deposition chambers under UHV conditions as long as possible), wearing breathing masks and gloves while working with targets and on open chambers, and swiping tests for lab cleanliness. Nevertheless, for thin film preparation these dangers are manageable since powders are not usually involved (except for target preparation) and the materials are contained in vacuum chambers or in solutions. The final film samples can be regarded as basically non-dangerous if handled reasonably. It should be noted that the apparent toxicity, especially of As, is sometimes discussed as drawback for potential manufacturing and using of FBS wires and tapes. However when the material is embedded in a metallic wire matrix or tape protection layer, the handling risks are limited. Additionally, toxic materials have been used in bulk form for thermoelectric materials such as Bi-Te and Pb-Te. Hence, the toxicity may not be the determining issue if the materials show excellent properties or functionalities.

In the following, the important first step, i.e. the choice of substrate, for the growth of FBS thin films is described. Then, mainly the growth of 11, 122, and 1111 thin films by PLD and MBE is reviewed. Two other compounds available as thin films [LiFeAs and (Li,Fe)OHFeSe] as well as other deposition methods besides PLD and MBE are mentioned briefly.

2.1. Choice of substrate and buffer layer

Various substrates and buffer layers have been used for FBS thin films, see table 1. The main criteria for the selection of substrate and buffer layer materials are: (i) small lattice mismatch between films and substrates, and (ii) no reaction between films and substrates (buffer layers). Depending on the desired application, other properties of the substrate might become important as well, such as flexibility, mechanical strength, magnetic and dielectric behaviour as well as costs and availability. The in-plane lattice parameters of FBS are in the range of $3.77 < a < 4.02$ Å, table 2. Therefore, for 001-oriented epitaxial films, (pseudo-) cubic or perovskite $YAlO_3(110)$ (YAO), $LaAlO_3(001)$ (LAO), $(LaAlO_3)_{0.3}(Sr_2TaAlO_6)_{0.7}(001)$ (LSAT), $SrTiO_3(001)$ (STO) and $MgAl_2O_4(001)$ (spinel, MAO) as well as Fe and CeO_2 layers, which are relatively close to the in-plane lattice

parameters of FBS, have been used mainly. However, MgO (001) and r-cut sapphire, $Al_2O_3(1\bar{1}02)$, with a large lattice misfit have also been used and FBS films (11, 122, and 1111) on MgO are grown epitaxially.

Among those substrates, almost no reaction has been observed for MgO (i.e. sharp interface between films and substrates), except for F-containing films such as $NdFeAsO_{1-x}F_x$, where a MgF_2 interlayer may be forming [82]. According to an empirical rule proposed by Hanawa *et al* [83], a substrate containing multi-valence elements and vacancy structures would not be appropriate for 11 systems. Hence, LAO and MgO substrates as well as Fe and CeO_2 buffer layers would be the best candidates. Indeed, sharp and clean interfaces between Fe(Se,Te) and those templates are observed [84–86], whereas thick reaction layers have been observed for Fe(Se,Te) films prepared by PLD on Y-stabilized $ZrO_2(001)$ (YSZ), STO, $LaSrAlO_4(001)$, and $LaSrGaO_4(001)$ [84]. However, Fe(Se,Te) and $Ba(Fe_{1-x}Co_x)_2As_2$ epitaxial thin films have been realized on STO [87–90]. In particular, a sharp interface between $Ba(Fe_{1-x}Co_x)_2As_2$ and STO has been observed by transmission electron microscopy (TEM) [91]. Hence, $SrTiO_3$ and its isostructure $BaTiO_3$ have been implemented as buffer layer for $Ba(Fe_{1-x}Co_x)_2As_2$ [91] and $Ba(Fe_{1-x}Ni_x)_2As_2$ [92]. Oxygen is easily released from STO at the deposition temperature of $Ba(Fe_{1-x}Co_x)_2As_2$ thin films by PLD under an ultra-high vacuum (UHV) condition, resulting in a vacancy structure [93], which leads to large electrical conductivity of the substrate and shunting effects impeding electrical transport investigations, e.g. [90, 91]. Additionally, Ti is a multivalence element. Hence STO should not be a suitable template for FBS. However, monolayers of FeSe have been fabricated only on STO so far [94–96], although these monolayers have been grown by MBE in contrast to the films by Hanawa *et al*. Therefore, Hanawa's empirical rule may be valid for limited systems and experimental conditions only.

Although reaction layers at the interface between FBS [$BaFe_2(As_{1-x}P_x)_2$ and $Ba(Fe_{1-x}Co_x)_2As_2$] and LSAT were forming, epitaxial growth with good crystalline quality without compromising superconducting properties have been reported by several groups, e.g. for $Ba(Fe_{1-x}Co_x)_2As_2$ and $BaFe_2(As_{1-x}P_x)_2$ [97–99]. It has been reported that fluoride substrates such as $CaF_2(001)$ and $SrF_2(001)$ are very suitable templates for epitaxial growth of various FBS with good crystalline quality as well as superconducting properties, although a reaction layer is present for some of the systems, 11 and 122 [100].

In general, compressive in-plane strain is present in FBS films grown on CaF_2 partly due to the larger thermal expansion mismatch between film and CaF_2 in comparison to the perovskite substrates (compare tables 1 and 3), leading to a change in the electronic structure and hence in T_c [101, 102]. Following the observations of Uemura *et al* that F has the tendency to diffuse from CaF_2 to the growing NdFeAsO film [103], fluoride substrates have been used intentionally as F source for SmFeAs(O,F) by Haindl *et al* [104]. Furthermore, LnFeAs(O,F) (Ln = Sm or Nd) films always show the highest T_c when grown on CaF_2 [103, 105]. The reason for this is not fully understood; however, additional F from the substrate and

Table 1. Relevant in-plane lattice parameter, thermal expansion coefficient at room temperature, and specifics of the substrate and buffer materials used so far for FBS thin film growth.

Material and surface	Abbreviations, other names	Structure type and symmetry	Relevant in-plane lattice parameter (Å)	Linear thermal expansion coefficient α at RT (10^{-6} K^{-1})	Specifics
Fe[a]		fcc	$a \cdot \sqrt{2} = 4.059$	11.8 [44]	Conducting, Co diffusion
Si		Cubic	$a/\sqrt{2} = 3.840$	2.57 ± 0.04 [45]	
Graphene/SiC(0001)		Hexagonal	$a = 2.46$	2.3 (4H-SiC) [46]	
GaAs		Cubic	$a/\sqrt{2} = 3.997$	5.7 [47]	Desorption of As above 580 °C
LiF		Cubic	4.027	33 [48]	
MgO(001)		NaCl, cubic	4.212	10.4 [49], 10.5 [50], 11.0 [51]	Hygroscopic
MgAl$_2$O$_4$(001)	Spinel	Cubic	$a/2 = 4.042$	6.78 [52]	
Al$_2$O$_3$(1$\bar{1}$02)	r-cut sapphire	Rhombohedral	3.48	5.0 ($\perp$c), 5.6 ($\|$c) [44], 8.4 [50]	
Al$_2$O$_3$(0001)	c-cut sapphire		4.758		
CeO$_2$[a]		CaF$_2$, cubic	$a/\sqrt{2} = 3.826$	—	
CaF$_2$(001)[b]		Cubic	$a/\sqrt{2} = 3.8679$	18 [50], 18.9 [53]	Brittle
SrF$_2$(001)		CaF$_2$, cubic	$a/\sqrt{2} = 4.107$	18.1 [53]	Brittle
BaF$_2$(001)		CaF$_2$, cubic	$a/\sqrt{2} = 4.681$	18.4 [53]	Brittle
TiO$_2$(100)	Rutile	Tetragonal	$b = 4.594$, $c = 2.959$	7.0 (a), 9.4 (c) [54]	
MgF$_2$ (001)		TiO$_2$, tetragonal	4.620	9.2 (a,b) [55]	Brittle
CaTiO$_3$(001)[a]	CTO	Perovskite, orthorhombic	$(a+c)/2\sqrt{2} = 3.822$	—	Phase transition at 1260 °C
(Nb:)SrTiO$_3$(001)[b]	STO	Perovskite, cubic	3.905	10.4 [50]	Conducting after UHV
BaTiO$_3$(001)[a]	BTO	Perovskite, tetragonal	3.992	—	
YAlO$_3$ (110)	YAO	Perovskite, orthorhombic	$(a+c)/2\sqrt{2} = 3.715$	5...10 [50], 8.9 (a) 8.5 (c) 3.8 (b) [56]	No phase transition
LaAlO$_3$ (001)	LAO	Perovskite, rhombohedral	$a/\sqrt{2} = 3.789$	11 [50],	Phase transition at 800 K (twin structure)
LaSrAlO$_4$ (001)	LSAO	K$_2$NiF$_4$, tetragonal	3.756	7.4 [50]	
LaSrGaO$_4$ (001)	LSGO	K$_2$NiF$_4$, tetragonal	3.844	10...19 [50]	
GdScO$_3$ (001)	GSO	Perovskite, orthorhombic	$(a+b)/2\sqrt{2} = 3.973$	6.7 (a), 11.5 (b), 14.5 (c) [57]	
LaMnO$_3$[a]	LMO	Perovskite, cubic	3.894	—	
KTaO$_3$	KTO	Perovskite, cubic	3.9885	5.3 [58]	
(LaAlO$_3$)$_{0.3}$(Sr$_2$TaAlO$_6$)$_{0.7}$ (001)	LSAT	Perovskite cubic	3.868	8.2 [59]	No phase transition,
Pb(Mg$_{1/3}$Nb$_{2/3}$)$_{0.72}$Ti$_{0.28}$O$_3$ (001)	PMN-PT	Perovskite, tetragonal/ rhombohedral	4.02	8.8 [60]	Several phase transitions
Y$_2$O$_3$:ZrO$_2$ (001)	YSZ	CaF$_2$, cubic	$a/\sqrt{2} = 3.624$	8.8 [50],	
Glass	—	Amorphous	—	4–9	
Mica	—	Monoclinic	—	18.4 (a,b), 5.8 (c) [61]	
Hastelloy[c]	—	fcc	—	10.8 [62]	Polycrystalline

[a] Only as buffer layer.
[b] Also as buffer layers.
[c] Only as template.

Table 2. Bulk lattice parameters at room temperature of some of the most common FBS materials used for thin film deposition (nominal compositions, mostly near or at optimal doping).

Material	a (Å)	c (Å)	References
FeSe, FeSe$_{0.92}$	3.77	5.52	[63, 64]
FeSe$_{0.5}$Te$_{0.5}$	3.78…3.80	5.98…6.08	[10, 65, 66]
FeSe$_{0.15}$Te$_{0.85}$	3.80	6.22	[67]
LiFeAs	3.78	6.35, 6.36	[11, 68]
BaFe$_2$As$_2$	3.96	13.01, 13.02	[69, 70, 71–73]
(Ba$_{0.6}$K$_{0.4}$)Fe$_2$As$_2$	3.91	13.3	[73]
Ba(Fe$_{0.92}$Co$_{0.08}$)$_2$As$_2$	3.96	12.98, 12.99	[70, 74]
Ba(Fe$_{0.95}$Ni$_{0.05}$)$_2$As$_2$	3.96	12.99	[75]
BaFe$_2$(As$_{0.7}$P$_{0.3}$)$_2$	3.93	12.82	[76]
(Sr$_{0.8}$K$_{0.2}$)Fe$_2$As$_2$	3.91	12.7	[77]
Sr(Fe$_{0.9}$Co$_{0.1}$)$_2$As$_2$	3.92	12.35	[77]
LaFeAsO$_{0.86}$F$_{0.14}$	4.02	8.70	[78]
NdFeAsO$_{0.82}$F$_{0.18}$	3.96	8.55	[79]
SmFeAsO$_{0.85}$F$_{0.15}$	3.93	8.48	[80]
GdFeAsO$_{0.85}$F$_{0.15}$	3.91	8.43	[80]
(Li,Fe)OHFeSe	3.79	9.26	[81]

Table 3. Linear thermal expansion coefficients α near room temperature of selected Fe-based superconducting materials along the [100] and [001] directions. Isotropic average calculated from volumetric thermal expansion coefficient α_{vol} is also shown.

Composition	$\alpha_{[100]}$ (10^{-6} K^{-1})	$\alpha_{[001]}$ (10^{-6} K^{-1})	$1/3$ α_{Vol} (10^{-6} K^{-1})	Reference
FeSe	17	33	21	[106]
BaFe$_2$As$_2$	9	35	27	[107]
Ba(Fe$_{0.962}$Co$_{0.038}$)$_2$As$_2$	8	36	26	[107]
Ba(Fe$_{0.926}$Co$_{0.074}$)$_2$As$_2$	8	34	26	[107]
Ba(Fe$_{0.92}$Co$_{0.08}$)$_2$As$_2$	8.5	(25)	—	[108]
	10	33	—	[109]
Ba(Fe$_{0.885}$Co$_{0.115}$)$_2$As$_2$	8.3	34	—	[108]
LaFeAsO	—	—	13	[110]
LaFeAsO$_{0.95}$F$_{0.05}$	—	—	14	[110]
LaFeAsO$_{0.9}$F$_{0.1}$	—	—	14	[110]
CeFeAsO[a]	—	—	12	[111]
PrFeAsO[a]	—	—	13	[111]
SmFeAsO[a]	—	—	12	[111]
GdFeAsO[a]	—	—	12	[111]

[a] At 250 K.

compressive strain by thermal mismatch may play the largest roles for higher T_c values.

From the above, the presence of a reaction layer neither much affects the crystalline nor the superconducting properties; however it may affect the chemical composition and stoichiometry of the film. It is general consensus that fluoride substrates, particularly CaF$_2$, seem to be the best template for FBS regarding T_c value and crystalline quality. Furthermore it is one of the substrates suited for microwave applications [112]. However, one has to keep in mind that CaF$_2$ is extremely brittle which makes it hard to handle in real applications. Furthermore, for the study on stoichiometrically well-defined films of FBS, the reaction layer as well as the possible F content in the film may be problematic. Therefore, alternatives for CaF$_2$ are still of interest.

To date, CeO$_2$ [86], BaTiO$_3$ and SrTiO$_3$ [91] as well as Fe [113] as buffer layers were shown by TEM to guarantee biaxially aligned or even coherent growth of Fe(Se,Te) and Ba(Fe$_{1-x}$Co$_x$)$_2$As$_2$, which is also a prerequisite for realizing superlattices. Indeed, SrTiO$_3$-Ba(Fe$_{1-x}$Co$_x$)$_2$As$_2$ superlattices [114] and Fe/Ba(Fe$_{1-x}$Co$_x$)$_2$As$_2$ multilayers [115] have been reported. CeO$_2$ had been used before, e.g. as very thin interlayers in multilayers with YBa$_2$Cu$_3$O$_7$ for increasing J_c [116], however so far has not been studied as interlayer material in FBS multilayers to our knowledge. Also CaF$_2$ has been used as buffer layer for FeSe$_{1-x}$Te$_x$: Ichinose *et al* [117] investigated PLD-grown CaF$_2$ on CaF$_2$ and LAO, and Yuan *et al* [118] investigated MBE-grown CaF$_2$ on LSAT. Even though CaF$_2$ grows with a pyramid structure in all cases, the FeSe$_{1-x}$Te$_x$ films on top grow epitaxially and with a smooth surface.

Quite recently, Kang *et al* pointed out the importance of the surface treatment of SrTiO$_3$ for the coherent growth of Ba(Fe$_{1-x}$Co$_x$)$_2$As$_2$ [119]. They concluded that TiO$_2$-terminated SrTiO$_3$ is prerequisite for the coherent growth of Ba(Fe$_{1-x}$Co$_x$)$_2$As$_2$. On the other hand, monoclinically distorted Ba(Fe$_{1-x}$Co$_x$)$_2$As$_2$ was grown on SrO-terminated SrTiO$_3$ due to the formation of BaFeO$_{3-x}$ at the interface, resulting in low T_c.

2.2. Pulsed laser deposition (PLD)

PLD is a very versatile deposition method, especially well-suited for quick-start experiments in the early stages of thin film research after the discovery of a new material or class of materials. Yet, equipped with *in-situ* analysis tools such as reflection high energy electron diffraction (RHEED), also extremely smooth, microstructurally clean, high-quality epitaxial thin films are possible to grow. A high-intensity laser beam focused or imaged on the surface of a target of the desired material rapidly heats up the material locally at the

surface. This leads to the development of a plasma plume, which is further heated by the laser pulse and expands almost perpendicular to the target surface towards the (in most cases heated) substrate, where the material is deposited and the film is growing. The pulsed nature of the deposition distinguishes PLD from many other, continuous, deposition processes. The film surface is flooded during the duration of one pulse (typically between 10 and 30 ns) with material of usually many more than one monolayer. At the same time, the incoming particles usually have high energies (∼10 eV), contributing to supplying the necessary energy for diffusion and site changes.

Two different excitation sources have been widely used for PLD, Nd:YAG solid state lasers and excimer gas lasers. The Nd:YAG lasers are usually operated in frequency-doubled ($\lambda = 532$ nm) or quadrupled ($\lambda = 266$ nm) state, seldom also under its basic frequency ($\lambda = 1064$ nm) [99, 120] or frequency-tripled ($\lambda = 355$ nm) [121–123]. These systems are relatively cost-efficient and can be operated with smaller energy densities due to the larger penetration depth of the laser irradiation at the target. The excimer laser is mostly operated with KrF ($\lambda = 248$ nm), seldom with XeCl ($\lambda = 308$ nm). The pulse duration is slightly larger than for Nd:YAG. The advantages of excimer lasers are their better energy homogeneity across the beam profile and the easier repetition rate adjustment besides the usually higher pulse energies.

2.2.1. 11 system.
As stated in the introduction, the 11 system is highly attractive due to the following reasons: (i) it is less toxic than the other systems like 122 and 1111; (ii) the simplest crystal structure, which is favourable for understanding basic physics, e.g. mechanism of superconductivity; and (iii) it is relatively feasible to fabricating thin films by both PLD and MBE. Excellent reviews on 11 thin films have already been published by Li *et al* [124], Mele [125], and Imai *et al* [126]. Hence the interested reader may also refer to them. Nevertheless, the recent results published after 2013 are briefly reviewed in chronological order. All studies discussed below used a KrF excimer laser.

2.2.1.1. *FeSe.*
To date, FeSe thin films with good superconducting properties by PLD are problematic. However, the use of CaF_2 substrate yields epitaxial FeSe thin films with high T_c up to 11.4 K, which is a 1.5-fold increase over bulk single crystals [127]. The enhanced T_c may be attributed to the in-plane compressive strain originating from the thermal expansion mismatch between the film and CaF_2 substrate, see section 3.1.1. Feng *et al* investigated in a very thorough study the influence of structural parameters on T_c of FeSe films on a variety of different substrates [128] by using epitaxial strain as well as in a high-throughput experiment on a single STO or CaF_2 substrate [129]. The films of the latter study were deposited by a dual-beam technique and used the fact that T_c (as well as the structural parameters) depend strongly on the deposition rate. The experimental time and the data quality were improved considerably in comparison to the many-substrate study. These data show a strong positive (negative) correlation between T_c and the lattice constant c (a).

2.2.1.2. *$FeSe_{1-x}Te_x$.*
Si *et al* used CeO_2 as a buffer layer to grow epitaxial Fe(Se,Te) thin films on both single crystalline YSZ and technical substrates [rolling-assisted biaxially textured substrate (RABiTS)] by PLD [130]. The resultant films showed a high T_c of over 20 K. Later, the same group reported on the microstructure of Fe(Se,Te) on CeO_2-buffered $SrTiO_3$ and revealed coherent growth of Fe(Se,Te) by TEM. The most striking point is the absence of the intercalated Fe, which is frequently observed in the 11 system. The intercalated Fe is harmful to the superconductivity and, therefore, the removal of the excess Fe is a key to good superconducting properties. It is not clear whether CeO_2 prevents Fe intercalation.

Molatta *et al* implemented non-superconducting Fe(Se, Te) as a buffer layer to grow high-T_c Fe(Se,Te) [131]. A 20 nm thick Fe(Se,Te) layer was primarily deposited on MgO at 400 °C, followed by a homo-epitaxial Fe(Se,Te) film at various temperatures. Thanks to the buffer layer, the homo-layer showed a high T_c of around 18 K in a wide range of growth temperatures (240 °C ⩽ T ⩽ 320 °C).

Imai *et al* reported on the phase diagram of $FeSe_{1-x}Te_x$ epitaxial thin films on CaF_2 substrates [132]. This study demonstrated one of the advantages of thin film growth, namely being able to stabilize metastable phases: $FeSe_{1-x}Te_x$ in the range of $0.1 \leqslant x \leqslant 0.4$ was realized, whereas the bulk crystals in this composition range cannot be grown due to phase separation into Te-rich and Se-rich phases. Another distinct feature in this study is that the Te content for the highest T_c of 23 K is located around $x = 0.2$. Later, Seo *et al* also fabricated Fe(Se,Te) thin films using a nominal $Fe_{0.94}Se_{0.45}Te_{0.55}$ PLD target (measured composition: $Fe_{0.97}Se_{0.39}Te_{0.61}$) [133]. The resultant films showed a Se content of around 0.7 because of the preference of Fe to bond with Se. Also Yuan *et al* found the resultant films showed a Se content of around 0.7 even though the PLD target with $FeSe_{0.5}Te_{0.5}$ was employed [134].

With the aim to produce free-standing and three-dimensional (3D) superconducting structures of FBS, such $FeSe_{0.7}Te_{0.3}$ films have been deposited recently on GaAs-based templates [135]. The films on STO/GaAs show the same $T_c = 11$ K as films directly on STO single crystals, whereas films directly on GaAs show a higher T_c of up to 17.4 K (depending on deposition temperature and thickness). On the GaAs/InGaAs/AlAs/GaAs templates necessary for the 3D structures, a maximum T_c of ∼16 K for 100 nm thick films was achieved. All these films showed a sharp biaxial texture of (001)[100]Fe(Se,Te)||(001)[110]GaAs.

Nabeshima *et al* reported on FeSe/FeTe superlattices on both CaF_2 and $LaAlO_3$ [136]. Because of the interdiffusion of Se and Te, the superlattice has a relatively high T_c of 15.8 K.

Recently, Huang *et al* have achieved superconducting $FeSe_{1-x}Te_x$ films directly on Si and SiO_x/Si by PLD [137].

These films are c-axis textured with a preferred in-plane orientation (on Si, FWHM $\sim 50°$) and no in-plane orientation (on SiO_x) which was related to interdiffusion at the interface. The films show a T_c of around 11 K. The same group recently showed $FeSe_{1-x}Te_x$ films on flexible Mica with T_c of $\sim$11 K [138]. To our knowledge, these are the first FBS films on mica.

In 2017, Bryja *et al* [139] reported on the first Fe-based superconducting films on single-crystalline vicinal substrates. They grew nominal $FeSe_{0.5}Te_{0.5}$ films by PLD on vicinally cut CaF_2 substrates with vicinal angles of 5°, 10°, 15°, and 20°. For low deposition temperatures (260 °C) and/or small vicinal angles, the c-axis of the film followed the c-axis of the substrate. However above 5° and at a higher deposition temperature of 400 °C, the growth direction turned towards the substrate normal leading to smaller vicinal angles of the film compared to the substrate. Although the crystallinity and therefore T_c as well as J_c values declined for larger vicinal angles above 10°, the anisotropy of the resistivity and of the critical current density could be evaluated. The former was found to be comparable to single-crystal values.

2.2.1.3. $FeSe_{1-x}S_x$. Whereas $FeTe_{1-x}S_x$ films have been grown by PLD and characterized rather early already by Mele *et al* [140–142], $FeSe_{1-x}S_x$ films were reported only recently. Fujiwara *et al* [143] used a multilayering deposition technique with alternating FeSe and FeS targets to grow tetragonal $FeSe_{1-x}S_x$ films on FeSe-buffered MgO with high sulphur contents up to $x = 0.78$. A linear dependence of the c-axis parameter with sulphur content was found, the films did not show full superconductivity, however onset T_c around 4 K for $x = 0.16$ has been measured.

Shortly after, Nabeshima *et al* [144] succeeded in growing fully superconducting $FeSe_{1-x}S_x$ films with $x \leqslant 0.43$ on LAO by using the same multilayering technique. This study illustrates that a careful composition analysis of 11 (and possibly all FBS) films is necessary since the real sulphur content is systematically lower than the nominal content, similar to the decrease in Se content in [133, 134]. As the sulphur content in the films increases, the nematic transition temperature as well as T_c decreases. Around $x = 0.18$, the nematic transition vanishes and a different (possibly antiferromagnetic) transition temperature appears. The films show different degrees of in-plane strain whose origin has been unclear at time of publication.

2.2.2. 122 system. PLD was mainly used for two members of the 122 family: $Sr(Fe_{1-x}Co_x)_2As_2$ and Ba122 compounds (doped mainly with K, *RE*, Co, Ni and P), as summarized in tables 4 and 5. The main focus lay on $Ba(Fe_{1-x}Co_x)_2As_2$ and recently $BaFe_2(As_{1-x}P_x)_2$. Two laser sources in PLD have been mainly used so far; a second harmonic Nd:YAG laser ($\lambda = 532$ nm) and a KrF excimer laser ($\lambda = 248$ nm).

The first report of epitaxial, superconducting $Sr(Fe_{1-x}Co_x)_2As_2$ thin films by Hiramatsu *et al* [164, 183] triggered a world-wide research competition of FBS thin films. These films with a thickness of 350 nm have been deposited on LSAT by PLD with a second harmonic Nd:YAG

laser. The film had a T_c of around 20 K; however, it showed only low critical current density J_c, suggesting electromagnetic granularity reduces J_c [184]. Later, it has been found that the parent compound $SrFe_2As_2$ is not stable against water, or in other words that superconductivity can be induced by water vapour [167]. Films exposed to wet air for 6 h showed decreased lattice parameters and a T_c of $\sim$25 K. For the induction of superconductivity, the authors proposed chemical pressure by water, OH or O molecules at interstitial sites (which however cannot explain the observed lattice shrinkage) or the formation of Sr vacancies due to hydroxide formation. *In situ* PLD processed $Sr(Fe_{1-x}Co_x)_2As_2$ thin films have also been realized by means of a KrF excimer laser [165]. The resultant thick films (700–800 nm) on LAO exhibited a very similar superconducting transition compared to the Nd:YAG grown films with a $T_{c,50\%}$ (50% of the normal state resistance) of 18.1 K. This first report on J_c data of Sr122 films showed a relatively low critical current density of $\sim$10 kA cm^{-2} at 5 K. Hiramatsu *et al* were able to deposit thin films of the non-equilibrium phase $(Sr_{1-x}La_x)Fe_2As_2$ [166], which is an indirectly electron-doped superconductor. Note that $(Sr_{1-x}La_x)Fe_2As_2$ is a metastable phase and, therefore, hard to obtain in bulk crystal form. The films showed a maximum T_c of 20.8 K and a very similar phase diagram to the directly electron-doped $Ba(Fe_{1-x}Co_x)_2As_2$. These films showed a large difference between magnetization and transport J_c, which was attributed to granularity and weak-link behaviour.

An attempt on fabrication of $(Ba_{1-x}K_x)Fe_2As_2$ by PLD has been made, since this system shows a relatively high T_c of around 40 K in the form of bulk crystals. However, *in-situ* $(Ba_{1-x}K_x)Fe_2As_2$ seems to be difficult to deposit due to the volatility of potassium. To date, only MBE yields superconducting $(Ba_{1-x}K_x)Fe_2As_2$ and $(Sr_{1-x}K_x)Fe_2As_2$, which will be reviewed later. In order to realize superconducting $(Ba_{1-x}K_x)Fe_2As_2$ films by PLD, a two-step process has been reported [151]. An amorphous precursor film of $Ba_{0.6}Fe_2As_{2.6}$ was deposited on Al_2O_3 and LAO at room temperature by PLD with a KrF excimer laser, operated at high repetition rate (48 Hz). The precursor films were sealed in quartz tubes with potassium chunks under high vacuum. The whole arrangement was heated to 700 °C, held at this temperature for 6 h, and then cooled to room temperature at a rate of 200 °C h^{-1}. The films were polycrystalline with a strong c-axis texture. Nevertheless, the films showed a high T_c of around 40 K. KFe_2As_2 thin films exhibiting large spin Hall conductivity have been deposited by a similar *ex-situ* phase formation process (annealing temperatures between 350 °C and 800 °C) by Hiramatsu *et al* [152]. The resultant superconducting film on LSAT with a T_c onset of 3.7 K showed a strong c-axis texture with a weak in-plane orientation. Due to extreme sensitivity to ambient atmosphere, all measurements were carried out without exposing the samples to air.

$Ba(Fe_{1-x}Co_x)_2As_2$ thin films have also been readily fabricated by PLD with both a second harmonic Nd:YAG and a KrF excimer laser. Most importantly, $Ba(Fe_{1-x}Co_x)_2As_2$ is more stable against H_2O than $Sr(Fe_{1-x}Co_x)_2As_2$, which is explained by a larger chemical stability due to more covalent

Table 4. Summary of 122 thin films grown by PLD (for $Ba(Fe_{1-x}Co_x)_2As_2$ films see table 5). For *in situ* process, T_{sub} indicates the deposition temperature and for *ex situ* process (*) the post-annealing temperature. T_c are estimated with 90% resistivity criterion or interpolation onset (see e.g. [145]) which is very similar.

Composition	Substrate	λ_L (nm)	T_{sub} (°C)	Thickness d (nm)	Highest T_c (K)	Remarks	References
$BaFe_2As_2$	$Fe/MgAl_2O_4$	248	670	$10 \sim 80$	10 ($t<30nm$)	Epitaxial	[146]
	MgO	532	850	$150 \sim 250$	—	Epitaxial	[147, 148]
	MgO	248	850	100	—	Epitaxial	[102]
	CaF_2	248	850	100	—	Epitaxial	[102]
$(Ba_{1-x}La_x)Fe_2As_2$	MgO	532	850	$150 \sim 250$	22.4 ($x = 0.13$)	Epitaxial	[147]
				200	30.3 ($x=0.13$, $p=3.2GPa$)	Applying pressure	[149]
$(Ba_{1-x}Ce_x)Fe_2As_2$	MgO	532	850	150…250	13.4 ($x = 0.15$)	Epitaxial	[150]
$(Ba_{1-x}Pr_x)Fe_2As_2$	MgO	532	850	150...250	6.2 ($x = 0.18$)	Epitaxial, not fully sc	[150]
$(Ba_{1-x}Nd_x)Fe_2As_2$	MgO	532	850	150…250	5.8 ($x = 0.13$)	Epitaxial, not fully sc	[150]
$(Ba_{1-x}K_x)Fe_2As_2^*$	LAO	248	700		38.5		[151]
	Al_2O_3	248	700		39.5		[151]
$KFe_2As_2^*$	LSAT	532	~500	100–200	3.7		[152]
$Ba(Fe_{1-x}Ni_x)_2As_2$	CaF_2	248	750	90–100	21.3 [153]	Epitaxial	[153–155]
	CaF_2	248	700–750	460	21.5	Slightly strained, epitaxial	[92]
	STO/LSAT	248	700–750	460	17.4	Epitaxial	[92]
	MgO	248	750	100	18.1		[135]
$BaFe_2(As_{1-x}P_x)_2$	MgO	532	800	90	26.5	Epitaxial	[156]
	MgO	248	850	~100	21.6 ($x = 0.19$), 24.9 ($x = 0.21$)		[157]
	LSAT		800	80	30.5 ($x = 0.33$)	Epitaxial	[97]
	MgO		N.A.	80	28.9 ($x = 0.33$)	Not mentioned	[158]
	MgO		800	$72 \sim 80$	28.0 ($x=0.33$)	Epitaxial	[159]
	MgO		1050	$150 \sim 200$	26.5 ($x = 0.30$)	Epitaxial	[160]
	IBAD-MgO		1050	$150 \sim 200$	26	Epitaxial	[161]
	IBAD-MgO		1200	185	28.3	Epitaxial	[162]
$Ba(Fe_{0.55}Ru_{0.45})_2As_2$	MgO	248	900	40	22.5		[163]
	LSAT	248	900	40	19		[163]
	LAO	248	900	40	12	Broad transition	[163]
	SrF_2	248	900	40	15		[163]
	BaF_2	248	900	40	10		[163]
	CaF_2	248	900	40	<2		[163]
$Sr(Fe_{1-x}Co_x)_2As_2$	LSAT	532	700	350	20.1	Epitaxial	[164]
	LAO	248	770	700	19.2		[165]
	c-cut Al_2O_3	248	770	700	—		[165]
$(Sr_{1-x}La_x)Fe_2As_2$	LSAT	532	750	200	20.8		[166]
$H_2O:SrFe_2As_2$	LSAT	532	700	200	24.4		[167]
$Ca(Fe_{1-x}Co_x)_2As_2$	LSAT	532	600–650	N.A.	—	Polycrystals	[168]
$CaFe_2As_2$	Fe/MgO	248	675	~100	—	$00l$ + FeAs	[169]
$(Ca_{1-x}Pr_x)Fe_2As_2$	Fe/MgO	248	675	~100	—	$00l$ + FeAs	[169]

bonds, a lower H_2O in-diffusivity due to smaller interstitial sites (due to larger ion size of Ba), and a lower Ba out-diffusivity due to a larger formation energy of Ba vacancies than Sr vacancies in 122 compounds [170]. This lead to a first realization of [001]-tilt bicrystal $Ba(Fe_{1-x}Co_x)_2As_2$ films on $SrTiO_3$ [89], as well as MgO and LSAT substrates [175]. Now, high-quality $Ba(Fe_{1-x}Co_x)_2As_2$ thin films have been realized on bare oxide substrates such as STO, LAO, MgO, and LSAT [90, 98, 171, 175] and fluoride substrates, such as BaF_2 and CaF_2 [101]. On the other hand, two groups

(University of Wisconsin-Madison, and IFW Dresden) have proposed buffer layers such as STO, $BaTiO_3$ [91] and Fe [113], respectively. Employing buffer layers brings another degree of freedom since it increases the number of possible substrates, whenever buffer layers grow epitaxially on the selected substrates and possible interface reactions [176] and shunting effects [185] are carefully taken into account. Indeed, high-quality $Ba(Fe_{1-x}Co_x)_2As_2$ thin films have been fabricated on STO-buffered LAO, Si(001), and $GdScO_3(110)$ [91].

Table 5. Summary of $Ba(Fe_{1-x}Co_x)_2As_2$ thin films grown by PLD. Most of the studies employed the optimum Co concentration ($x = 0.1$ or 0.08) for the PLD target.

Substrate/Template	Wavelength (nm)	Deposition rate information	T_{sub} (°C)	Thickness t (nm)	Highest T_c (K)	Remarks	References
LSAT(001)	532	—	700	500	19.3		[170]
LSAT(001)	248	5 Hz	700	30	22.3		[98]
LSAT(001)	248	20 Hz	700	40	23.5		[90]
LSAT(001)	532	—	—	—	22.6		[171]
LSAT(001)	532	2.8–3.3 Å s^{-1}	800–850	300	25.5 (x=0.075)		[168]
LSAT(001)	248, 532, 1064	Variation	850	200–300	—	Only structural data	[99]
LSAT	248	29.1 Hz	725	60–950	18.8		[172]
STO/LSAT	248	—	730–750	350	22.8		[91, 173]
STO/LSAT	248	—	730–750	24×(1.2 S TO /13 Ba122) (~340)	18.9	Superlattice	[114, 174]
STO/LSAT	248	—	730–750	24×(3.3 Ba122/13.3 Co: Ba122) (~400)	23.7	Multilayer	[114, 174]
Fe/LSAT	248	10 Hz	700	130	24.8	(110) misorientation	[113]
[001]-tilt LSAT(001) symmetric bicrystal	532		850	250–350	21.6		[175]
STO	248	10 Hz	650	40	24.5		[90]
STO	248	29.1 Hz	725	60–950	21.2		[172]
STO [001]-tilt symmetric bicrystal	248	—	—	350	20.8 (0°), 20.3 (6°)		[89]
LAO	248	10 Hz	650	40	18.1		[90]
LAO	248		725	60–950	19.2		[172]
STO/LAO	248		730–750	350	22.2	BTO buffer was also used	[91, 173]
YAO	248	10 Hz	650	40	16.9	45° misorientation	[90]
STO/GdScO$_3$(110)	248		730–750	350	22.1	BTO buffer was also used	[91, 173]
Fe/MgAl$_2$O$_4$	248		630	(10 Ba122/5 Fe/20 Ba122)	29.4	Multilayer	[115]
STO/Si(001)	248		730–750	350	19.0		[91, 173]
MgO	248	7 Hz	850	100	22.6 (x=0.04)	Phase diagram	[102]
MgO	248	29.1 Hz	725	60–950	19.2		[172]
MgO [001]-tilt symmetric bicrystal	532	10 Hz	850	250–350	20.7		[175]
Fe/MgO	248	10 Hz, ~0.8 Å s^{-1}	750	~100	27.9 (x = 0.035)	Phase diagram	[176]
Fe/MgO	248	10 Hz	700	130	24.4		[113]
CaF$_2$ (001)	248	7 Hz	750 700	85 50	27.9 26.9		[101]
CaF$_2$ (001)	248	29.1 Hz	725	60–950	24.2		[172]
CaF$_2$(001)	248		850	100	28.4 (x=0.075)	Phase diagram	[102]
CaF$_2$(001)	248		730–750	330 350	25.4 ($T_{c,0}$) 26.0 ($T_{c,0}$)	Single-layer Multilayer	[177]
CaF$_2$(001)	248	40 Hz	700	460	27.1 (0 mol% BZO)	BaZrO$_3$ addition	[178]
BaF$_2$ (001)	248	7 Hz	700–750	40	21.4		[101]

Table 5. (Continued.)

Substrate/Template	Wavelength (nm)	Deposition rate information	T_{sub} (°C)	Thickness t (nm)	Highest T_c (K)	Remarks	References
BaF$_2$ (001)	248	29.1 Hz	725	60–950	23.0		[172]
SrF$_2$ (001)	248	7 Hz	700–750	40	22.1		[101]
IBAD-MgO/…/Hastelloy	532	—	—	150	22.0		[179]
Fe/IBAD-MgO/…/Hastelloy	248	10 Hz	700	50 55 (70 nominal)	22.0 23.0		[180, 181]
STO/LMO/IBAD-MgO/…/ Hastelloy	248	9 Hz	850	110	20.2		[182]

10
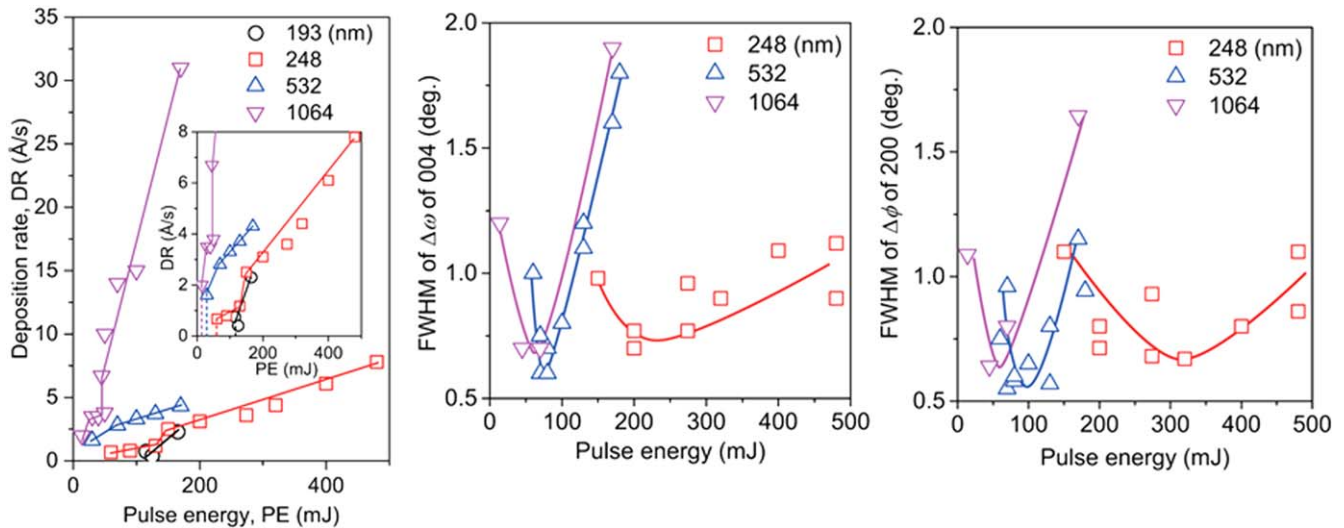
Figure 2. Dependence of deposition rate and texture quality on the pulse energy for $Ba(Fe_{1-x}Co_x)_2As_2$ films grown by PLD with different laser wavelengths. Reprinted from [99], with the permission of AIP Publishing.

Superconducting epitaxial $Ba(Fe_{1-x}Ni_x)_2As_2$ films have been fabricated on $CaF_2(001)$, STO-buffered LSAT and MgO substrates by KrF excimer laser [92, 135, 153–155]. The $Ba(Fe_{1-x}Ni_x)_2As_2$ films on CaF_2 showed slightly lower T_c than $Ba(Fe_{1-x}Co_x)_2As_2$, although the films are strained similar to the $Ba(Fe_{1-x}Co_x)_2As_2$. However, the self-field J_c (2.8 MA cm^{-2} at 4.2 K) of $Ba(Fe_{1-x}Ni_x)_2As_2$ measured by magnetization is almost comparable to that of $Ba(Fe_{1-x}Co_x)_2As_2$. Due to the epitaxial strain on MgO, the maximum T_c which was reached was 18.1 K for a Ni content as low as $x = 2.1\%$ [135].

In 2014, it has been concluded that not only the deposition temperature [168] but also the deposition rate significantly affects the epitaxial growth of $Ba(Fe_{1-x}Co_x)_2As_2$ [99]. By employing the optimum deposition rate around 3 Å s^{-1}, it is possible to fabricate sharply-textured epitaxial $Ba(Fe_{1-x}Co_x)_2As_2$ thin films without buffer layers on LSAT regardless of the laser wavelength, figure 2.

Isovalently P-doped Ba122 epitaxial thin films have been prepared on MgO without any buffer layers by PLD with a second harmonic Nd:YAG laser [156]. The films showed an onset T_c of 26.5 K, although the P content of around 0.34 was almost at optimum level (i.e. 0.33 for single crystal). This may be due to the strain effect, which will be discussed in subsection 3.1.1. High J_c values have been obtained: self-field J_c of 3.5 MA cm^{-2} at 4.2 K and over 1 MA cm^{-2} in the presence of an applied field of 1 T.

In 2015, Langer et al reported on PLD of isovalently Ru-doped Ba122 films and their comparison to single crystal data [186]. Epitaxial $Ba(Fe_{0.55}Ru_{0.45})_2As_2$ films can be grown on a variety of oxide (MgO, LAO, LSAT) and fluoride (CaF_2, BaF_2, SrF_2) substrates which leads to a large range of electrical properties from antiferromagnetic region (on fluorides) via optimally doped (on MgO) to the overdoped region, which was attributed mainly to the substrate effect [163]. Out-of-plane and in-plane texture qualities of 0.7° and 0.8° respectively can be achieved, e.g. on MgO at 900 °C although with a slight 45° in-plane rotated component. For lower deposition temperatures (~700 °C), the main texture component is not as sharp, however no rotated component is observed. Maximum T_c of these films was 22.5 K, which corresponds well to single crystal data [71] of same lattice parameters yet smaller Ru content (~0.3).

Whereas $AE(Fe_{1-x}Co_x)_2As_2$ (AE: alkali earth elements, Ba, and Sr) thin films can be fabricated by in-situ PLD relatively easily, the PLD process is not as suitable for realizing $Ca(Fe_{1-x}Co_x)_2As_2$ thin films due to the high vapour pressure of Ca. Katase et al grew $CaFe_2As_2$ films by PLD from a stoichiometric $Ca(Fe_{0.97}Co_{0.03})_2As_2$ target [168]. Only impurity phases such as Fe-As compounds and Fe were observed rather than Ca-containing phases, except for a substrate temperature $T_s = 650$ °C, where $Ca(Fe_{1-x}Co_x)_2As_2$ may be formed, figure 3. However, neither signs of superconductivity nor resistivity anomaly was observed in transport measurements. By chemical analysis, 14 at% of Ca were measured in the film deposited at $T_s = 650$ °C. Further increasing $T_s = 700$ °C led to a severe loss of Ca (7 at%). The authors concluded that an amorphous phase with Ca was formed. In order to compensate the loss of Ca, a Ca-rich target (33.3 at% of Ca) was used; however, the amount of impurities could not be reduced. To conclude, it is hard to obtain $CaFe_2As_2$ thin films by PLD due mainly to high vapour pressure of Ca. Since then, the research activity on $CaFe_2As_2$ thin films had been inactive.

After the discovery of high-T_c over 40 K in $Ca_{1-x}La_xFe_2As_2$ [187–189], followed by two-site-doped $Ca_{1-x}La_xFe_2(As_{1-y}P_y)_2$ with $T_c = 45$ K [190], the research on $CaFe_2As_2$ thin films regained strong interest. Iida et al used the Fe-buffer layer for growing $CaFe_2As_2$ similar to Ba122/Fe bilayers. These films were deposited on Fe-buffered MgO by ablating $CaFe_2As_2$ and Pr-doped $CaFe_2As_2$ sintered pellets using a KrF excimer laser (frequency of 7 Hz and energy density of 3 J cm^{-2}) at 675 °C and showed c-axis orientation. These results illustrate possible phase formation of $CaFe_2As_2$ by PLD. However, Pr may not be incorporated into $CaFe_2As_2$ since no peak shifts between $CaFe_2As_2$ and Pr-doped

Figure 3. Deposition temperature windows for PLD-grown $AE(Fe_{1-x}Co_x)_2As_2$ (AE: Ca, Sr, Ba) films of different texture and impurity quality. Reproduced from [168]. © IOP Publishing Ltd. All rights reserved.

$CaFe_2As_2$ were observed. No signs of superconductivity were detected for both Pr-doped $CaFe_2As_2$ and undoped $CaFe_2As_2$ thin film in resistivity measurements down to 2 K [169].

Also, Ba122 has been investigated in its indirectly electron-doped, i.e. *RE*-substituted, form e.g. as $(Ba_{1-x}La_x)Fe_2As_2$ by Katase *et al.* Also for Ba122, the phase diagram seems only to depend on charge carrier density and not on whether it is changed directly (within the FeAs layer) or indirectly (from Ba interlayers) [147]. Pressure effects [149] and magnetic scattering [150] have been investigated on these *RE*-substituted films. Exchanging La with Ln = Ce, Pr, Nd leads to a systematic decrease in solubility and T_c and increase of the structural phase transition temperature [150].

Besides superconducting 122 films, also non-super-conducting 122 films have been deposited by purpose. For example, the Mott insulator $TlFe_{1.6}Se_2$ has been grown epitaxially on CaF_2 and LSAT by PLD with a KrF excimer laser for realizing carrier-induced superconductivity by electric double-layer transistors (EDLT) [191]. Another example is $Ba(Fe_{1-x}Cr_x)_2As_2$ thin films showing meta-magnetic transitions [192]. Furthermore, semiconducting $BaZn_2As_2$ epitaxial films have been grown by a reactive solid-phase epitaxy technique using a KrF excimer laser [193].

In short conclusion, the *in-situ* PLD technique for both laser sources (i.e. KrF and Nd:YAG) produces a wide range of superconducting, epitaxial 122 films except for Ca122, KFe_2As_2, and $Ba_{1-x}K_xFe_2As_2$ which contain volatile elements. A two-step process involving a deposition of precursor films by PLD followed by a heat treatment is however effective for realizing K-containing films.

2.2.3. 1111 system. The number of PLD studies regarding 1111 compounds is very limited, see table 6, mainly due to the difficulties in avoiding the formation of $LnOF$ phases which are very stable and hinder the stoichiometric and epitaxial growth.

In the early stage of Fe-based thin film studies, the main effort has been dedicated to the 1111 system, firstly because FBS was discovered in this crystal structure class, and secondly thin films in this material class, such as LaCuOSe, had already been investigated for their semiconducting and optical properties [202]. Later, work continued on these systems due to the highest superconducting transition temperature of 58 K among FBS in bulk [35] and thin film

[203] form, disregarding the exceptional high T_c values in FeSe monolayers found later [94]. First epitaxial LaFeAs(O,F) thin films have been fabricated by Hiramatsu *et al* [200], continuing and extending their work on LaCuOSe. They had fabricated LaMnAsO by PLD with an ArF excimer laser ($\lambda = 193$ nm) [183]. Because LaFeAs(O,F) is isostructural to LaMnAsO, they simply applied the same technique as for LaMnAsO. However, epitaxial LaFeAs(O,F) thin films could not be grown by this technique. After changing the excitation source from an ArF excimer laser to a second harmonic Nd:YAG laser and optimizing the deposition conditions, epitaxial LaFeAs(O,F) films on MgO and LSAT have been realized [200]. However, the films did not show any sign of superconductivity due to the lack of F.

Backen *et al* applied a two-step process, in which amorphous precursor films of LaFeAsO were deposited on LAO and MgO at room temperature by PLD with a KrF laser, followed by *ex-situ* annealing. This method is very similar to *ex-situ* phase formation of $Ba_{1-x}K_xFes_2As_2$ (which however was annealed together with K lumps or KFe_2As_2 powder [152]). As a result, the polycrystalline film showed sign of superconductivity [194]. After further tuning of the processing conditions, LaFeAs(O,F) films with a full superconducting transition [195] and finally epitaxial, superconducting LaFeAs(O,F) thin films [196, 197] were achieved. Also GdFeAs(O,F) [195], SmFeAs(O,F) [198], and (Sm,La)FeAs(O,F) films [199] have been shown by this method. Whereas the GdFeAs(O,F) films were not fully superconducting, the latter showed full superconductivity with $T_c \sim 31$ K and 29.5 K respectively. After these initial investigations, PLD of 1111 systems has been given up for some time since the two-step process is not suitable for fabricating superlattices, stack type junctions and long processing times, and no reports on *in-situ* PLD-grown superconducting, epitaxial 1111 films had been published. Only recently, Haindl *et al* showed that superconducting 1111 films are possible with a one-step *in-situ* process [104]. They deposited SmFeAsO on CaF_2, which lead to F-doping from the substrate during film growth. The films had a T_c of up to 35 K with a transition width of around 10 K. This process is, after further optimization, very interesting for the growth of smooth, thin superconducting 1111 film. The same group investigated the growth behaviour of non-superconducting $SmFeAsO_{1-\delta}$ films on MgO [201].

Table 6. Summary of PLD-grown 1111 films.

Composition	Substrate	λ (nm)	T_{sub} (°C)	Thickness d (nm)	Highest T_c (K)	Remarks	References
LaFeAs(O,F)[a]	LAO	248	1030 (4 h)	600	11.1	Epitaxial, weak fibre component	[194]
	LAO	248	1060	750	27.5	Polycrystalline, broad transition	[195]
	LAO	248	960 (7 h)	200	25	Epitaxial, $\Delta\phi = 1°$	[196]
	LAO	248	~1000	150	23	Epitaxial, LaOF inter- and cap layer	[197]
	MgO	248	1030 (4 h)	600	—	Non-sc.	[194]
GdFeAs(O,F)[a]	LAO	248	1060		~41	Not fully sc, polycrystalline	[195]
SmFeAs(O,F)[a]	LAO	248	1060		~31	Epitaxial	[198]
SmFeAs(O,F)	CaF$_2$	532	860	60	~35	Epitaxial	[104]
	Ba122/MgO	532	860	16	—	Non-sc.	[104]
(Sm,La)FeAs(O,F)[a]	LAO	248	940–970 (5–7 h)		29.5	c-axis texture, most likely biaxially textured	[199]
LaFeAsO	MgO	532	700–880	300	—	Epitaxial, $\Delta\omega_{003} = 1.5°$	[200]
	LSAT	532	700–880	300	—	Epitaxial, $\Delta\omega_{003} = 0.8°$, less impurities	[200]
SmFeAsO$_{1-\delta}$	MgO	532	820–900	11–91	—	Microstructural study	[201]

[a] *Ex-situ* phase formation with PLD at room temperature.

Table 7. Summary of MBE-grown FeSe films. All films were grown from individual sources and showed c-axis oriented epitaxy.

Substrate	T_{sub} (°C)	Thickness d (nm)	Max. T_c (K)	References
YAlO$_3$(110)	350	500	7.5	[204]
LaAlO$_3$(001)	RT-500	500 [204], 200 [205]	sc. [204], non-sc.[205]	[204, 205]
r-cut Al$_2$O$_3$	RT-500	200	13	[205]
Graphene/SiC	180–480	1.2–4	7	[96]
Se-etched Nb:STO, STO	450 + 550(annealing)	0.6	37[a], 42[b], 52[c]	[206]
Se-etched Nb:STO	450 + 550(annealing)	0.6	65[b]	[95]
TiO$_2$-terminated Nb:STO	450 + 550(annealing)	0.6	99.3 ± 0.2[a]; 111 ± 4[a]	[94]

[a] 90% resistivity.
[b] BSC gap.
[c] Fluctuation onset.

2.3. Molecular beam epitaxy (MBE)

MBE, widely used for III/V semiconductors, is a suitable method for fabricating thin films containing volatile elements such as K and F, since precise control of each molecular beam is possible. Unlike PLD and sputtering methods, molecules or atoms have a relatively low energy, resulting in the absence of possible interdiffusion between film and substrate. Additionally, due to the relatively slow growth process in UHV condition, the grown films are usually considered microstructurally clean. MBE has been employed in a wide range of FBS (11, 111, 122 and 1111), which will be reviewed shortly in the following sections.

2.3.1. 11 system.
MBE research in the 11 system has concentrated on FeSe so far, table 7. No studies on MBE-grown films of FeTe, FeSe$_{1-x}$Te$_x$ or the sulphides have been reported until now. Unlike the thin film growth of GaAs by MBE, a self-adjustment of Fe:Se = 1:1 (i.e. re-evaporation of excessive Se) does not occur and FeSe$_2$ having the pyrite structure is formed for too high a Se flux. Therefore, the precise control of each flux should be monitored.

Prior to the monopoly of monolayer research [206], thick FeSe films have been prepared by MBE. Jourdan and ten Haaf have prepared epitaxial FeSe thin films (500 nm) on pseudo-cubic YAlO$_3$(110) with a T_c of 7 K by MBE using elemental Fe and Se solid sources [204]. According to their studies, the superconductivity was obtained in a very narrow composition range of FeSe$_x$ with $x = 1.04 ± 0.02$. Superconducting films were also achieved on YAlO$_3$(010), SrLaAlO$_4$(001), and LaAlO$_3$(001) (without T_c values being given). Almost at the same time, FeSe films (200 nm) have been deposited on both LaAlO$_3$(001) and r-cut Al$_2$O$_3$ at growth temperatures ranging from room temperature (RT) to 500 °C by a combinatorial approach [205] due to the complicated phase diagram [207] close to Fe:Se = 1:1. A deposition temperature above 160 °C leads to a streaky RHEED pattern evidencing c-axis oriented epitaxial films with smooth surfaces. For films grown on r-cut sapphire substrates, the formation of γ-Fe$_7$Se$_8$ could be suppressed. Additionally, the growth window of β-FeSe (the tetragonal phase) was slightly expanded. Despite the onset T_c of 13 K for Se-rich films, zero resistance was not observed.

To date, the highest T_c of FBS of ∼111 K has been confirmed by *in-situ* transport measurements on MBE-processed FeSe monolayer on SrTiO$_3$ [94]. This opens a new avenue for exploring mechanism of this new material class. The first FeSe monolayer (with a T_c of 37 K) was deposited on Nb:SrTiO$_3$(001) [206]. These monolayer FeSe films have brought a huge excitement in the condensed matter physics [95]. Prior to the deposition, the substrate is thermally treated at 950 °C under Se flux for 30 min in UHV condition. Then Fe and Se flux from Knudsen cells are emitted to the substrate at 450 °C. Here, the Se flux is almost ten times higher than the Fe one. After the deposition, the resultant film was annealed at 550 °C for several hours. This annealing process is reportedly crucial for an electronic band structure leading to superconductivity. The superconducting gap was around 20 meV measured by scanning electron microscopy (STM). The ratio of $2\Delta/k_B T$ was around 5.5 for bulk FeSe, where Δ is the superconducting gap and k_B the Boltzmann constant. Assuming that the same mechanism for superconductivity holds for both bulk and monolayers, the T_c of the monolayer will be around 80 K. Interestingly, the superconductivity is destroyed already for a layer thickness of two unit cells. Lattice parameters and electronic structure also clearly change as the layer thickness increases [96]. The in-plane lattice parameter is ∼3.9 Å for monolayer films, indicative of ∼1 % tensile strain, and falls to ∼3.75 Å for thicker films. For monolayers, the hole-like Fermi surface at the Γ point in k-space (0,0) is not visible, i.e. there is only an electron-like Fermi surface around M(π,π). Already for a layer thickness of three unit cells, the Fermi topology has completely changed towards bulk behaviour, figure 4. However, the T_c of FeSe films on graphene/SiC substrate was observed to increase with increasing layer thickness [208]. Such differences may originate from the processing conditions (with or without annealing process after the deposition). To date, several scenarios are discussed for such high T_c. (i) Charge transfer from the STO substrate due to the loss of oxygen and/or Se vacancies. Both cases correspond to electron doping. (ii) Interfacial coupling between electrons in FeSe and oxygen phonon [209].

2.3.2. 111 system.
In 2015, the successful deposition of epitaxial LiFeAs, so-called 111, via MBE on a Nb:STO single crystal has been reported by Chang *et al* [210]. This is remarkable since LiFeAs had been disregarded so far from thin
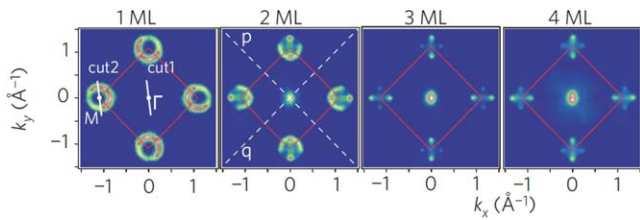
Figure 4. Thickness dependence of the Fermi surface as represented by photoemission intensity maps at the Fermi energy at 30 K for 1–4 monolayers (ML). For 1 ML, the hole-like Fermi surface at the Γ point in k-space (0, 0) is not visible, it reappears for 2 ML, and the whole pattern is bulk-like already for 3 ML. [96] (2013) (Copyright © 2013, Springer Nature). With permission of Springer.

film research due to the high vapour pressure of Li and the high reactivity of LiFeAs with atmosphere. During the growth, Li and Fe were evaporated from standard Knudsen cells. For As flux, FeAs compound was used for obtaining reactive atoms of As. Epitaxial LiFeAs films with thickness ranging from 1 to 26 uc, where uc is the unit cell of LiFeAs (6.36 Å), have been deposited at 450 °C and subsequently transferred to an STM chamber for topography and spectroscopy without breaking UHV condition. The in-plane lattice parameters changed from 3.91 Å to 3.77 Å with increasing layer thickness. A layer thickness of 15 uc leads to a fully relaxed LiFeAs film. Unlike FeSe monolayers, a well-defined superconducting gap with sharp coherence peaks was observed for a film thickness larger than 13 uc. A superconducting gap of $2\Delta \sim 14$ meV was recorded. Additionally, the authors have performed transport measurements *ex situ* on a 100 uc (63 nm) thick LiFeAs film. The measurements revealed a T_c of 16 K, which is only slightly lower than the bulk value (18 K).

2.3.3. 122 system. Besides later studies on $BaFe_2(As_{1-x}P_x)_2$, MBE has been mainly employed for 122 compounds containing volatile elements such as K, and Ca, which are hard to grow by PLD, table 8.

In-situ $Ba_{1-x}K_xFe_2As_2$ and $Sr_{1-x}K_xFe_2As_2$ thin films on sapphire, LAO, MgO, and STO have been fabricated by MBE using an In-K alloy as a solid source rather than pure K [211, 216–218]. These studies have constructed the phase diagrams for both systems. The maximum T_c values were 38.3 K at $x = 0.3$ in $Ba_{1-x}K_xFe_2As_2$ and 33.4 K at $x = 0.4$ in $Sr_{1-x}K_xFe_2As_2$. However, the films are not stable in air. Therefore, the film surface was covered by polystyrene resin, commercially called 'Q-dope', in order to avoid possible degradation [219].

Similarly, $CaFe_2(As_{1-x}P_x)_2$ and $Ca_{1-x}Nd_xFe_2As_2$ have been grown epitaxially on LSAT [212]. The former showed a T_c of 21.4 K at $x = 0.14$ and the latter was not superconducting, which is in contrast to bulk studies. Unlike the $AE_{1-x}K_xFe_2As_2$ mentioned before, these films are rather stable. Hatano *et al* also reported on the growth of parent compound $CaFe_2As_2$ on various substrates by MBE [220]. The films on CaF_2, LAO and MAO showed an onset superconductivity due to the local strain originating from water vapour similar to the results reported by Hiramatsu *et al* [167] or the antiphase domain structure reported by Xiao *et al* [221].

$K_xFe_{2-y}Se_2$ epitaxial thin films have also been realized by MBE [213]. *In-situ* low-temperature STM studies revealed two phases in $K_xFe_{2-y}Se_2$: one is an insulating phase with Fe-vacancies and the other one is the stoichiometric, superconducting phase KFe_2Se_2. These studies imply that local Fe-vacancies destroy superconductivity.

MBE has also been applied to $BaFe_2(As_{1-x}P_x)_2$, which yields a high T_c of around 30 K and a very high self-field J_c of 10 MA cm^{-2} at 4.2 K [214]. Additionally, bicrystal experiments on $BaFe_2(As_{1-x}P_x)_2$ revealed that a large J_c of over 1 MA cm^{-2} at a grain boundary (GB) angle as large as 24° at 4 K, which is far beyond that of $Ba(Fe_{1-x}Co_x)_2As_2$. The optimum P content is lower than the optimum level for single crystals (i.e. $x = 0.33$). Since the films have been prepared on MgO, a large lattice misfit of 6% between film and substrate leads to tensile in-plane strain. This strain shifts the whole superconducting dome for $BaFe_2(As_{1-x}P_x)_2$ towards the underdoped regime compared to single crystals [215].

Besides superconducting, Fe-based 122 compounds, epitaxial $BaMn_2As_2$ thin films have been grown on GaAs (001) by MBE [222]. These films show semiconducting behaviour and a change of charge carriers from electrons at low deposition temperatures to holes for high deposition temperatures, which was explained by different band anisotropies.

2.3.4. 1111 system. In the case of 1111 compounds, MBE has mainly been used for Nd1111 at Nagoya University and for Sm1111 at the Tokyo University of Agriculture and Technology, table 9.

The first epitaxial films of NdFeAsO were realized on GaAs, although F was not incorporated into the matrix [223]. These films had a thickness of 15 and 30 nm. An elongation of the growth time (to more than 5 h) and consequently a film thickness above 75 nm yielded superconducting NdFeAs(O,F) [224] and also LaFeAs(O,F) [226] epitaxial films. The respective T_c of NdFeAs(O,F) and LaFeAs(O,F) were 48 and 4.5 K. Auger spectroscopy on the superconducting films revealed that a NdOF layer was formed at the surface for growth times above 5 h. Hence, it is most probable that F diffused into NdFeAsO from NdOF layer. Later, also Kawaguchi *et al* identified GaAs a suitable substrate for growing the 1111 phase. Further investigation revealed that Ga works as a getter of F as the following sublimation reaction at 280 °C: $NdF_3 + Ga \rightarrow Nd + GaF_3$. Employing this reaction made it possible to utilize various substrates such as MgO, LAO and CaF_2 [103, 225]. However, films prepared on such substrates always have too low a fluorine content, i.e. are not superconducting.

In order to dope F into the grown matrix, a NdOF over-layer was deposited on parent NdFeAsO layer. As a result, superconducting NdFeAs(O,F) thin films have been realized. Ueda *et al* have applied a similar method to grow SmFeAs(O,F) thin films on fluoride substrates such as CaF_2, SrF_2 and BaF_2 [105]. A record transition temperature of 57.8 K [203] was obtained for the film on CaF_2. Additionally, the magnetization J_c at self-field and 5 K was around 2 MA cm^{-2}.

Table 8. Summary of MBE-grown 122 films.

Material	Substrate	Sources	Temperature (°C)	Thickness (nm)	T_c (K)	Reference
$Ba_{1-x}K_xFe_2As_2$	LSAT	Ba, Fe, As, In-K	340	130	38.3 ($x = 0.3$)	[211]
$Sr_{1-x}K_xFe_2As_2$	LSAT	Sr, Fe, As, In-K	340	120	33.4 ($x = 0.4$)	[211]
$CaFe_2(As_{1-y}P_y)_2$	LSAT	Ca, Fe, As, GaP	700	70	21.4	[212]
$Ca_{1-x}Nd_xFe_2As_2$	LSAT	Ca, Fe, As, Nd	700	70	non-sc	[212]
$Ca_{1-x}Nd_xFe_2(As_{1-y}P_y)_2$	LSAT	Ca, Fe, As, GaP, Nd	700	70	<21.4	[212]
$K_xFe_{2-y}Se_2$	6H-SiC (0001)	K, Fe, Se	440	20	22–25 (gap closing)	[213]
$BaFe_2(As_{1-x}P_x)_2$	MgO, bicrystal	Ba, Fe, As, GaP	850	100	28.8…30.5 (depending on stoichiometry)	[214]
	LAO	Ba, Fe, As, GaP	710	100	30 ($x = 0.23$)	[215]
	MgO	Ba, Fe, As, GaP	800–900	100	31 ($x = 0.23$)	[215]

Although superconducting Ln1111 films have been realized, LnOF (Ln: Sm, Nd) over-layers are necessary which may become obstacles for stack-type Josephson junctions and other microelectronic and surface-sensitive applications and experiments. In 2015, a one-step process has been realized by Sugawara *et al* which yielded SmFeAs(O,F) superconducting thin films on LAO and CaF$_2$ without an over-layer [228]. The key for this achievement was the use of FeF$_2$ as a fluorine source. These films showed a high T_c above 50 K and a similar in-field $J_c(B)$ performance as SmFeAs(O,F) films with SmOF over-layer. Similarly, and at the same time, Chihara *et al* [229] succeeded in the one-step growth of superconducting NdFeAs(O,F) films with T_c of 50 K and J_c values exceeding 1 MA cm^{-2} at 4 K for applied fields up to 9 T.

2.4. Other deposition methods

Besides PLD and MBE as the major deposition methods for Fe-based superconducting thin films, other methods have been used in recent years as well, especially for 11 materials, but also for Nd1111 and (Li,Fe)OHFeSe, the so-called 11111 or 5–1 compound.

2.4.1. 11 system. Due to the interesting photochemical, photovoltaic, and magneto-mechanical properties of this compound, FeSe films have been prepared for a long time by several methods, such as co-evaporation [230], metal-organic [231, 232] and aerosol-assisted chemical vapour deposition (CVD) [233, 234], and chemical bath deposition [235]. Most of these methods produced α-FeSe, i.e. the hexagonal non-superconducting crystal structure, sometimes a mix of this phase and the tetragonal β-FeSe. Only after the discovery of superconductivity in β-FeSe [8] and related compounds in 2008 were the deposition possibilities of this phase preferably in superconducting and epitaxial form investigated.

Speller *et al* [236] and later Mousavi *et al* [237, 238] investigated the *in-situ* phase formation of $Fe_y(Se_{1-x}Te_x)$ during RF magnetron sputtering from a single mixed target on a variety of single crystal substrates. Despite the largest misfit to $Fe_y(Se_{1-x}Te_x)$, MgO substrates yielded the sharpest texture qualities [236], which is concurrent to the fact that biaxially

c-axis-textured $Fe_y(Se_{1-x}Te_x)$ can even be grown (by PLD) on amorphous surfaces like glass [239, 240]. Due to the different sputtering rates of different elements, the Te content x and the Fe content y are correlated to each other in these films and depend strongly on the *in-situ* deposition and, occasionally, *ex-situ* annealing conditions [238]. Best samples concerning phase purity, texture, and T_c value (10.2 K, $T_{c0} = 6.9$ K) are deposited around 315 °C and thicknesses not larger than 50 nm [237], figure 5.

FeSe films were deposited on MgO by RF magnetron co-sputtering from an FeSe and a Se target by Schneider *et al* in order to investigate thickness effects on T_c and finite-size resistivity scaling [241]. Highest T_c values of $\sim$9 K with largest residual resistivity ratios of $\sim$5 are deposited around 500 °C. The films are polycrystalline, yet highly c-axis-textured [242] with strong in-plane orientation and contain only minor amounts of the (101)-oriented component and of the hexagonal phase [243]. On one of these films with a thickness of 500 nm, the fluctuation conductivity as well as the Berezinskii–Kosterlitz–Thouless (BKT) transition between 2D and 3D behaviour has been observed [244]. Similarly textured films with $T_c \sim 11$ K ($T_{c0} = 7.5$ K) have been prepared on [110]-oriented STO substrates, which enabled the investigation of anisotropic grain boundary networks and their influence on J_c and resistivity [245]. Chai *et al* employed reactive sputtering from an Fe target in H$_2$S atmosphere followed by *ex-situ* selenization at elevated temperatures for growing FeSe$_x$ films [246]. These films grow polycrystalline with Fe$_7$Se$_8$ impurities and show T_c onset values up to 10.2 K and T_{c0} around 4 K.

High temperature solution via SeSn flux, a method similar to single crystal growth, via the precipitation of FeSe on an LAO substrate was a relatively early attempt to grow FeSe films besides PLD, MBE, and sputtering. Qi *et al* [247, 248] achieved phase-pure (by x-ray diffraction) β-FeSe films with T_c onset value of around 6 K, slightly lower than for the comparable bulk samples.

Also chemical methods have been used in the attempt to deposit the superconducting FeSe phase. Chen *et al* deposited β-FeSe on indium tin oxide (ITO) electro-chemically with Pt as counter electrode and a H$_2$SeO$_3$/FeSO$_4$·7H$_2$O solution

Table 9. Summary of MBE-grown 1111 films. All films showed *c*-axis oriented epitaxy.

Material	Substrate	Source	T_{sub} (°C)	Growth rate (nm h^{-1})	d (nm)	T_c (K)	References
NdFeAsO	GaAs(001)	Fe, As, NdF$_3$, Fe$_2$O$_3$	670	15	15, 30	*Non sc.*	[223]
NdFeAs(O,F)	GaAs(001)	Fe, As, NdF$_3$, Fe$_2$O$_3$	700	15	15–90	48 (90 nm)	[224]
	MgO(001)	Fe, As, NdF$_3$, Fe$_2$O$_3$, Ga	650	15	15	45 [225], 44 [103]	[103, 225]
	GaAs(001)	Fe, As, NdF$_3$, Fe$_2$O$_3$, Ga	650	15	15	37	[103]
	CaF$_2$(001)	Fe, As, NdF$_3$, Fe$_2$O$_3$, Ga	650	15	15	56	[103]
	LAO(001)	Fe, As, NdF$_3$, Fe$_2$O$_3$, Ga	650	15	15	45	[103]
LaFeAs(O,F)	GaAs(001)	Fe, As, LaF$_3$, Fe$_2$O$_3$	650	15	9	4.5	[226]
SmFeAs(O,F)	CaF$_2$(001)	Sm, Fe, As, O$_2$ atm.	650	90–180	100–170	57.8	[105]
		Sm, Fe, As, O$_2$ atm., no cap layer	650	90–180	100–170	~10	[227]
		Sm, Fe, As, FeF$_2$, O$_2$ atm.	645	510	85	52.9 (1step) 57.8 (2step)	[228]
	SrF$_2$(001)	Sm, Fe, As, O$_2$ atm.	650	90–180	100–170	56.7, 57.3	[105], [227]
		Sm, Fe, As, O$_2$ atm., no cap layer	650	90–180	100–170	~30	[227]
	BaF$_2$(001)	Sm, Fe, As, O$_2$ atm.	650	90–180	100–170	55.3, 56.4	[105], [227]
	Al2O3	Sm, Fe, As, O$_2$ atm.	650	90–180	100–170	48.2 (very broad transition)	[227]
	YAO	Sm, Fe, As, O$_2$ atm.	650	90–180	100–170	48.7	[227]
	LAO(001),	Sm, Fe, As, FeF$_2$, O$_2$ atm.	645	510	85	51.9 (1step)	[228]
		Sm, Fe, As, O$_2$ atm.	650	90–180	100–170	50.3	[227]
	MgO	Sm, Fe, As, O$_2$ atm.	650	90–180	100–170	55.3	[227]
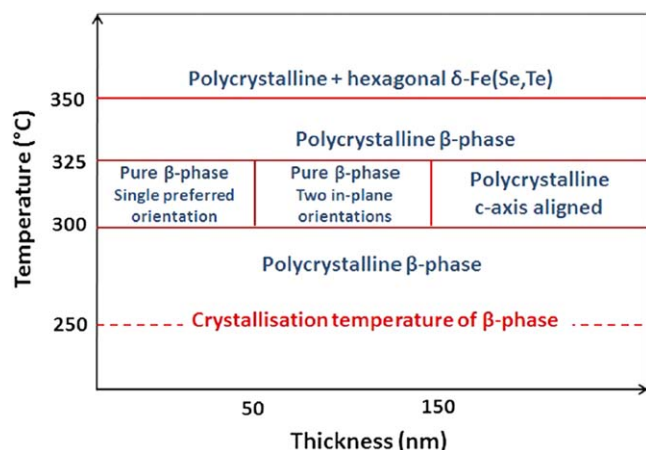
Figure 5. Temperature-thickness parameter windows for sputtered Fe(Se,Te) films of different texture qualities and crystal structures on MgO. [237] (2015) (Copyright © 2015, Springer Nature). With permission of Springer.

[249]. Later, Yamashita *et al* deposited phase-pure β-FeSe on ITO using an H_2SeO_3/$FeCl_2 \cdot 4H_2O$/Na_2SO_4 solution [250]. No information on superconductivity was given in those publications. This same method was also used by Demura *et al* with an iron plate as anode. Initial investigations clarified the role of electrical potential and pH value of the electrolyte for the Fe-Se composition of the films, and T_c values of 3.5 K [251] and later 8.1 K [252] were recorded. Later, Demura [253], Yamashita *et al* [254] adapted this method for the use of RABiTS tapes as anode with regard to possible low-cost coated conductor production of 11 materials. On this substrate, zero-resistance superconducting state was found with a T_c of 2.5 K. Metal-organic vapour deposition (MOCVD) has been used by Li *et al* for FeSe films [255]. They investigated the influence of substrate (Si and GaAs) and stoichiometry on the superconducting and magnetic properties. The film with optimized stoichiometry on Si showed full superconductivity with $T_c = 10.5$ K and $T_{c0} \sim 2.4$ K, whereas the films with higher Fe content and on GaAs showed only partial superconductivity ($T_c \sim 6.5$ K) or semiconducting, ferromagnetic behaviour respectively. Recently, chemical transport deposition (CTD) has been used by Feng *et al* for growing FeSe films [256]. This process makes use of the high vapour pressure of Se which is transported in Ar flow of $1\,l\,min^{-1}$ to an Fe foil at elevated temperatures up to 600 °C. The films obtained so far contain both α-FeSe and β-FeSe, and the maximum onset T_c is 7.8 K without full superconductivity.

The sulphur-containing phase $Fe(Te_xS_y)$ has been prepared in form of thin films in an *ex-situ* phase formation process from amorphous layers which were deposited by PLD. Yoshimoto *et al* [257] were able to grow fully superconducting, highly biaxially oriented films with T_c up to 9.0 K when the precursor film was annealed together with an $Fe(Te_{0.8}S_{0.2})$ pellet.

2.4.2. 1111 system. A two-step aerosol-assisted MOCVD process has been investigated by Corrales-Mendoza *et al* with

regard to possible deposition of superconducting Nd1111 films. The authors used neodymium-hexafluoro-pentanedionate and iron-pentanedionate to grow $(Nd,Fe)O_{1-y}F_{1+2y}$ precursor films, which were loaded with As during an annealing step. The annealing with As powder did not result in superconducting films although a structural change to the rhombohedral (Nd,Fe) OF phase was observed [258]. Changing to fluorine-free neodymiumTris(2,2,6,6-tetramethyl-3,5-heptanedionato) (Nd-Tris) as chemical precursor and annealing at $T > 1050$ °C with a superconducting $NdFeAsO_{0.75}F_{0.25}$ pellet led to non-superconducting NdFeAsO films since F was not incorporated in the crystal structure [259]. In 2015, the authors showed that MOCVD of superconducting 1111 films is indeed possible by changing from F-doping to Co-doping [260]. Annealing with $NdFe_{0.9}Co_{0.1}AsO$ pellet resulted in $NdFe_{0.88}Co_{0.12}AsO$ films with an onset T_c of around 15 K and full superconducting transition ($T_{c0} \sim 12.5$ K). These were the first Co-doped Nd1111 thin films reported. And recently, Corrales-Mendoza *et al* reported on superconducting SmFeAs(O,F) films grown by MOCVD, which was achieved by an *ex-situ* F-diffusion annealing step [261]. The films showed onset T_c values of up to 53 K and a double transition due to the grain boundary networks. All MOCVD *Ln*1111 films are polycrystalline and without a strong preferential texture so far.

2.4.3. 11111 system. Only recently, a fifth crystal structure of FBS has been successfully prepared in the form of thin films: (Li,Fe)OHFeSe, the so-called 11111 (or 5–1) phase [23], which may be regarded as chalcogenide crystallographic equivalent of the pnictide 1111 phase (if the OH group is regarded as single entity). This material consists of widely separated FeSe layers and therefore shares electronic similarities with the FeSe monolayer films [262], is highly anisotropic and shows 2D behaviour. Similar to the single crystal growth of this material by ion exchange [23], these films are grown by Huang *et al* via matrix-assisted hydrothermal epitaxial growth (MAHEG) [263], where the K layers of a precursor $K_{0.8}Fe_{1.6}Se_2$ single crystal on $LaAlO_3$ single crystal are exchanged by (Li,Fe)OH layers in a soft-chemistry process. These films are highly epitaxial with $T_{c0} = 42.4$ K, an anisotropy near T_c of ~ 5.6 and self-field J_c values of 0.5 MA cm^{-2} at 24 K [24]. Due to the large anisotropy, the multiband superconductivity, and the proximity to magnetism, these films show a rich vortex phase diagram and additional features in flux pinning behaviour [264], which deserve further investigation.

2.5. Summary on film preparation

For the large variety of literature on FBS thin film preparation techniques in the recent decade, several conclusions and summaries may be drawn:

- The main two deposition techniques for FBS films are PLD and MBE, usually in UHV:

  (a) PLD is mainly used for 122 and 11 compounds. For 1111, PLD is possible yet difficult to achieve epitaxy and high T_c simultaneously;

(b) MBE is mainly used for 1111 compounds, 122 compounds with volatile elements, and ultra-thin FeSe films.

- Many other methods, such as sputtering and chemical deposition (CVD, CTD, ECD) have been employed for FeSe and Fe(Se,Te). Most of these techniques need further optimization.
- Typical deposition temperatures are around 700 °C–850 °C for 122 and 1111 compounds (except P-doped Ba122 at >1000 °C) and 200 °C–400 °C for 11 compounds.
- Singular studies have been reported for LiFeAs by MBE and (Li,Fe)OHFeSe by MAHEG.
- For many two-step processes, the phase formation takes place *ex situ*, and the final properties of the film are less determined by the deposition technique (may it be PLD, MOCVD, sputtering, etc) than by the phase-formation step (atmosphere, temperature profile etc).

3. Tuning superconducting transition temperature and upper critical field

It is of major importance to understand which factors influence the superconducting transition temperature as well as the upper critical field in FBS thin films in order to tune these critical parameters for possible applications. The parent compounds of FBS have typically an antiferromagnetic order. It was shown that superconductivity is induced in these materials either by carrier doping, isovalent substitution (i.e. chemical pressure) or structural modification under external pressure, for a review see [265]. In all cases, changes in the structural parameters of the parent compound are observed, which led to the assumption that an optimal arrangement of the atoms is required to achieve high T_c values. It is assumed that the superconducting transition is particularly sensitive the atomic arrangement in the FeAs or FeSe layer. It was already discussed early after the discovery of FBS, that the As–Fe–As bond angle plays an important role [266]. Other authors proposed that T_c is closely correlated with the pnictogen (or chalcogen) height above the Fe plane [267, 268].

The growth of thin films results often in a change of the structural parameters in comparison to bulk materials due to the boundary conditions at the substrate-film interface. This dependence might be used in thin film technologies to modify or even tune the superconducting parameters. In the following, we will discuss the effect of strain on the critical parameters as well as methods to modify either strain in these films or the electronic subsystem by electrochemical gating.

3.1. Effect of crystallographic parameters on superconducting properties

As mentioned above, T_c of FBS compounds is strongly influenced by the exact atomic arrangement in the unit cells, either discussed by the As–Fe–As bond angle [266] or via the pnictogen/chalcogen height [268]. Besides by chemical

substitution (i.e. charge carrier or isovalent doping), these parameters are influenced and determined by the lattice parameters a and c. For a given compound and stoichiometry, applying stress to one of these lattice parameters (e.g. by uniaxial pressure along c or epitaxial strain along a) usually leads to strain not only on this parameter but also to other directions. This is characterized by the (in general direction-dependent) Poisson ratio ν. It can be calculated by the elastic stiffness coefficients C_{ij} and for the isotropic or polycrystalline case by $\nu_{iso} = 3(B^{-2}G)/\{2(3B + G)\}$, where the bulk modulus B and the shear modulus G are averages in the so-called Voigt-Reuss-Hill approximation and determined by C_{ij} themselves, see e.g. [269]. For uniaxial distortion along the fourfold symmetry axis (c-axis) of the tetragonal FBS systems, the more relevant parameter is $\nu_{12} = C_{13}/C_{11} + C_{12}$ [270], which is equivalent to $\nu_{001} = \epsilon_\perp/\epsilon_\perp - 2\epsilon_\parallel$ for epitaxial c-axis grown films, where $\epsilon_\parallel$ is the in-plane strain and $\epsilon_\perp$ the strain perpendicular to the film surface, i.e. along [001]. These data are given in table 10 for selected compounds as available in literature or calculated from the relevant literature data. FeSe, for which most usable data are available, shows a rather large data scatter. That might be explained by a strong dependence on the exact stoichiometry. Hanzawa *et al* [271] pointed out recently that the strain state in very thin MBE-grown FeSe films depends strongly on the Fe:Se ratio, which was related to excess interstitial Fe or disordered Fe vacancies. Kawaguchi *et al* [215] have shown the dependence of the Poisson ratio of BaFe$_2$(As$_{1-x}$P$_x$)$_2$ films on MgO on the P content x, more or less linearly increasing from around 0.2 at $x = 0$ to 0.35 at $x = 0.45$. Similar dependencies can in principle be deduced from literature data for Ba(Fe$_{1-x}$Co$_x$)$_2$As$_2$ [102] and FeSe$_{1-x}$Te$_x$ [132] films as well as FeSe$_{1-x}$Te$_x$ bulk [272]. However, due to the large experimental errors (especially in a-axis parameter), data scatter, and differences between experimental and theoretical values [272], such plots would be premature without exact knowledge about the experimental conditions. Further studies on the Poisson ratio of FBS are highly desired in order to complete the picture on epitaxially strained films.

It was already observed from the beginning that different substrates result in a wide range of of the critical temperatures in epitaxial FBS films, and several studies were explicitly dedicated to T_c's substrate dependence, e.g. for FeSe [128, 274], FeSe$_{1-x}$Te$_x$ [83, 84, 118, 279, 280], Ba(Fe$_{1-x}$Co$_x$)$_2$As$_2$ [90, 172], and Ba$_{1-x}$K$_x$Fe$_2$As$_2$ [151]. This dependence is often attributed to strain in these layers, i.e. to a pure deformation of the unit cell due to the epitaxial growth on substrates with a different lattice misfit. However, such a correlation between strain and critical parameters is not straightforward. In particular, it is difficult to prepare purely epitaxially strained films as this requires a coherent growth at the interface between substrate and film without the incorporation of misfit dislocations or other defects. As an example, Yamagishi *et al* [211] observed no substrate dependence of the film's c-axis lattice parameter for MBE-grown Ba$_{1-x}$K$_x$Fe$_2$As$_2$ films irrespective of the different misfit, indicating relaxed growth. Coherent growth is typically achieved in semiconductors or simple perovskite oxides by a layer-by-layer growth mode verified by reflection high-energy

Table 10. Poisson ration ν of Fe-based superconducting materials determined on polycrystalline bulk samples, theoretically, or deduced from film studies involving several substrates (marked with [*]). Due to the large experimental errors and data scatter, all values were rounded to two decimal places.

Material	Poisson ratio ν_{iso}	Poisson ratio ν_{21} or ν_{001}	References
FeSe	0.18, 0.20	0.10, 0.18	[272, 273]
FeSe[*]	—	0.28 ± 0.02, 0.21, 0.25 ± 0.02, 0.28 ± 0.02, 0.36 ± 0.04, 0.27 ± 0.01	[129, 132, 144, 271, 274, 275]
$FeSe_{0.5}Te_{0.5}$[*]	—	0.11 ± 0.04	[132]
LiFeAs	0.24; 0.24	0.19, 0.27	[276, 277]
$SrFe_2As_2$	0.28	0.19	[278]
$RbFe_2As_2$	0.31	0.34	[278]
KFe_2Se_2	0.25	0.20	[269]
$Ba(Fe_{1.9}Co_{0.1})As_2$[*]	—	0.29 ± 0.02	[90]
$LaFeAsO_{0.86}F_{0.14}$	0.26	0.25	[277]
$SmFeAsO_{1-x}F_x$[*]	—	0.29 ± 0.01	[227]

electron diffraction (RHEED) oscillations. To our knowledge, such a growth mode has not been observed so far for FBS thin films. Instead, streak-like features are often observed in RHEED studies [101, 115, 181, 281], which indicate smooth surfaces with extended flat areas; however, do not prove coherent growth. Additionally, a coherent growth is normally restricted to layers below a misfit-dependent critical thickness as it is energetically more favourable to include lattice defects if the volume strain energy gets too high. Completely strained films have been observed for undoped $BaFe_2As_2$ on Fe-buffered $MgAl_2O_4$ below a critical thickness of about 30 nm [146]. In this case, strain induces bulk superconductivity with a T_c of about 10 K by a pure lattice deformation without any chemical doping. Nevertheless, there are also defects present as the Fe buffer has already a grain structure resulting in small orientation changes [282]. Recent cryo-EBSD measurements by Pukenas *et al* [283] on these films support these results by revealing that for thicknesses below 30 nm the structural phase transition is absent in contrast to $BaFe_2As_2$ single crystals, even though a clear island growth mode also of these thinnest films is apparent.

Additionally to the incorporation of misfit dislocations, other factors need to be taken into account, if epitaxially grown films on different substrates are compared. At first, the interface between the substrate and the film plays an important role for epitaxial growth (for a more general discussion see for example [284]). A layer-by-layer growth often requires similar crystal structures, i.e. a perovskite unit cell for both template and film. Therefore, it makes already a difference if a substrate with a perovskite, fluorite or rocksalt structure is used. Furthermore, the specific atomic arrangement at the interface has an influence as it determines the binding between the uppermost substrate atoms with the first film atoms and influences in this way also the nucleation of the film. As a result, it might be difficult to achieve epitaxial films even if the lattice misfit is small (for example 11 on LSAT, where no epitaxial growth [83], epitaxial growth with large mosaic spread [118], or good epitaxial growth [274] was reported). Secondly, an interdiffusion might occur at the

interface. In particular 122 and 1111 films are deposited at high temperatures, which favours such diffusion processes. This might be especially important for substrates which easily loose one of their elements (for example O in STO or F in CaF_2). As a result, a reaction layer might be formed or composition gradients appear in such films (see for example the extended discussion in [285]). Finally, compositional inhomogeneities need to be taken into account. They might be related to different defect structures in films grown on different substrates resulting from processes during nucleation and coalescence of the film, which are strongly influenced by the misfit and the interface properties [83, 84, 122, 172, 227].

In the following, two major approaches will be summarizes, where the superconducting properties are mainly tuned by strain. At first, strain can be induced by the application of substrates with different thermal expansion coefficient. In this case the strain arises during cool-down after film deposition at high temperatures. Secondly, the strain might be varied after preparation by external forces. Examples are the application of piezoelectric substrates, hydrostatic pressure cells, and the uniaxial straining of films grown on flexible metal tapes.

3.1.1. Influence of thermal expansion coefficient. As already mentioned above, a misfit of the thermal expansion coefficient between substrate and film might result in the incorporation of significant strain values in FBS thin films. This is in particular the case when films are deposited at high temperatures (typically 700 °C–850 °C) as for the 122 or the 1111 material system. The cooling rate after deposition is typically high enough to avoid major defect rearrangements or diffusion processes resulting in a deformation of the film lattice cell due to the clamping of the thin layer on the significantly thicker substrate. However, most substrates used for the growth of FBS have similar thermal expansion coefficients as the superconducting material itself (tables 1 and 3), i.e. result in negligible strain values. In contrast, CaF_2 shows a significantly higher coefficient of around 18×10^{-6} K^{-1} at room temperature, table 1, resulting in a compressive strain

state after cool-down. This was studied in detail for the growth of $Ba(Fe_{1-x}Co_x)_2As_2$ films on CaF_2 and MgO substrates [102]. In this comparative investigation, a clear difference for the film lattice parameters was found for various doping contents, which were traced back to thermal expansion by temperature dependant x-ray diffraction measurements. As a result, the complete phase diagram is shifted to higher (on CaF_2) or lower (on MgO) doping levels. A similar behaviour was also found for the $Ba(Fe_{1-x}Ni_x)_2As_2$ system [135]. In a recent study, Langer *et al* [286] nevertheless argue that thermal mismatch between CaF_2 and $Ba(Fe_{1-x}Co_x)_2As_2$ alone cannot explain the observed change in lattice parameters. Full understanding of the film growth on CaF_2 should regard the strong tendency of F to diffuse into the film (as also observed for $FeSe_{0.5}Te_{0.5}$ films by Ichinose *et al* [100]), therefore include the formation of foreign phases and misoriented components as well as a possible incorporation of F into the crystal structure.

Similarly, also 11 films grown on CaF_2 reveal higher T_c values compared to layers on other substrates [118, 275, 287]. Also in this case, a difference in the *a*-axis lattice parameter was found, which can be traced back to the incorporated strain by the mismatch in the thermal expansion coefficient which is even lower for 11 in comparison to 122 materials due both to the lower deposition temperatures and a larger in-plane expansion coefficient of 11 compounds, table 3. Tsukada *et al* [288] attribute the decreased *a*-axis parameter furthermore to a Se-deficient interlayer due to Se diffusion into the substrate. A lower T_c value was found, when CaF_2 was used only as buffer layer instead of as substrate. In this case, the thermal expansion of the film architecture is governed by the value of the significantly thicker LSAT substrate and not by the CaF_2 [118].

3.1.2. External tuning of the critical parameters after deposition. Since typically also the microstructure is changed, it is difficult to modify the strain state for one particular composition by the application of different lattice matching substrates in a controlled way. The alternative is to modify the strain state of the grown film dynamically by external forces. However, this is not straightforward as the films are typically clamped to rigid ceramic substrates. Nevertheless, different approaches were used in the last years to realize such an external tuning of the superconducting properties on one and the same substrate.

At first, piezoelectric substrates might be applied for such studies. If an electric field is applied to such piezocrystals, their lattice parameters can be changed reversibly to a certain amount. As an example, single-crystalline $Pb(Mg_{1/3}Nb_{2/3})_{0.72}Ti_{0.28}O_3$ (PMN-PT) was tested for the growth of FBS by PLD. It was found that $Ba(Fe_{1-x}Co_x)_2As_2$ films can be epitaxially grown on these substrates using either $CaTiO_3$ or $SrTiO_3$ buffer layers [289]. These samples showed a maximum T_c of 18.5 K. Applying a strain of 0.02 % resulted in a change of T_c of about 0.3 K [290]. Furthermore, a shift of the upper critical field H_{c2} with strain is observed, which is explained by the T_c change. However, no influence of the strain state on the anisotropy of the upper critical field was found, if the temperature is normalized to
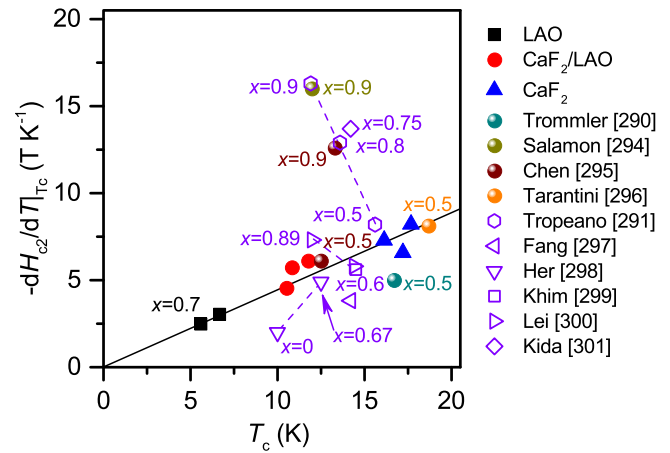

Figure 6. T_c dependence of the $H_{c2}^{\|c}$ slope near T_c of $FeSe_{1-x}Te_x$ films (full symbols: Yuan *et al* [134], and balls) and bulk samples (open symbols, Tropeano: polycrystalline, otherwise single crystals). A clear positive linear correlation for the films is apparent. Bulk values, especially with higher Te content x, differ due to different compositions as well as dirty-limit effects.

T_c. A similar study was also done for nominal $FeSe_{0.5}Te_{0.5}$ [290]. In this case, a two-step process as described above was used without any additional buffer layer material. The change in T_c with strain of about 0.2 K for a strain of 0.02 % was slightly lower compared to the $Ba(Fe_{1-x}Co_x)_2As_2$ sample. Whereas the magnitude of the $H_{c2}(T)$ slope near T_c slightly increased for $Ba(Fe_{1-x}Co_x)_2As_2$ (since magnitude and anisotropy were constant at given reduced temperature), it did not depend on T_c for the $FeSe_{1-x}Te_x$ film. This may be compared to results on polycrystalline $FeSe_{1-x}Te_x$ bulk samples by Tropeano *et al* [291] where T_c was altered via Se-Te composition and to a recent thin film study by Yuan *et al* [134] on $FeSe_{0.7}Te_{0.3}$ where T_c was changed by growth conditions and different strain states on different substrates. In the former case, the slope was decreasing with increasing T_c, which was related to the dirty-limit superconductivity due to the polycrystalline nature of the samples. In the latter case, a clear positive linear correlation between slope and T_c was found, which has been explained with a clean-limit two-band description. This behaviour has been found before also for clean-limit 1111 [291, 292] and 122 compounds [292, 293], however could not have be deduced from the bulk sample literature data for $FeSe_{1-x}Te_x$, as illustrated by figure 6 which compares the data of [134] to other thin film [290, 294–296] and bulk data [291, 297–301]. The opposite or indifferent behaviour of the films on PMN-PT [290] is due to the small changes in T_c (within symbol size).

Even though the piezo-crystal approach was tested successfully, it is suitable for small strain variations only, due to the restricted lattice changes of the single-crystalline piezocrystals at low temperature [302]. Alternatively, flexible substrates might be used for such strain studies. A typical example is the use of biaxially textured templates based on metal tapes, which were mainly developed for the $YBa_2Cu_3O_{7-\delta}$ (YBCO) coated conductor approach. It was shown already soon after the discovery of FBS, that such coated conductor templates are also suitable for growth of epitaxial 122 and 11 films, for a review see [43]. These metal templates can be stretched or bent elastically

and therefore be used as a platform for strain investigations. Indeed, such experiments have been carried out. Trommler, for example, showed that such samples can be used in two-point bending experiments [303]. With a custom-made insert for the PPMS, bending strain on the metal tape up to 1% could be applied and a parabolic T_c dependence on strain in Ba(Fe$_{0.9}$Co$_{0.1}$)$_2$As$_2$/Fe/IBAD-MgO/Hastelloy samples [181] with maximum T_c reduction of 1 K at 1% strain has been found. Similar reports for uniaxial in-plane stress have been reported recently by Iida *et al* [123] using the piezo-based strain device according to [304]. A total shift in T_c of 0.1 K for varying the strain along [110] between +0.018 % and −0.030 % has been resolved for Ba(Fe$_{0.92}$Co$_{0.08}$)$_2$As$_2$/IBAD-MgO/Hastelloy, which corresponds to a pressure derivative of $dT_c/dp_{[100]} = -4$ K GPa^{-1}. Similar experiments might be possible for FeSe$_{1-x}$Te$_x$ films on Mica [138], if sharp c-axis texture or even better biaxial texture is given.

Finally, hydrostatic pressure was applied to epitaxial FBS thin films using a piston-cylinder clamp cell with a liquid pressure medium. The application of a pressure of up to 1.7 GPa resulted in a T_c increase of up to 8 K for FeSe$_{0.5}$Te$_{0.5}$ films grown on MgO substrates [305]. A dependence of the relative increase of T_c with pressure on the anion height above the Fe plane was found in this study; however, changes in the band structure or the Fermi level may play an important role for these effects. Shortly after, Katase *et al* [149] found a strong dependence of T_c on applied pressure in the whole phase diagram of (Ba$_{1-x}$La$_x$)Fe$_2$As$_2$ films in contrast to K-, Co-, and P-doped BaFe$_2$As$_2$ films. This was associated with the lattice shrinkage which led to an optimization of the crystal and electronic structure and therefore to reduced electron scattering and increased carrier density.

3.2. Gating experiments (carrier injections and etching)

An EDLT is a powerful tool for exploring new superconducting materials, e.g. gate-induced superconductivity in KTaO$_3$ [306] and MoS$_2$ [307]. One of the biggest advantages of EDLTs is to generate a significantly large electric field of 50 MV cm^{-1} at the interface between ionic liquids (ILs) and given materials, resulting in a two-dimensional carrier density of ~8 × 10^{14} cm^{-2} [308]. This value is not achievable for a conventional field effect transistor with a solid gate insulator. Additionally, carrier doping by electrostatic gating introduces less disorder than that by chemical substitution. Hence, phase transitions due to more or less pure carrier doping can be investigated.

The first EDTL experiments on FBS were conducted using FeSe$_{1-x}$Te$_x$ (x = 0.9 and 1) single crystals [309]. The thin FeSe$_{1-x}$Te$_x$ samples, fabricated by the scotch tape method [310], were placed on SiO$_2$-covered Si substrates, followed by device fabrication. After the device fabrication, bmim[PF$_6$] as IL was placed on the channel. The authors observed a depletion of holes by applying a positive gate voltage (V_g) of 3 V, even though relatively thick samples (100–150 nm) were used. Almost one year later, Katase *et al* attempted to induce superconductivity in TlFe$_{1.6}$Se$_2$ in a EDLT transistor using

DEME-TFSI as an IL [191]. TlFe$_{1.6}$Se$_2$ is a Mott insulator with a Néel temperature above 450 K. Hence, one can expect a high T_c for this material if the long-range antiferromagnetic order is suppressed by carrier doping, which is a conventional concept for the cuprates. Indeed, a phase transition from insulator to metal was observed in 20 nm thick TlFe$_{1.6}$Se$_2$ films. However, superconductivity was not induced, probably due to insufficient charge carrier density. Hanzawa *et al* pointed out that the temperature dependence of the resistivity of FeSe thin films showed semiconducting behaviour, which may render this material possible for gate-tuned superconductivity. Indeed, their hypothesis has been proved experimentally. An EDLT using MBE-grown FeSe films (~10 nm) on SrTiO$_3$ was fabricated. The resultant device depicted a superconductor–insulator transition with a maximum T_c of 40 K by electrostatic gating [311]. According to He *et al*, only the electron-like Fermi surface was observed at the M point in the k-space for FeSe monolayers on SrTiO$_3$ with T_c = 65 K [95]. A similar band structure may be realized by heavy electron doping (i.e. electrostatic gating) on the assumption that a Lifshitz transition occurs in FeSe.

At the same time, Shiogai *et al* have reported on gate-enhanced T_c in FeSe thin films on both SrTiO$_3$ and MgO substrates [312]. They fabricated EDLT structures using FeSe thin films grown by PLD with thickness over 10 nm. The thickness of FeSe was controlled by electrochemical etching, which was conducted at around 250 K under a V_g of 5 V. Once the target thickness was reached, electrostatic carrier doping was carried out at T = 220 K. As a result, a T_c over 40 K was achieved for both films on MgO and SrTiO$_3$ substrates with thickness below 10 uc of FeSe with V_g = 5 V. These results suggest that the presence of the artificial interface between SrTiO$_3$ and FeSe is not a prerequisite for the exceptionally high T_c values. This hypothesis is further strengthened by the following report of Lei *et al* [313]. They have reported on a high T_c of 48 K for thin FeSe flakes (10 nm) achieved by sole electrostatic carrier injection. Later, Shiogai *et al* fabricated EDLTs with FeSe/MgO, FeSe/STO and FeSe/KTaO$_3$ (KTO), and successfully induced superconductivity for all devices [314]. In that study, the critical thickness (d_c), for which zero resistance was obtained by V_g = 5 V, was determined for all devices. The respective d_c values for FeSe/MgO, FeSe/STO and FeSe/KTO were 4.5 nm, 12 nm and 26 nm. Additionally, another critical thickness (d_H), for which a negative Hall coefficient was observed, was determined as 2.6 nm, 7 nm, and 16 nm for FeSe/MgO, FeSe/STO and FeSe/KTO, respectively. The difference in the length scale for each substrate is due to a different amount of charge transfer from the substrates. Noteworthy, no charge transfer occurs for FeSe/MgO. Another distinct feature is that T_c for all devices was scaling with the Hall coefficients at 50 K, see figure 7. Very recently, the same group reported exceptionally high thermoelectric power coefficients $\alpha^2/\rho > 10.000$ μW cm^{-1} K^{-2} (α Seebeck coefficient, ρ resistivity) on samples prepared by the method of [312] for lowest film thicknesses and temperatures [315]. This is very promising for possible energy harvesting applications.
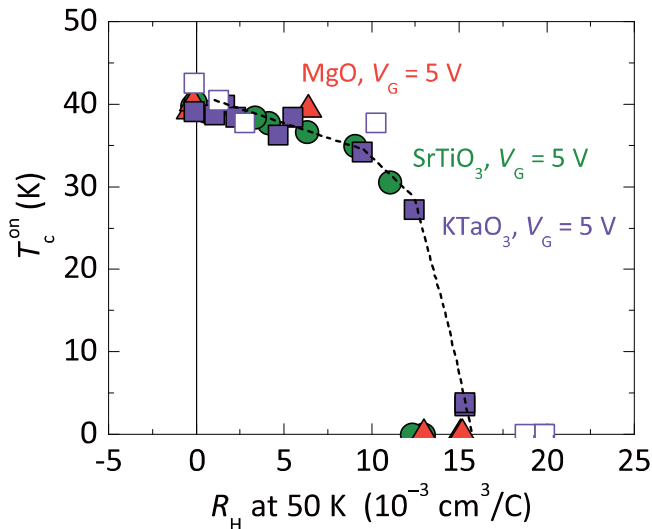
Figure 7. T_c^{on} as function of R_H at 50 K for FeSe deposited on various substrates. Reprinted (figure 7) with permission from [314], Copyright (2017) by the American Physical Society.

Kouno *et al* have fabricated EDLTs with superconducting $FeSe_{0.8}Te_{0.2}$ films on STO, LAO and CaF_2 to strengthen the superconductivity by electrostatic gating [316]. A maximum T_c of 38 K was obtained by $V_g = 5$ V irrespective of the substrate material and hence the initial value of T_c. However, the critical thickness for which the onset T_c enhancement was observed depends on the substrates. Here, the respective critical thickness for $FeSe_{0.8}Te_{0.2}$/STO and $FeSe_{0.8}Te_{0.2}$/LAO were 12 and 30 nm. For some of the $FeSe_{0.8}Te_{0.2}$/STO and $FeSe_{0.8}Te_{0.2}$/CaF_2 samples, the d_c values were below 10 nm. The authors argued that the film homogeneity caused such differences.

Although the interface between STO and FeSe seems not to be necessary for T_c values above 40 K [312], there is a gap in T_c between ~40 K for FeSe-based EDLTs and 65 K for FeSe monolayers on STO (determined by ARPES) [317]. To further increase T_c for FeSe EDLTs, multivalent ILs have been employed instead of conventional monovalent ones [318]. As a result, T_c was enhanced to 50 K, which is about 7 K higher than for the conventional FeSe EDLTs with monovalent ILs.

Electrostatic gating has been implemented not only for tuning T_c but also J_c. Harada *et al* reported on the enhancement of J_c for ion-gated FeSe films [319]. The self-field J_c reached 10 MA cm^{-2} at 2 K, which is almost three orders of magnitude higher than for bulk FeSe. The reason for such high J_c is the suppression of superconducting fluctuations by the increase of the superfluid density with gating. Additionally, the BKT transition temperature T_{BKT} was increased in the same manner as T_c.

The gate-tuned superconductor–insulator transition was also observed in thin flakes of (Li,Fe)OHFeSe [320]. However, the gate-controlling effect was attributed to Li ion doping rather than electrostatic charge carrier accumulation. To further confirm the effect of Li ions on T_c, a Li solid ion conductor (SIC) has been implemented as gate dielectric for

fabricating FeSe [321] and $FeSe_{0.5}Te_{0.5}$ [322] SIC field effect transistors. For FeSe, Li ions were intercalated by gating, resulting in $Li_yFe_2Se_2$, which has $ThCr_2Si_2$ structure. The maximum T_c was around 47 K. For $FeSe_{0.5}Te_{0.5}$ on the other hand, Li ions were accumulated at the interface between $FeSe_{0.5}Te_{0.5}$ and the gate dielectric resulted in electrostatic doping. Hence, T_c was decreased in $FeSe_{0.5}Te_{0.5}$ SIC transistors and finally dropped to zero with applied gate voltage.

Quite recently, Piatti *et al* reported on the modulation of the normal state resistance of a 10 nm thick $BaFe_2(As_{0.8}P_{0.2})_2$ film by field-effect doping [323]. Additionally, the authors observed a broadening of the transition by both electron and hole doping, indicating that the film was near optimally doping.

4. Tuning critical current density

The critical current density, J_c, of FBS films significantly improved over time for different reasons. First of all, the optimization of the growth conditions improved the homogeneity and the connectivity of the superconducting layer: this in general improved the self-field J_c. Then the growth conditions have been tuned in order to improve the in-field performance. This has been done following different approaches: by introducing natural growth defects that could act as effective pinning centres maintaining the superconducting layer 'clean' (i.e. without secondary phases, not in the sense of *clean limit*), by irradiation damage or by introducing secondary phases via mixed PLD targets, modifying the deposition environment, performing annealing in controlled atmosphere or by multilayer deposition. In the following, all these aspects will be summarized. In section 4.1 the properties of clean films with and without growth defects will be discussed. Section 4.2 is dedicated to films containing secondary phases that significantly alter the in-field performance. Section 4.3 will discuss the effect of irradiation on FBS films. Since the film properties are extremely sensitive to the deposition methods (e.g. PLD and MBE) and the growth conditions (substrate or buffer layer, pressure, deposition rate, etc), every group developed its own recipe to improve J_c obtaining films with quite unique properties. These results will be summarized and the main sample properties discussed and compared.

In this section, we use T_{c0} as critical temperature parameter, since this more strongly influences the J_c properties. H_{irr} is in most cases determined from J_c measurements at 100 A cm^{-2} or by fitting the pinning force density. Most of the J_c results reported here are obtained by transport. In few cases J_c was calculated from magnetization measurements: those values are in general larger than those obtained by transport (in particular in early samples which suffer from granularity). For this reason, we will clearly identify magnetically-obtained data and they will be differently marked in the graphs.
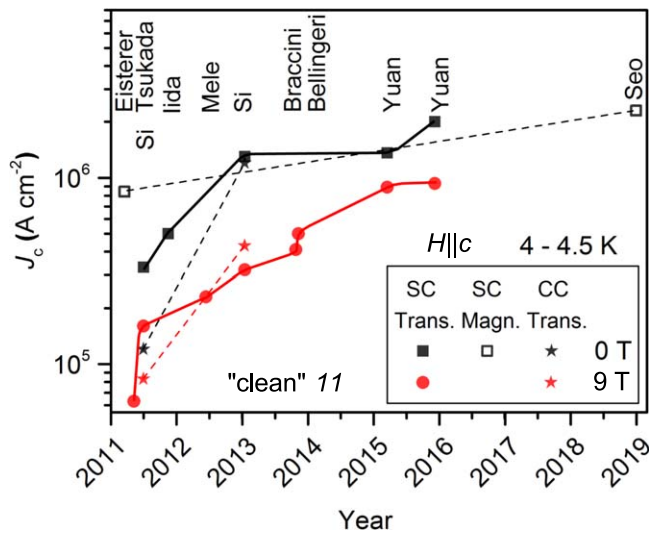
Figure 8. Development of maximum achieved J_c around 4 K for 11 films in self-field and at 9 T ($H\|c$). Data are taken from [130, 324–327, 328–332, 333]. All data are of nominal $FeSe_{0.5}Te_{0.5}$.

4.1. Microstructurally clean films and growth defects

4.1.1. 11 system.
The performance of 11 films progressively improved over time. Since most of the groups characterized these samples in the 4–4.5 K range in magnetic fields up to 9 T, the J_c improvement is reported in figure 8 at 0 and 9 T for films on single crystals (SC) and for coated conductor samples (CC). Most of the J_c investigations in the 11 system have been done on PLD-grown films, only singular studies on MBE and *ex-situ* films have been reported.

4.1.1.1. FeSe, FeTe, Fe(Te,S).
The first J_c characterizations of 11 films were reported for the FeTe phase [334] and for compositions with a lower T_c ($FeTe_{0.8}S_{0.2}$) [142]. From the fundamental prospective, the demonstration that superconductivity can be induced in films by strain in the otherwise non-superconducting FeTe phase is interesting, see section 3.1.1. Han *et al* [334] performed an experiment using different substrates (MgO, STO, LSAT and LAO), varying thickness from 60 to 150 nm and changing the deposition temperature: the best results led to a T_{c0} of ~9 K in a 90 nm thick film deposited on STO and $J_c(2K, 0–7 \text{ T}) = 6.7–3 \times 10^4 \text{ A cm}^{-2}$ was obtained.

Mele *et al* [142] compared $J_c(H)$ for PLD-grown ($FeTe_{0.8}S_{0.2}$) films on two different substrates, STO and MgO with high orbital $H_{c2}(0)$ values of around 61 T and 74 T, respectively. Due to the low T_{c0} values of 5.4 K (MgO) and 3.5 K (STO), J_c did not exceed 10^4 A cm^{-2} at 2 K for MgO. J_c of the STO film is two orders of magnitude lower, due to the lower T_c value as well as enhanced granularity. Yoshimoto *et al* [257] reported shortly after on a similar film grown by *ex situ* solid-phase crystal growth process from $Fe(Te_{0.65}S_{0.16})$ precursor. They found the highest T_{c0} value of 9.0 K and $J_c(2 \text{ K}, 0 \text{ T})$ value of $1.4 \times 10^4 \text{ A cm}^{-2}$ for the sample with shortest reaction time (10 min) due to lower crystallinity and changed composition for longer reaction times.

In 2014, Zhang *et al* determined critical currents on a one-unit-cell MBE-grown FeSe layer sandwiched between FeTe on STO substrate [335]. This film with a T_{c0} of 23.5 K (basically coinciding with the BKT transition) showed $J_c(2 \text{ K}, 0 \text{ T})$ of 1.7 MA cm^{-2} and only a weak field dependence at low T ($J_c(2K, 16T) = 0.5 \text{ MA cm}^{-2}$). These values are comparable to the data obtained on $FeSe_{0.5}Te_{0.5}$ coated conductor samples [130], see below. Recently, Harada *et al* [319] measured $V(I)$ curves of FeSe films on STO with different thicknesses by EDLT and ion-liquid etching technique. For the 0.8 nm sample with T_{c0} of around 35 K, the highest $J_c(2 \text{ K}, 0 \text{ T})$ value of 15 MA cm^{-2} was found.

4.1.1.2. $FeSe_{0.5}Te_{0.5}$.
Due to the relatively high T_c and the possibly stable deposition conditions of $FeSe_{0.5}Te_{0.5}$, most of the J_c improvement studies have been performed on films with that nominal composition. In 2010–2011, it was demonstrated by Bellingeri *et al* that T_c in $FeSe_{0.5}Te_{0.5}$ films strongly depends on the thickness and that strain can enhance T_{c0} up to about 19 K (onset at 21 K) [336, 337]. In similar films with thickness $t = 150$–200 nm deposited on LAO, J_c was estimated by magnetization to $J_c(4.5 \text{ K}, 0–5 \text{ T}) \sim 8.4$–2 $\times 10^5 \text{ A cm}^{-2}$ and a relatively low ratio between $J_c^{\|ab}$ and $J_c^{\|c}$ at low field was also reported with, in one case, signs of possible c-axis correlated pinning [324].

A first example of the beneficial effects of growth on CaF_2 substrate was reported by Tsukada *et al* in 2011 [325]. Although not yet optimized, the films revealed a rather weak field dependence of J_c, reaching 5.9–4.2 $\times 10^4 \text{ A cm}^{-2}$ at 10–14 T and 4.5 K ($T_{c0} \sim 15$ K, $t = 36$ nm). The weak field dependence of 11 films was soon confirmed by Si *et al* who performed high-field characterization of a film on LAO ($T_{c0} \sim 15$ K) [326]. With a $J_c(4.2 \text{ K}, 0 \text{ T}) \sim 3.3 \times 10^5 \text{ A cm}^{-2}$ they demonstrated that J_c can exceed $\sim 10^5 \text{ A cm}^{-2}$ in fields up to ~ 20 T and 10^4 A cm^{-2} up to ~ 35 T. Later in 2013, the same group reported even better high-field performance using a CeO_2 buffer layer on yttria-stabilized zirconia (YSZ) leading to a better film quality with T_{c0} exceeding 18 K, $J_c(4.2 \text{ K}, 0 \text{ T})$ larger than 1 MA cm^{-2} and J_c remaining at $\sim 5 \times 10^4$–1.4 $\times 10^5 \text{ A cm}^{-2}$ at 31 T [130].

A different approach was taken by Iida *et al* in 2011 to improve the crystalline quality of 11 films [327]. They introduced an Fe buffer layer that facilitates the growth of clean 11 films on MgO and prevents the diffusion of oxygen into the film ($T_{c0} \sim 16.9$ K, thickness $t = 95$ nm). This produced a clean and well-connected film with a self-field J_c at 4.2 K increasing with respect to previous films up to 0.5 MA cm^{-2} and with a strong field dependence for $H\|c$ ($J_c(9 \text{ T}, 4.2 \text{ K}) = 3 \times 10^4 \text{ A cm}^{-2}$) because of the absence of effective pinning centres. On the other hand, it was suggested that the weak field dependence of $J_c(H\|ab)$ might be related to intrinsic pinning. A later paper in 2013 on a similar, 75 nm thick film investigated pinning properties in details ($J_c(0 \text{ T}, 4 \text{ K}) > 1 \text{ MA cm}^{-2}$) [85]. Analysing the angular dependences of J_c and n-value, where n is the exponent of $E(J) \sim J^n$ near J_c, an inverse correlation between them was found at low temperatures for fields approaching the ab-planes. This was a clear evidence for intrinsic pinning due to the 11 layered structure and, hence, to a modulation of the order

parameter along the c-axis. Such inversion occurs when the vortex core becomes smaller than the interlayer distance ($2\xi_c < d$). Since even small particles could produce buckling of the layered structure able to wash out this feature, the signature of intrinsic pinning evidences the clean microstructure of those films. From a more fundamental point of view, the appearing of intrinsic pinning at low temperatures implies that the orbital anisotropy (determined by the band structure) is much larger than the J_c anisotropy, γ_{Jc}, which was estimated by Blatter's J_c rescaling approach to range between 2 and 3.5 with γ_{Jc} decreasing approaching T_c. This temperature dependence and magnitude of γ_{Jc} are similar to the penetration depth anisotropy γ_λ. This seems to be another evidence of the structural cleanness with weak pinning, where J_c is mainly determined by vortex-vortex interaction and so following the penetration depth anisotropy. Because of their clean microstructure, the films on Fe/MgO are of course not the best-performing at high fields.

Very different properties and peculiar microstructure were instead found for films deposited on STO substrate by Bellingeri *et al* ($t = 100$ nm) in 2012 [338]. Despite a lower self-field J_c (3×10^5 A cm^{-2} at 4 K) with respect to previous results by other groups, a strong c-axis correlated pinning was found enhancing $J_c(H||c)$ above $J_c(H||ab)$ in the whole measured field range (J_c(9 T, 4 K)$\sim$70–110 kA cm^{-2}). The origin of such increase was found in a high density of threading dislocations formed during the film growth with an effective diameter comparable to ξ_{ab} and a matching field close to 20 T. Those defects appeared to be uniquely obtained in films deposited on STO substrate by PLD with a KrF excimer laser ($\lambda = 248$ nm).

Further improvements were shortly after obtained in films on CaF$_2$. In 2012, Mele *et al* performed an optimization experiment on different substrates and, varying the deposition conditions, obtained for films on CaF$_2$ a J_c(4.2K) ranging from 0.41 to 0.23 MA cm^{-2} at 0 and 9 T ($T_{c0} \sim 16.2$ K, $t = 189$ nm) [339]. Also in this case a c-axis-correlated peak was clearly detected but the microstructural origin was not identified. No c-axis peak was instead detected in films on CaF$_2$ deposited by Braccini *et al* ($T_{c0} = 19$ K, $t = 180$ nm) [328], however the in-field J_c was improved up to J_c(4 K, 9 T) $\sim 5 \times 10^5$ A cm^{-2} [329]. Those films present lattice disorder on the scale of 5–20 nm that appears to be responsible for isotropic pinning. Similar lattice disturbance was found in films on CaF$_2$ investigated by Yuan *et al* in a comparative investigation of properties for clean samples grown on different substrates (CaF$_2$, LAO, and MgO; $t \sim 140$–250 nm) [330]. They also identified several defect structures: in the film on LAO islands that disperse and modulate the structure, and in films on bare MgO defects parallel to the c-axis with crystal distortion or rotation. As a consequence, LAO and CaF$_2$ did not generate c-axis-correlated pinning, whereas bare MgO did. Interestingly, γ_{Jc} values found for films on LAO and CaF$_2$ were still between 2 and 3 but with the opposite temperature dependence with respect to the cleaner film on Fe/MgO described previously in [85]. This suggests that, with sensitively stronger pinning centres, γ_{Jc} follows the H_{c2} and ξ anisotropy trends because the vortices interact with the defects via ξ. Because of the increased disorder induced by

the defects, the stronger pinning effectiveness and the larger ξ_c, these films showed no sign of intrinsic pinning, differently from samples on Fe/MgO. More recent results by Yuan *et al* using again CaF$_2$ substrate reached a J_c(s.f., 4.2 K) = 1.36 MA cm^{-2} and J_c(9 T, 4.2 K) = 0.89–0.97 MA cm^{-2} with a pinning force density F_p of $\sim$80–87 GN m^{-3} at 4.2 K and 9 T ($T_{c0} = 19$ K, $t = 200$ nm) [331]. Later, a similar film reached a J_c(4.2 K, 0–9 T) of the order of $\sim$2–0.9 MA cm^{-2} with a rather low anisotropy (1.28 at 15 K as estimated by Blatter's rescaling) [332]. The prevalent pinning mechanism was identified to be by point defects, and also in this case no c-axis peak was observed. Also with regard to possible high-field applications, Grimaldi *et al* [340] recently investigated the temperature, field and angular dependences of the vortex instability, i.e. the onset of flux flow, in Fe(Se,Te) films. Defining the (I^*, V^*) point in the I–V characteristic as the transition between the flux flow and the normal state, these films show an instability current I^*, which is insensitive to the underlying pinning mechanism (in contrast to I_c) and much more robust and smooth than for cuprate HTS such as Bi$_2$Sr$_2$Ca$_{n-1}$Cu$_n$O$_{2n+4+\delta}$.

More recently, Seo *et al* [333] obtained in a 11 film a slightly larger self-field J_c at 4.2 K of about 2.3 MA cm^{-2} (by magnetization): the sample was however very clean as demonstrated by a stronger field dependence.

From a prospective of possible applications, 11 film deposition on technical substrates was also performed and the samples characterized in high fields. A 11 film deposited by Si *et al* on an IBAD-MgO template in 2011 showed inferior J_c performance with respect to a comparable sample on LAO single crystal, however J_c(0 T) was still $\sim 1.2 \times 10^5$ A cm^{-2} and J_c(25 T) $\sim 10^4$ A cm^{-2} at 4.2 K [326]. More successful was the result obtained in 2013 with the deposition on Ni-W RABiTS substrate with CeO$_2$ buffer layer ($T_{c0} > 18$ K) [130]. The self-field J_c at 4.2 K exceeded 1 MA cm^{-2} and remained close to $\sim 9 \times 10^4$–2×10^5 A cm^{-2} at 31 T. In this case, the film performed better than the reference sample on CeO$_2$/YSZ despite the 6° in-plane misorientation for the RABiTS sample. This unexpected result has likely the same origin as lately identified in BaFe$_2$(As$_{1-x}$P$_x$)$_2$ films by Sato *et al*, namely being due to pinning effects at GBs [161], see below.

4.1.2. 122 system

4.1.2.1. Ba(Fe,Co)$_2$As$_2$, Sr(Fe,Co)$_2$As$_2$.
Because of the larger critical temperature of the 122 phase with respect to 11, several groups reported on the performance of 122 films in wider temperature and field ranges. For this reason, the J_c improvement of Ba(Fe$_{1-x}$Co$_x$)$_2$As$_2$ films are reported in figure 9 in two temperature ranges, 3.5–5 K and 10–12 K, and in the field range from 0 to 9 T for films on single crystal substrates (SC) and for CC. The first reports on Co-doped 122 films were on the Sr122 compound with still quite a low transport J_c: 16 kA cm^{-2} at 5 K in Sr(Fe$_{1-x}$Co$_x$)$_2$As$_2$ on LAO with $T_{c0} = 16.4$ K, $t = 700$–800 nm, with sign of c-axis pinning [165], and J_c(0 T, 4.2 K) = 13 kA cm^{-2} in Sr(Fe$_{1-x}$Co$_x$)$_2$As$_2$ film on LSAT with $T_{c0} <$ 16.2 K, $t = 450$ nm [184]. However, higher J_c values measured
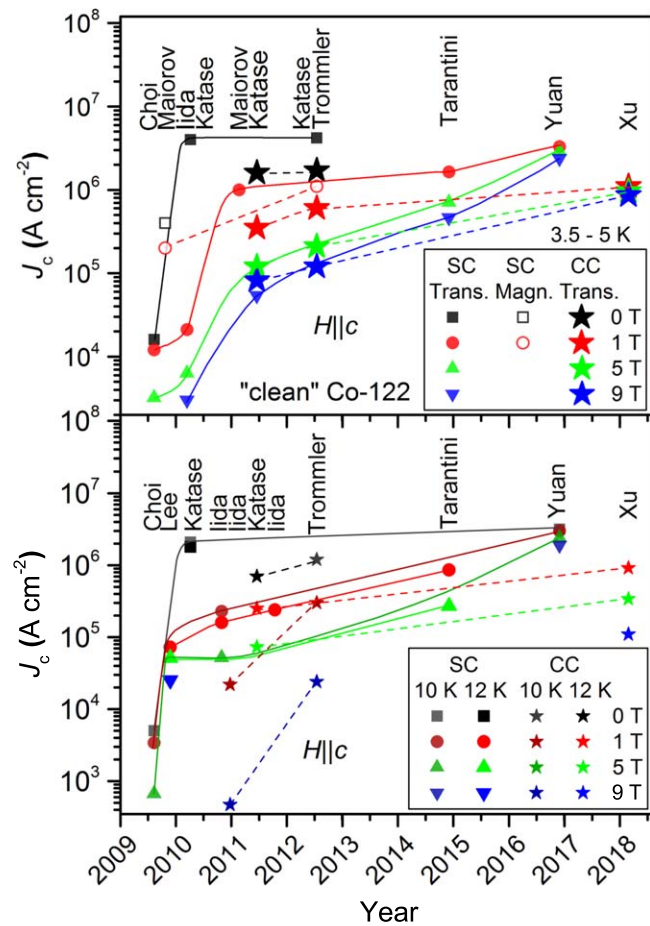
Figure 9. Development of maximum achieved J_c around 4 K (above) as well as 10 and 12 K (below) for Ba(Fe$_{1-x}$Co$_x$)$_2$As$_2$ films in self-field, 1 T, 5 T, and at 9 T ($H||c$), SC single crystal substrates, CC coated conductor templates. Data are taken from [89, 98, 165, 168, 177, 181, 182, 184, 281, 341–344].

by magnetization of J_c(4.5 K, 0 T) = 0.4 MA cm^{-2} suggested a higher potential, and the authors concluded that both the difference between magnetization and transport and the strong field dependence of J_c were likely determined by either granularity/weak link issues or pinning from soft magnetic inclusions. A c-axis peak was also found at low field ($B \leqslant 1$ T) and ascribed to possible grain boundaries due to the columnar growth, as well as to linear/planar defects along the c-axis. Significantly larger J_c values were soon realized by Lee *et al* in Ba(Fe$_{1-x}$Co$_x$)$_2$As$_2$ films on STO with $T_{c0} \sim 19.7$ K and $t = 350$ nm in the first bicrystal study on FBS [89]. The intragrain self-field transport J_c at 12 K was between ~ 60 and ~ 100 kA cm^{-2} with an irreversibility field exceeding 16 T for $H||c$.

The structural and transport properties of Ba(Fe$_{1-x}$Co$_x$)$_2$As$_2$ films appear to be strongly affected by the deposition technique. In fact, already in an early research stage Katase *et al* [168] were able to achieve a large self-field J_c of 2 and 4 MA cm^{-2} at 11 and 4 K, respectively, in thick films (250–1000 nm) on bare substrates using a Nd:YAG laser. Iida *et al*, using a KrF laser, obtained clean microstructures in thin films (<100 nm) deposited on LSAT [98] and later on Fe-buffered MgO [341].

Lee, Tarantini *et al*, using a KrF laser on STO and on STO- and BTO-templated LSAT substrates, were able to obtain thick films (350–500 nm) affected in general by secondary phases (discussed in a following section) but also studied clean thick films with self-field J_c of 3.3 MA cm^{-2} at 4.2 K with weak field dependence on CaF$_2$ [177]. Even better performance was then obtained with similar deposition technique by Yuan *et al* with J_c above 1 MA cm^{-2} at 9 T [344]. In the following we will first describe the properties of the thin films and then of thicker films. Finally, we will summarize the results obtained for CC samples.

In 2010 Iida *et al* carefully analysed the anisotropic properties of clean Ba(Fe$_{1-x}$Co$_x$)$_2$As$_2$ on LSAT using Blatter's J_c rescaling ($t = 30$ nm, J_c(1–9 T)$\sim$20–3 kA cm^{-2} at 4.2 K) and finding that γ_{Jc} increases with increasing temperature from ~ 1.55 at 4.2 K to ~ 2 at 17.5 K [98]. This trend appeared consistent with the Ginzburg–Landau value found at 21.5 K for the $H_{c2}(\theta)$ analysis. Random defects appeared to affect most of the $J_c(\theta)$ curves with only some *ab*-correlated pinning and no *c*-axis peak. The formation of a biaxially oriented Fe interlayer was observed by TEM [113], and this gave the authors the idea to deposit an Fe buffer layer on MgO substrate [341]. They found a significant performance improvement with a 15 nm thick Fe layer thanks to an ameliorated crystalline microstructure (T_{co} up to ~ 21 K, $t = 100$ nm), and interestingly J_c(0 T,12 K) increased by a factor of 40 to 0.45 MA cm^{-2} with respect to films on LSAT. Because of the clean microstructure, $J_c(H||c)$ is always smaller than $J_c(H||ab)$ and the angular dependence can be rescaled with γ_{Jc} similar to the ones for the LSAT films (~ 1.4–2.1 at 6–16 K). In 2011, a clear dependence between the film thickness and both T_c and J_c was found in films on Fe/MgO [281]. Very thin films ($t = 30$ nm) suffered from poor connectivity with J_c one order of magnitude smaller than for thicker films ($t \geqslant 70$ nm). These latter showed a systematic increase of T_{c0} with film thickness due to stress relief and a change in the J_c angular dependence due to emerging *c*-axis pinning by increased amount of *c*-axis correlated defects. Up to 90 nm, a progressive increase of both $J_c(H||ab)$ and $J_c(H||c)$ was observed, whereas at 150–225 nm, despite a more evident *c*-axis peak that maintained $J_c(H||c)$ at the same level of the 90 nm film, $J_c(H||ab)$ started to be slightly suppressed but still larger than $J_c(H||c)$. The *c*-axis peak was ascribed to GB pinning and to the emerging of the 110 orientation in thicker films. Despite a small amount of these defects positively decreases the ratio between $J_c(H||ab)$ and $J_c(H||c)$, a threshold is reached between 90 and 150 nm and the presence of these defects started to be slightly detrimental. A similar *c*-axis peak was observed in Ba(Fe$_{1-x}$Co$_x$)$_2$As$_2$ thin films on LSAT(001) deposited at a relatively low temperature of 675 °C in UHV condition [345]. These films contained round and *c*-axis elongated Fe precipitates near or within 45° [001] tilt grain boundaries. These Fe particles, together with the threading dislocations in the GBs contributed to *c*-axis enhanced pinning.

In 2013, Kurth *et al* demonstrated the effect of the substrate on the superconducting properties of Ba(Fe$_{1-x}$Co$_x$)$_2$As$_2$ comparing fluoride substrates (CaF$_2$, SrF$_2$, BaF$_2$) to LSAT, LAO and STO [101]. They found a correlation between T_c and the c/a

ratio and an enhanced T_c for films on CaF_2. For a 85 nm thick film with T_{c0} of about 25 K, they obtained a self-filed J_c at 10 K over 1 MA cm^{-2}. In 2015 the field and angular dependence of a $Ba(Fe_{1-x}Co_x)_2As_2$ film on Fe/MgO was investigated in high fields ($T_{c0} \sim 23.1$ K, $t = 170$ nm) [346]. This film had a complicated microstructure due to the presence of a high density of stacking faults (effective along the ab-planes) and small angle grain boundaries (acting as c-axis pinning centres). The c-axis peak was however evident only at low fields and disappeared at fields larger than 0.2 $H_{irr}^{||c}$. It was also shown that J_c was differently affected depending on the field range. In fact, at low fields the standard Blatter rescaling was able to explain most of the angular dependence, whereas at high fields an empirical rescaling related to $H_{c2}(\theta)$ has to be used. This empirical scaling has recently been generalized by Talantsev and Mataira [347].

As mentioned above, the use of a Nd:YAG laser allowed Katase *et al* to grow $Ba(Fe_{1-x}Co_x)_2As_2$ films with good connectivity on bare LSAT already in 2010 [342]. Studying a Josephson junction, they reported an intragrain self-field J_c of 2 MA cm^{-2} at 11 K and about 4 MA cm^{-2} at 4 K ($T_{c0} \sim 20.5$ K, $t = 250$ nm). In 2011, an in-field investigation revealed a c-axis peak due to correlated defects with $J_c(H||c)$ exceeding $J_c(H||ab)$ up to 12 T at 4 K ($T_{c0} \sim 19$ K, $t = 200$ nm, $J_c(1$ T, 4 K$) \sim 1$ MA cm^{-2}, $J_c(1$ T, 4 K$) \sim 230$ kA cm^{-2}) [343]. No microstructural origin of the correlated pinning was found and F_p maximum at 4 K was estimated to 30 GN m^{-3} at 12 T. After a detailed investigation of the growth conditions on LSAT, Katase *et al* found that the deposition temperature strongly influences the crystalline quality and, as a consequence, J_c [168]. The optimal temperature range with ameliorated microstructure and maximum $J_c(4$ K$) > 1$ MA cm^{-2} is between 800 °C and 850 °C. Within this range, they also investigated the thickness dependence finding that up to 480 nm $J_c(4$ K$)$ is about 2 MA cm^{-2} or higher, whereas at larger thickness (up to 1080 nm) J_c drops to ~ 1 MA cm^{-2}.

In 2014, the enhanced high-field properties of a thick $Ba(Fe_{1-x}Co_x)_2As_2$ film deposited on CaF_2 were also reported by Tarantini *et al* [177]. A clean single layer film ($T_{c0} = 25.4$ K, $t = 330$ nm), whose only defects were dislocations with a corresponding matching field of $B_\phi = 3$ T and a large splay angle (up to 45°), was characterized up to 35.1 T. At 16 K, the self-field J_c exceeded 1 MA cm^{-2} (more than twice as high as for films on STO/LSAT), and $H_{irr}||c$ increased up to 15.5 T. Despite the low density of dislocations, this sample presented an evident c-axis peak at 4.2 K exceeding the ab direction up to 10 T and still reducing the effective anisotropy at larger field. $J_c(4.2$ K, 35.1 T$)$ still exceeded 0.1 MA cm^{-2} for $H||ab$ and was about 20 kA cm^{-2} for $H||c$. Moreover, a J_c of the order of 0.17–0.25 MA cm^{-2} at 20 T was found in every field orientation (F_p peaks at 12.5 and 20 T for $H||c$ and $H||ab$, respectively). Since the performance improvement of this film on CaF_2 was beyond expected simply from T_{c0} enhancement, the authors suggested the presence of a significant pinning contribution by point defects becoming particularly effective at low temperatures.

The properties of $Ba(Fe_{1-x}Co_x)_2As_2$ films on CaF_2 were further improved in 2017 by Yuan *et al* ($T_{c0} = 24.2$ K,

$t = 150$ nm) [344]. They were able to achieve J_c values at 4.2 K of 3.5 MA cm^{-2} in self-field and 2.37–2.65 MA cm^{-2} at 9 T. The sample had a large density of stacking faults and a low density of vertical defects. Despite this, they observed a c-axis peak with $J_c(H||c)$ larger than for $H||ab$ up to 2 T and reduced effective anisotropy at larger fields.

From the point of view of possible applications, in 2011, considering the positive effect of the Fe layer, Iida *et al* used the same approach to grow $Ba(Fe_{1-x}Co_x)_2As_2$ on IBAD-MgO-covered metal substrate ($t = 50$ nm) [180]. T_{c0} was suppressed and J_c lower than for the similarly deposited films on single crystal MgO substrates. However, $J_c(0$ T, 8 K$)$ already exceeded 10^5 A cm^{-2} and maintained a similar field dependence ($J_c(9$ T, 8 K$) \sim 30$ kA cm^{-2}). A similar approach was employed by Katase *et al* who deposited directly on the IBAD-MgO template [179]. In this case, T_{c0} was enhanced in comparison to similarly deposited films on MgO single crystal. The self-field J_c at 2 K of films on IBAD ranged from 1.2 to 3.6 MA cm^{-2} depending on the in-plane misorientation of the MgO ($\Delta\phi_{MgO}$) with the best results obtained with the largest $\Delta\phi_{MgO}$ (in spite of the similar $\Delta\phi_{Ba122}$). The higher-temperature characterization revealed that films on IBAD have better in-field performance than on MgO substrate, where it should be noted that films on MgO single crystals were also inferior to the one on LSAT possibly due to the absence of c-axis pinning. Moreover, $J_c(H||c) > J_c(H||ab)$ was found at high temperature and low field suggesting that films on IBAD do have effective c-axis pinning centres related to their microstructures. J_c at 4K, 9 T was $\sim 8 \times 10^4$ A cm^{-2} for $H||c$ and $\sim 1.6 \times 10^5$ A cm^{-2} $H||ab$. In 2012, the performance of $Ba(Fe_{1-x}Co_x)_2As_2$ on Fe/IBAD-MgO was improved by Trommler *et al* ($T_{c0} \sim 19.3$ K, $t = 70$ nm) reaching a J_c above 2 MA cm^{-2} in self-field at 4 K and remaining at about 0.1–0.2 MA cm^{-2} at 9 T [181]. For $H||c$, the F_p maximum was about 11 GN m^{-3} and the estimated H_{irr} above 35 T at 4 K. In this case, c-axis correlated pinning was detected at low fields: wide-spread defects of low density originating from defects and grain boundaries in the MgO template were observed and might be the origin of the correlated pinning. The most recent result was reported in 2018 by Xu *et al* for $Ba(Fe_{1-x}Co_x)_2As_2$ films grown on IBAD-MgO templates with $LaMnO_3$ epilayer and additional STO buffer layer ($T_{c0} \sim 19$ K, $t = 110$ nm) [182]. J_c at 4.2 K reached 1.14 MA cm^{-2} in self-field and remained at 0.86–0.98 MA cm^{-2} at 9 T. A variation of pinning mechanism was found by changing temperature: at low T an additional ab-correlated pinning was identified, whereas at higher temperature also a weak c-axis contribution slightly affected the angular dependence.

4.1.2.2. BaFe$_2$(As,P)$_2$. Thanks to the previous growth experience on the $Ba(Fe_{1-x}Co_x)_2As_2$ compound and the higher T_c with similar anisotropy, $BaFe_2(As_{1-x}P_x)_2$ films showed soon very good J_c performance (figure 10). Since two different techniques, PLD (Nd:YAG) and MBE, were mainly employed for the realization of $BaFe_2(As_{1-x}P_x)_2$ films, in the
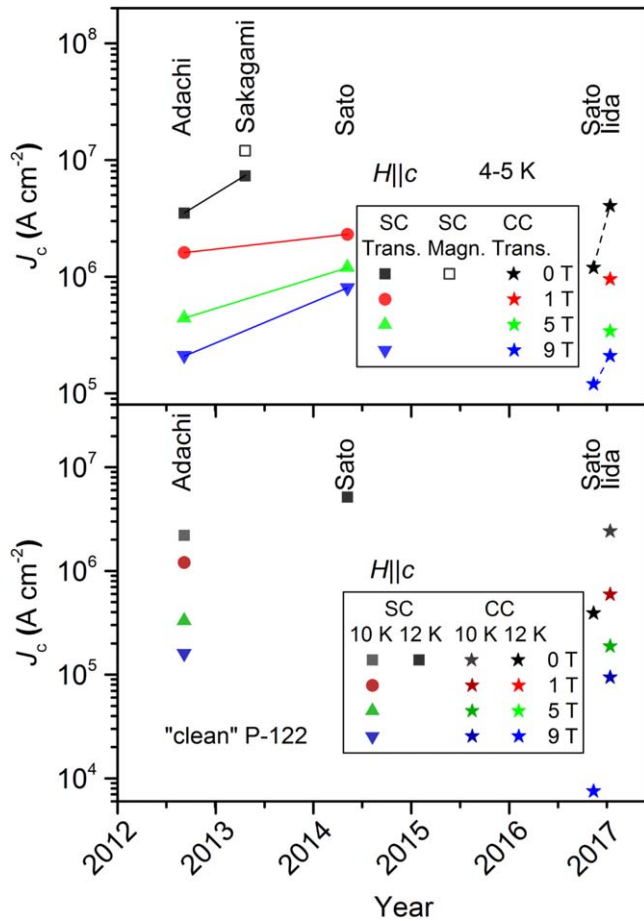
Figure 10. Development of maximum achieved J_c around 4 K (above) as well as 10 and 12 K (below) for $BaFe_2(As_{1-x}P_x)_2$ films in self-field, 1 T, 5 T, and at 9 T ($H\|c$), SC single crystal substrates, CC coated conductor templates. Data are taken from [156, 160–162, 214].

following we will describe the achieved properties accordingly.

In 2012, $BaFe_2(As_{1-x}P_x)_2$ films with nominal $x = 0.4$ were grown by PLD using a Nd:YAG laser on MgO substrate by Adachi *et al* ($T_{c0} = 24$ K, $t = 90$ nm) obtaining a self-field J_c at 4.2 K of 3.5 MA cm^{-2} [156]. The in-field properties for $H\|c$ at 4.2 K ($J_c(9$ T$) \sim 0.3$ MA cm^{-2}) were comparable to the ones reported for the best $Ba(Fe_{1-x}Co_x)_2As_2$ films at that time, but because of the larger T_c the advantage of $BaFe_2(As_{1-x}P_x)_2$ was more obvious at higher temperature with $J_c(10$ K, 0–9 T$) \sim 2.0$–0.16 MA cm^{-2}. Investigating the effect of P-doping (nominal $x = 0.25$–0.5, effective film composition $x = 0.19$–0.45), Miura *et al* found an optimal film composition x of 0.28 (nominal $x = 0.33$) with $T_{c0} = 26.5$ K, $J_c(5$ K, 0 T$) = 3.05$ MA cm^{-2} and $J_c(5$ K, 7 T$) \sim 0.3$ MA cm^{-2} ($t \sim 80$ nm) [158]. The growth on LSAT substrate from a target with similar nominal $x = 0.33$ instead produced inferior properties probably because of a lower doping level in the film ($x = 0.144$) [97]. In 2014, the effect of growth conditions by PLD (Nd:YAG) were investigated by Sato *et al* [160]. They prepared 150–200 nm films on MgO varying the growth rate from 2.2 to 3.9 Å s^{-1}. They found that by decreasing the rate the self-field $J_c(12$ K$)$ increased from

2.7 to 5.15 MA cm^{-2}, and correlated pinning generated a c-axis peak that exceeded the ab-peak at 3 T. At 4 K, J_c reached 7 MA cm^{-2} in self-field and varied from 1.1 to 0.8 MA cm^{-2} at 9 T. The fact that $J_c(H\|c)$ becomes larger than $J_c(H\|ab)$ around 1 T suggests a change of pinning effectiveness with temperature in this sample. Despite the defect density appeared similar for varying growth rate, their microstructure was different: the most effective defects in the 2.2 Å s^{-1} films were more vertical and ascribed to dislocations, whereas the other defects formed larger angles with regard to film normal and were identified as domain boundaries.

In 2016, Sato *et al* investigated the effect of the IBAD-MgO quality on the performance of PLD-grown $BaFe_2(As_{1-x}P_x)_2$ films (Nd:YAG; $t = 150$–200 nm) [161]. They used two substrates with different in-plane crystallographic alignments: an MgO top layer with $\Delta\phi_{MgO} = 4.0°$ (well-aligned) generated a $\Delta\phi_{P:Ba122} = 2.7°$ whereas $\Delta\phi_{MgO} = 8°$ (poorly-aligned) resulted in $\Delta\phi_{P:Ba122} = 8.0°$. Despite the poorly aligned substrate induced a T_c suppression ($T_{c0} = 19$ K versus 23 K), self-field J_c values of both samples were almost identical at both 12 K (~ 0.4 MA cm^{-2}) and 4 K (~ 1 MA cm^{-2}). Moreover, at least at 4 K the in-field performance of the poorly-aligned sample was significantly better than for the well-aligned one with a marked c-axis peak effective also at 9 T [$J_c(4$ K, 9 T$) \sim 0.12$ and 0.16 MA cm^{-2} for $H\|c$ and $H\|ab$, respectively, for $\Delta\phi_{MgO} = 8°$]. The origin of this J_c enhancement in the poorly aligned sample was identified in a larger density of dislocation arrays forming the low-angle grain boundaries. Having a misorientation angle smaller than the critical angle $\theta_c \sim 9°$, those grain boundaries mainly act as effective pinning centres along the c-axis. A similar sample on IBAD-MgO ($t = 185$ nm, $T_{c0} \sim 25.5$) was also characterized in high-field [162]. The $V(I)$ characteristics revealed a non-Ohmic linear differential (NOLD) behaviour in the low-field regime up to 10 T at 4.2 K indicating that J_c was limited by GB weak-links. At higher fields, a typical power-law regime was found suggesting that intragrain pinning is the dominant mechanism. $J_c(4.2$ K$)$ was 4 MA cm^{-2} in self-field and still exceeded 50 kA cm^{-2} at 20 T. The shape of $F_p(H)$ confirmed the pinning-effective nature of the dislocation arrays for $H\|c$, which also generated a strong c-axis peak effective up to H_{irr}, whereas for $H\|ab$ the pinning mechanism seemed to change with temperature becoming more dominated by point defects at low T.

In 2013, $BaFe_2(As_{1-x}P_x)_2$ films were also realized by MBE on MgO substrate by Sakagami *et al* ($t \sim 100$ nm), finding that J_c was significantly affected by the film composition with the best performance obtained in an Fe-rich film (2.42 instead of 2) with $x = 0.32$ [214]. The maximum self-field J_c at 4.2 K was estimated to 12 MA cm^{-2} by magnetization, and the corresponding (extrapolated) transport J_c value of that sample was 7.3 MA cm^{-2}. The authors suggested that this behaviour might be due to Fe nanoparticles acting as pinning centres. A similar $BaFe_2(As_{1-x}P_x)_2$ film grown by MBE was also investigated in high field by Kurth *et al* ($t = 107$ nm, $T_{c0} \sim 28.5$ K) [145]. Transport $J_c(4.2$ K, 0 T$)$ reached a similar level of 6.3 MA cm^{-2}, and the F_p maxima were 77 GN m^{-3} at 15 T and 35 GN m^{-3} at 10 T for $H\|ab$ and $H\|c$, respectively.

Table 11. Selected J_c data at 4–5 K together with T_{c0} of 1111 films.

Material	Texture	T_{c0} (K)	Self-field J_c (MA cm^{-2})	$J_c(1\mathrm{T}\|c)$ (MA cm^{-2})	$J_c(H\|ab)$ (MA cm^{-2})	References
LaFeAs(O,F)	Polycrystalline	20	0.002	—	—	[348]
	Epitaxial	17	∼0.8	0.01	0.02 (9 T)	[197]
SmFeAs(O,F)	Epitaxial	51	1.25	0.95	∼0.75 (35 T)	[349]
		55.3	1.8[a]	1.5[a]	—	[229]
NdFeAs(O,F)	Epitaxial	∼40	3.1	2.9	—	[105]
		42.5	3.3	2.0	1.2 (35 T)	[350]
(Sm,La)FeAs(O,F)[b]	c-axis texture, most likely biaxially textured	25	∼0.3	0.1	0.1 (9 T)	[199]

[a] Magnetization measurements.

[b] J_c data at 2 K.

Despite a rather clean microstructure without obvious c-axis correlated or other defects, $J_c(H\|c)$ at 4.2 K still reached $\sim 10^4$ A cm^{-2} at 35 T and the presence of shoulders in the angular dependence suggested that some composition variation might actually act as strong pinning centres.

4.1.2.3. Other 122 compounds. In 2017, Ba(Fe$_{1-x}$Ni$_x$)$_2$As$_2$ films were grown by PLD on both STO/LSAT and CaF$_2$ substrates by Yoon *et al* (T_{c0} = 16.0 K and 20.5 K, respectively; t = 460 nm) [92]. Self-field J_c obtained by magnetization at 4.2 K was 2.8 MA cm^{-2}, and at 13 T J_c still exceeded 60 kA cm^{-2}. High-field properties of a PLD-grown Ba(Fe$_{1-x}$Ni$_x$)$_2$As$_2$ film on CaF$_2$ [155] were characterized by Richter *et al* (t = 100 nm) [154]. Because of the relatively low T_c of this compound, the self-field J_c determined by transport was limited to 0.57 MA cm^{-2} at 4.2 K, and H_{irr} was of the order of 21 and 33.5 T for $H\|c$ and $H\|ab$. Also in this compound a low anisotropy of 1.8 at 4.2 K was determined by Blatter's rescaling.

(Sr$_{1-x}$La$_x$)Fe$_2$As$_2$ was grown by PLD on LSAT varying the La-doping level (t = 200 nm) [166]. The best results were obtained with a La content x = 0.32 ($T_{c0} \sim$ 12.2 K) reaching a magnetic J_c of 0.2 MA cm^{-2} at 2 K. However, a significantly lower transport J_c of 5 kA cm^{-2} was found due to granularity.

An interesting experiment was performed by Engelmann *et al* on undoped Ba122 films to investigate the superconducting properties induced by strain [146]. They grew 122 films on Fe-buffered MgAl$_2$O$_4$ with superconducting layer thickness varying between 10 and 80 nm. The strongest induced superconductivity was obtained in the 10–30 nm thick films with a T_{c0} of 8–10 K. The 30 nm film has the largest self-field J_c of $\sim$12 kA cm^{-2} at 4 K with an H_{irr} of 1.5 T; whereas the 10 nm film, despite a lower J_c(0 T) $\sim$ 4 kA cm^{-2}, had a larger H_{irr} of about 6.5 T.

4.1.3. 1111 system. So far, transport J_c measurements on LnFeAs(O,F) thin films have been limited to the following compounds with Ln=La, Sm, Nd: polycrystalline LaFeAs(O,F) [348] as well as epitaxial LaFeAs(O,F) [197], SmFeAs(O,F) [105, 349] and NdFeAs(O,F) [229, 350] thin films, table 11. Unlike for 11 and 122 systems, an attempt on improving $J_c(H)$

properties for LnFeAs(O,F) thin films by APCs has not been reported. Table 11 summarizes the transport critical current properties of LnFeAs(O,F) (Ln=La, Sm, Nd). Because of the clean microstructure of those films, in-field J_c properties for $H\|c$ are inferior to the pinning enhanced 11 and 122 systems. On the other hand, J_c for $H\|ab$ shows superior behaviour over 11 and 122 due to the intrinsic pinning as discussed ahead.

4.1.3.1. LaFeAs(O,F). Films of La1111 were initially difficult to grow. In 2010 Haindl *et al* [348] reported the growth of a thick film (700 nm) deposited by PLD on LAO at room temperature and post-annealed. This resulted in polycrystalline films with limited J_c of 600 A cm^{-2} at 2 K, which had been interpreted as clear indication for GB limitation of J_c in LnFeAs(O,F) compounds. Clear improvements were obtained by the same group one year later [197] with the growth of a clean epitaxial 150 nm thick film. The sample presented only the ab-peak in the angular dependence of J_c. Deviations from Blatter's rescaling near ab indicated that here J_c is mainly determined by intrinsic pinning due to the layered structure, whereas point defects act isotropically. The scaling parameter γ_{Jc} shows a clear temperature dependence ranging from 3.2 at 2 K to 4.2 at 15 K. For this sample J_c appears to probe the H_{c2} anisotropy since the J_c anisotropy merges at intermediate temperatures with the H_{c2} anisotropy obtained close to T_c. Moreover, there was no significant change in the pinning mechanism by changing temperature, and the $F_p(B)$ curves were reasonably reproduced by the Kramer parameters.

4.1.3.2. SmFeAs(O,F). Sm1111 films (t = 100–170 nm) prepared by MBE with post-growth fluorine diffusion were reported by Ueda *et al* in 2011 [105]. Three different fluoride substrates were used with the best results on CaF$_2$ with T_{c0} up to 56.4 K. J_c, characterized by magnetization, reached 1.8 MA cm^{-2} in self-field at 5 K and revealed a weak field dependence [J_c(5 T, 5 K) $\sim$ 0.6 MA cm^{-2} for $H\|c$]. Similar films (t = 80 nm) were later characterized in transport at high field [349]. The low-field J_c values were similar to the magnetic ones but a very weak suppression at increasing field was shown with J_c(4.2 K, $H\|c$) still exceeding 0.1 MA cm^{-2}

at 45 T. Quite peculiar was the field dependence of J_c(4.2 K, $H\|ab$): after an initial gradual drop, J_c remains approximately constant at 0.75 MA cm^{-2} above 28 T. This behaviour was already observed in YBCO films and attributed to a combination of extrinsic and intrinsic pinning. The latter dominated at higher field and is due to the quasi-2D nature of the system with $2\xi_c$ being smaller than the interlayer distance of the FeAs planes below 30–40 K. The effect of the intrinsic pinning was also confirmed by the n-value analysis that, instead of a monotonic decrease with increasing field observed in 3D materials, reveals a clear increase above 28 T. More recently, a systematic study of the growth conditions of Sm1111 prepared by a single-step method were developed by using FeF$_2$ as fluorine source [228]. Although the films are more homogeneous with a more controllable stoichiometry, the F concentration is lower than for the two-step deposition, leading to films with a slightly suppressed T_{c0} (maximum 54.0 K). Although the J_c of that film at 5 K was improved in self-field with 3 MA cm^{-2}, it was more temperature and field sensitive ($\sim$ 0.13 MA cm^{-2} at 5 T).

4.1.3.3. NdFeAs(O,F).
In 2015, the one-step growth by MBE and J_c performance of NdFeAs(O,F) films on MgO were reported by Chihara *et al* ($t = 30$ nm) [229]. The microstructure showed no significant defects apart from some Nd/O-rich regions close to the film surface. The onset T_c was about 50 K and J_c measured at 4 K was ranging from 3 MA cm^{-2} in self-field to almost 1 MA cm^{-2} at 9 T ($H\|c$) indicating a weak field dependence. A similar sample ($T_{c0} \sim 42.5$ K, $t = 60$ nm) which was later investigated in high fields [350] confirmed the weak field dependence of J_c: J_c(4.2 K, 0 T) $\sim$ 3.3 MA cm^{-2}, J_c(35 T, 4.2 K) $\sim 4.8 \times 10^4$ A cm^{-2} for $H\|c$, and exceeding 1 MA cm^{-2} for $H\|ab$. Blatter's rescaling was employed to determine the temperature dependence of γ_{Jc}. In this case, γ_{Jc} decreased with increasing temperature (from $\sim$2.2 at 4.2 K to $\sim$1.4 at 35 K). This temperature dependence, similar to that of 11 films and opposite to that of La1111 ones, suggested that J_c in Nd1111 is more affected by the anisotropy of the penetration depth γ_λ.

Another interesting observation results from the investigation of J_c and the n-value on a wide range of temperature, field and orientation: in fact, it was possible to recognize the 2D nature in Nd1111 as well. Moreover two different 2D pinning regimes were clearly observed at low temperature studying $n(\theta)$ when the applied field approaches the *ab*-planes. When the transition between the 3D (high temperature) to the 2D (low temperature) behaviours occurs, the formation of the vortex staircase structure is first identified by a dip in the $n(\theta)$ curves appearing near the *ab*-planes. Then, at a closer angle with the *ab* direction, a peak emerges in the $n(\theta)$ dip corresponding to the vortices being entirely locked parallel to the *ab*-planes. The properties of Nd1111 were then further improved reaching self-field J_c(10 K) $\sim$5 MA cm^{-2} and F_p maxima at 10 K 2.3–2.8 times larger than those previously obtained [351].

4.2. Addition of secondary phases and tailoring growth defects

4.2.1. 11 system.
Oxygen annealing of FeSe$_{0.5}$Te$_{0.5}$ films has been shown to be extremely effective in increasing J_c by Zhang *et al* [352]. Keeping the sample at 90 °C for 1–2 h had doubled the self-field J_c from 1.24 to 2.54 MA cm^{-2} at 5 K and increased the in-field performance above 1.5 T by about 300%. Although less effective, also annealing in vacuum for 1–2 h improved J_c (in self-field by 38% and in-field by up to 180%). The authors hypothesized as possible reason for the J_c enhancement an oxidation of the excess Fe that changed from magnetic and pair-breaking to non-magnetic (which however does not explain the vacuum annealing effect) or a possible phase change during the annealing. No hard evidence was, however, found for any of the two explanations.

The introduction of secondary phases to increase J_c in FeSe$_{0.45}$Te$_{0.55}$ films was also achieved by multilayer deposition of the 11 phase and CeO$_2$ [333]. This approach led to an increase in J_c(4.2 K) by about 40% at self-field (from 2.3 to 3.2 MA cm^{-2} measured by magnetization) and by about 120%–90% in the 5–13.5 T range (from 0.22 to 0.43 MA cm^{-2} at 13.5 T measured by magnetization). The transport data were also measured at 6 K obtaining a self-field value of $\sim$3.6 MA cm^{-2}. Despite the multilayer deposition is clearly effective to improve J_c with respect to its own reference sample, the in-field performance are still inferior to those previously reported for a nominally clean sample in [331].

4.2.2. 122 system.
Ba(Fe,Co)$_2$As$_2$ films deposited on STO and STO (respective BTO)-templated LSAT substrates in 2010 showed quite remarkable performance: the self-field J_c (magnetization) reached up to 4.5 MA cm^{-2} at 4.2 K (on BTO/LSAT) and pinning properties of samples on STO and STO/LSAT are significantly ameliorated showing only a weak field dependence [353]. The high self-field J_c values were attributed to the excellent crystalline structure obtained with the STO (BTO) buffer layer. The enhancement in the in-field J_c was obtained thanks to the presence of vertically-aligned secondary-phase defects, which were later shown to be a Ba–Fe–O phase, namely BaFeO$_2$ [354]. This is an isostructure of the tetragonal SrFeO$_2$ ($a = 3.991$ Å and $c = 3.474$ Å) with slightly larger a-axis parameter due to the larger ionic radius of Ba compared to Sr and the coherently strained state in the Ba122 matrix, according to the authors. These strong pinning centres generate a clear c-axis peak in the angular dependence of J_c which is effective up to high magnetic field.

It was later shown in similar samples that the film quality and J_c can be tuned by modifying the STO layer thickness [355]. In the best case, the self-field J_c exceeded 0.1 MA cm^{-2} at 12 K but, more importantly, the weak field dependence of J_c($H\|c$) makes it surpass J_c($H\|ab$) up to 16 T, the maximum applied field in this study. The irreversibility fields H_{irr} of these samples were estimated to $\sim$ 20 and 24 T at 12 K for $H\|c$ as well as $H\|ab$, respectively, compared to about 9 T for $H\|c$ in clean films. With a mean separation of the nanocolumns of 16–17 nm and a corresponding matching

field of 7–8 T, a shift of the F_p maximum at 12 K to ~9.5 T (corresponding to $H/H_{irr} \sim 0.5$) was obtained. The other samples in this study, despite their inferior J_c performance in most of the field range, indicate that the columnar defect density can be tuned by changing the STO thickness, and the F_p maximum can be shifted up to 12.5 T suggesting that further improvement could be possible.

In order to tune the defect density in Ba(Fe,Co)$_2$As$_2$, in 2012 films with different oxygen content and multilayers thereof were prepared on STO/LSAT by PLD using targets with different amount of oxygen. High T_{c0} values of ~21–22.8 K were reached for film thicknesses $t \geqslant 400$ nm [174]. Since oxygen generates self-assembled Ba–Fe–O nanorods and nanoparticles 4–5 nm in diameter, low and high oxygen content targets were employed: the latter, despite causing some J_c suppression at low fields due to the reduced cross-section, generates films with strong in-field performance improvement due to $B_\phi(H||c)$ up to 13.2 T. The irreversibility field for $H||c$ at 4.2 K shifts from 34 T (low oxygen) to more than 40 T. The F_p maximum at 4.2 K for $H||c$ increases from 39 to 53 GN m^{-3} and moves up to 15 T which is close to B_ϕ. J_c at 4.2 K has a weak angular dependence thanks to the combined effects of nanorods (c-axis-aligned) and nanoparticles (ab-aligned with additional isotropic contribution) and exceeds 0.15 MA cm^{-2} at 20 T.

The second approach to improve the pinning performance when using low-oxygen targets is to artificially introduce interlayers of undoped Ba122. This results in a pinning landscape including flat ab-aligned precipitates, round nanoparticles and short c-axis nanorods. This multilayer structure shows no negative effects on the low-field behaviour due to the absence of reduced cross-sections; both single and multilayer films show J_c(12 K,0 T) > 1 MA cm^{-2}. Whereas increasing the oxygen content in single-layer films increased J_c preferentially in c-axis direction at medium and high magnetic fields, multilayering low- and high-oxygen layers uniformly increases J_c in the entire angular and field range due to the combined effects of different APCs. For the latter films, an H_{irr} of 40.5 T was measured for $H||c$, and F_p increased by ~20% in both main orientations.

The microstructure of similar films and superlattices made of Ba122 and STO layers was further investigated in detail in [114]. It was shown that the STO interlayers suppress T_c and, despite a significant pinning effect along the ab-plane, lead to inferior J_c performance with respect to films with undoped Ba122 interlayers that have both the c-axis-correlated pinning by self-assembled nanorods and the strong pinning by flat precipitates along the ab-planes.

The multilayer approach for introducing multiple APCs in Ba122 films was further investigated in 2014 on CaF$_2$ substrates for its advantageous effect on T_c (~26 K compared to ~23 K on LSAT) [177]. Ba(Fe,Co)$_2$As$_2$ layers were alternated with BaO-enhanced Ba(Fe,Co)$_2$As$_2$ layers leading to oxygen-rich short c-axis nanorods, ab-plane precipitates and round nanoparticles with a $B_\phi(H||ab)$ between 3.2 and 5.7 T. At 16 K, J_c(0 T) of such a film on CaF$_2$ exceeded 1 MA cm^{-2}, J_c($H||ab$) was more than one order of magnitude larger than for a similar film on STO/LSAT, and $H_{irr}(H||c)$

increased from 11 T to about 17.5 T. The improvement with respect to the clean single layer on CaF$_2$ was evident on the entire field range reaching 126% J_c increase at 16 T for $H||ab$, and $H_{irr}(H||c)$ was enhanced by about 2 T. At 4.2 K, self-field J_c was about 5.6 MA cm^{-2} and remained above 0.18 MA cm^{-2} and 3.3×10^4 A cm^{-2} for $H||ab$ and $H||c$, respectively. The F_p maximum increased by 62%–65% with respect to the single layer sample reaching 84 GN m^{-3} at 22.5 T for $H||ab$ and 70 GN m^{-3} at 10 T for $H||c$.

Recently, Lee et al successfully introduced BaZrO$_3$ (BZO) nanocolumns in ~460 nm thick Ba(Fe,Co)$_2$As$_2$ films on CaF$_2$ [178]. The BZO concentration was varied between 0 and 8 mol% by using mixed targets containing 0, 2, 4, and 8 mol% BZO and a KrF excimer laser for PLD operated at 40 Hz and an energy density at the target of 3 J cm^{-2}. T_c is on average suppressed by 1 K mol%$^{-1}$ and still ~22 K at 8 mol%, and the in-plane texture spread increases systematically with increasing BZO content. Magnetization J_c(4.2 K, 0 T) increased from 2.9 MA cm^{-2} for 0 mol% to 4.4 MA cm^{-2} for 2 mol% and decreased for higher concentrations. An in-field improvement is observed for both 2 and 4 mol%, reaching 14 times enhancement for 2 mol% compared to 0 mol% at 13 T (maximum applied field). The 8 mol% sample showed lower J_c values in the entire measurement range due to a more suppressed T_c value as well as disturbed phase formation as deduced from highly increased normal state resistivity. The origin of the improvement for the low concentrations was identified in the high density of short c-axis-aligned BZO nanorods with a matching field of about 20 T.

Already in 2013, Miura et al studied the effect of BZO nanoparticles in PLD-grown BaFe$_2$(As,P)$_2$ films of around 80 nm thickness on MgO by varying the concentration between 1 and 3 mol% [159]. The size of the BZO nanoparticles was about 8 nm with an average separation of 24 nm. Their presence causes minimal T_c suppression (also with an initial slope of ~1 K mol%$^{-1}$). Moreover, BZO nanoparticles increase H_{irr} near T_c in particular for $H||c$. The self-field J_c(5 K) monotonically increases from 3 to 5.2 MA cm^{-2}. The field decay is also clearly suppressed going from an intermediate-field power-law behaviour to non-power-law typical for uniformly dispersed pinning by nanoparticles [J_c(5 K, 7 T) ~ 0.7 MA cm^{-2}]. J_c increases in all field orientations. For $H||c$ F_p reaches 59 GN m^{-3} with a plateau from 3 to 9 T (maximum applied field), and the maximum increase with respect to the reference sample is at 3.5 T for 3 mol% of BZO. The authors demonstrated that the position of maximum increase in J_c is proportional to $n^{1/3}$ where n is the particle density.

4.3. Irradiation effects

4.3.1. 11 system.
11 films on LAO were subjected to neutron irradiation but no significant J_c increase was found [324].

Irradiation with 190 keV protons at fluence of 10^{15} cm^{-2}, on the other hand, shows clear improvement of the in-field J_c [86]. The pinning force density increases by 30% for $H||c$ and it doubles for $H||ab$ at 4.2 K. Such a strong increase was ascribed to cascade defects and nanoscale strain field. The
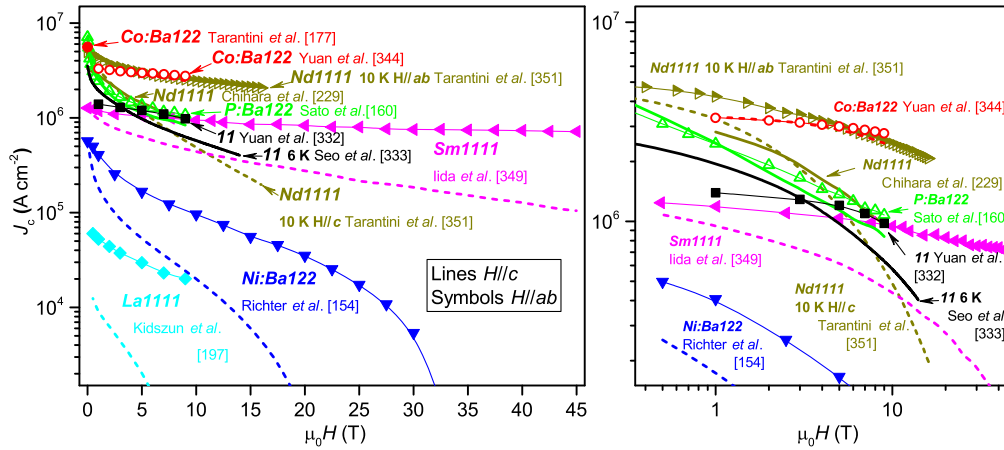
Figure 11. Field dependence of J_c for films of several FBS compounds. Multiple datasets for the same compound are shown if obvious performance differences are noted in different field ranges. Most of the data are reported at 4–4.2 K. Data at higher temperatures (6–10 K) are included only if showing better performance than the 4.2 K data in part of the field range. Right side: same data in double-log scale for better clarity at low fields. An editable graph is available at nationalmaglab.org.

effect of high energy proton irradiation (3.5 MeV) was also investigated with a fluence up to $\sim 7 \ 10^{16} \ cm^{-2}$ with and without an aluminium foil to change the implantation depth that in both cases occurs inside the substrate [356]. J_c was suppressed by using the foil (with the implantation depth being closer to the superconducting layer) whereas enhancements were found with direct irradiation. For instance, J_c(7 T) increased by 40% at 4.2 K and 50% at 12 K.

An improvement in the performance with respect to the pristine sample was found also for Au irradiation [357]. Although small changes were observed at 0 T, the increase at 9 T was of $\sim 20\%$ at 4.2 K and $\sim 70\%$ at 10 K. Moreover, irradiation shifts the F_p maximum to higher fields, from 4 to 8 T, with about 40% increase in the peak intensity. The defects are clearly different from the cascade defects found for proton irradiation. Here, they are cluster-like defects appearing as 10–15 nm particles slightly elongated along the a-axis with lattice similar to the main phase but larger lattice parameters.

4.3.2. 122 system. Proton irradiation was performed on Ba(Fe$_{1-x}$Co$_x$)$_2$As$_2$ films with high density of c-axis correlated pinning in the pristine sample producing a rather complex pinning landscape [358]. Protons induce a slight decrease of T_c negatively effecting J_c at high temperature. At 4 K, the introduction of additional point defects has a strong effect on the high-field J_c for $H\|ab$ that increases from ~ 0.19 to ~ 0.27 MA cm^{-2} at 9 T reducing the visibility of the c-axis pinning (~ 0.25–0.26 MA cm^{-2} at 9 T). The changes for $H\|c$ are moderate with some suppression at low field and small improvement (or no change) at high field.

4.3.3. 1111 system. A NdFeAs(O,F) film was irradiated with α-particles to study the effect of such irradiation on T_c, H_{c2}, and J_c [351]. Very different behaviour of these three properties was found but what was surprising was a weak effect of J_c despite the enhanced low-temperature H_{c2} with increasing disorder. The $F_p(H\|c)$ maximum shifted

from 4.5 to 6 T with irradiation but the peak amplitude remained constant at intermediate fluence and was clearly suppressed at large irradiation levels. The origin of this behaviour was found analysing the pinning contributions. The pinning contributions were initially affected by the T_c suppression and by both T_c suppression and changes in the density of states at high fluences. Despite these negative effects, the point defect contribution alone was actually increasing up to $\sim 20\%$ at intermediate fluence and the increased defect density was in fact proportional to the fluence. This implies that, although α-particle irradiation is an effective method to increase the point defect density, the overall pinning force density is too strongly affected by the concomitant T_c suppression.

4.4. Summary on critical current density

The compounds that showed the most significant performance improvement over time are the 11 and the 122 phases (Co- and P-doped in particular). Because of their intrinsically lower J_c anisotropy, they have been more widely studied for their promising application potential with respect to the highest-T_c, but also largest-anisotropy, 1111 counterparts. Figure 11 summarizes the best performance obtained so far by transport in FBS films; most of the data are reported at ~ 4–4.2 K with multiple sources for the same compound when obvious differences in performance were achieved in different field ranges. Some data at 6–10 K are included as well for the cases where higher J_c values at low fields were obtained despite the larger measuring temperatures.

Comparing the 1111 compounds, it is clear that the Sm and Nd ones are the best-performing. At 4.2 K, the field dependence trend $J_c(H\|c)$ is fairly similar, however Nd1111 data [229] reveal a 2.6 times larger self-field J_c with respect to Sm1111 [349] despite the lower T_c. Moreover, more recent results showed for Nd1111 a self-field J_c at 10 K of almost 5 MA cm^{-2} [351], suggesting that better performances are obtainable.

In the case of the 11 phase, recent results showed a surprisingly high self-field J_c up to $\sim$3.5 MA cm^{-2} at 6 K in a clean sample (though with a strong field dependence) [333]. However, the even more important result is a weak field dependence with almost no anisotropy at 4.2 K and J_c exceeding 0.9 MA cm^{-2} at 9 T [332]. Despite its significantly lower T_c, 11 films have better 4.2 K performance at 9 T with respect to $J_c(H\|c)$ of the 1111 compounds. Although a stronger field dependence at higher fields is expected for the 11 phase because of the lower H_{c2} and H_{irr}, the lower anisotropy is a clear advantage, and this material could anyway be preferable in the low/middle field range.

The most promising phase appears, however, to be 122. With an intermediate T_c between 11 and 1111, 122 compounds reach the highest 4.2 K self-field J_c values ($\sim$5.6 MA cm^{-2} for Ba(Fe$_{1-x}$Co$_x$)$_2$As$_2$ [177] and $\sim$7 MA cm^{-2} for BaFe$_2$(As$_{1-x}$P$_x$)$_2$ [160, 214]), they have a J_c anisotropy close to 1, and, in the case of Co, a very week field dependence with J_c of the order of 2.5–3 MA cm^{-2} at 9 T [344].

In all cases, the best in-field performances for each phase reported in figure 11 are for samples with only native, mostly growth-related defects without APCs like secondary phases and irradiation defects. Although secondary phases and irradiation were demonstrated to be effective to enhance the pinning properties with respect to their reference sample in FBS films [43], later growth optimization has surpassed the performance of APC samples. This means that combining growth optimization and APC could lead to further improvements of FBS materials.

5. Conclusion, outlook and perspectives

In the past 11 years since the discovery of high-T_c superconductivity in FBS compounds, thin films of these materials have not only been used to evaluate their application potential (e.g. in microelectronic devices or on coated conductor architectures) but also played an integral part in fundamental physical investigations, e.g. by widening the accessible experimental range in materials (e.g. metastable phases such as RE-substituted 122 structures or Fe(Se$_{1-x}$Te$_x$) with low Te content) and characterization tools (e.g. EDLT structures, strain experiments, transport J_c measurements). With different deposition methods, where MBE and PLD are the main techniques, a plethora of dopant-matrix combinations in three classes of FBS (11, 122, and 1111) have been realized; 111 as well as 11111 thin films have been shown in singular studies.

In order to further and better use the advantages and potential of films, i.e. foremost their geometry and the possibility to apply in-plane strain either during deposition process or during measurements, detailed nanoscale stoichiometric and microstructural characterizations within the film or at the film-template interface might grow in importance. Furthermore, fully strained films grown in a layer-by-layer growth mode have not been shown so far for FBS films, possibly due to their metallic nature and large surface energies. This together with higher precision in the determination of a-axis parameters and taking into account the Poisson ratios will be the next important steps in (epitaxial) in-plane strain experiments to detangle strain and stoichiometry dependencies of T_c and H_{c2}.

Even though the addition of pinning centres (growth defects, irradiation, nanoparticles) have been shown to improve the J_c properties, such films have always been surpassed by high-quality films at a later time. To reach the performance limits of these materials, it is therefore important to start with reference sample deposited at optimized conditions and find defect structures without detrimental effects on T_c, H_{c2} and H_{irr}.

Finally, such a review can only be a snapshot in time and topics and will never be complete. Several interesting studies, such as spectroscopy on FBS films or bicrystal grain boundary junction had to be omitted here in order to keep the focus, and several new interesting manuscripts are being written during the final stages of our review, which we could not include any more. Nevertheless, we do hope we gave a round and fair picture of all FBS film activities regarding possible deposition techniques and tuning the films' basic properties, and we apologize for any important paper we might have missed.

ORCID iDs

J Hänisch https://orcid.org/0000-0003-2757-236X
K Iida https://orcid.org/0000-0003-1038-9630
R Hühne https://orcid.org/0000-0002-0030-6048
C Tarantini https://orcid.org/0000-0002-3314-5906

References

[1] Kamihara Y, Hiramatsu H, Hirano M, Kawamura R, Yanagi H, Kamiya T and Hosono H 2006 *J. Am. Chem. Soc.* **128** 10012–3
[2] Kamihara Y, Watanabe T, Hirano M and Hosono H 2008 *J. Am. Chem. Soc.* **130** 3296–7

[3] Chubukov A V and Hirschfeld P J 2015 *Phys. Today* **68** 46–52

[4] Canfield P C and Bud'ko S L 2010 *Annu. Rev. Condens. Matter Phys.* **1** 27–50

[5] Putti M *et al* 2010 *Supercond. Sci. Technol.* **23** 034003

[6] Girolami G S 2009 *J. Chem. Educ.* **86** 1200–1

[7] Tanabe K and Hosono H 2012 *Japan. J. Appl. Phys.* **51** 10005

[8] Hsu F-C *et al* 2008 *Proc. Natl Acad. Sci. USA* **105** 14262–4

[9] Yeh K-W, Ke C-T, Huang T W, Chen T K, Huang Y L, Wu P M and Wu M-K 2009 *Cryst. Growth Des.* **9** 4847–51

[10] Sales B C, Sefat A S, McGuire M A, Jin R Y, Mandrus D and Mozharivskyj Y 2009 *Phys. Rev.* B **79** 094521

[11] Pitcher M J, Parker D R, Adamson P, Herkelrath S J C, Boothroyd A T and Clarke S J 2008 *Chem. Commun.* **130** 5918

[12] Parker D R, Pitcher M J, Baker P J, Franke I, Lancaster T, Blundell S J and Clarke S J 2009 *Chem. Commun.* **130** 2189

[13] Sasmal K, Lv B, Lorenz B, Guloy A M, Chen F, Xue Y-Y and Chu C-W 2008 *Phys. Rev. Lett.* **101** 107007

[14] Rotter M, Tegel M and Johrendt D 2008 *Phys. Rev. Lett.* **101** 107006

[15] Katayama N *et al* 2013 *J. Phys. Soc. Japan.* **82** 123702

[16] Burrard-Lucas M *et al* 2013 *Nat. Mater.* **12** 15–9

[17] Guo J, Jin S, Wang G, Wang S, Zhu K, Zhou T, He M and Chen X 2010 *Phys. Rev.* B **82** 180520R

[18] Ogino H, Sato S, Kishio K, Shimoyama J-I, Tohei T and Ikuhara Y 2010 *Appl. Phys. Lett.* **97** 72506

[19] Shirage P M, Kihou K, Lee C-H, Kito H, Eisaki H and Iyo A 2011 *J. Am. Chem. Soc.* **133** 9630–3

[20] Shirage P M, Kihou K, Lee C-H, Takeshita N, Eisaki H and Iyo A 2012 *J. Am. Chem. Soc.* **134** 15181–4

[21] Singh S J, Bristow M, Meier W R, Taylor P, Blundell S J, Canfield P C and Coldea A I 2018 *Phys. Rev. Mater.* **2** 074802

[22] Pachmayr U, Nitsche F, Luetkens H, Kamusella S, Brückner F, Sarkar R, Klauss H-H and Johrendt D 2015 *Angew. Chem. Int. Ed.* **54** 293–7

[23] Dong X-L *et al* 2015 *Phys. Rev.* B **92** 064515

[24] Huang Y *et al* 2017 *Chin. Phys. Lett.* **34** 077404

[25] Matthias B T 1960 *J. Appl. Phys.* **31** S23–6

[26] Matthias B T, Compton V B and Corenzwit E 1961 *J. Phys. Chem. Solids* **19** 130–3

[27] Raub E, Raub C J, Röschel E, Compton V B, Geballe T H and Matthias B T 1967 *J. Less Common Met.* **12** 36–40

[28] Collings E W and Ho J C 1975 *J. Less Common Met.* **41** 157–64

[29] Braun H F 1980 *Phys. Lett.* A **75** 386–8

[30] Matthias B T and Corenzwit E 1955 *Phys. Rev.* **100** 626–7

[31] Chandrasekhar B S and Hulm J K 1955 *J. Phys. Chem. Solids* **7** 259–67

[32] Graham A W, Kurmoo M and Day P 1995 *J. Chem. Soc., Chem. Commun.* **58** 2061–2

[33] Wang C *et al* 2008 *Europhys. Lett.* **83** 67006

[34] Ren Z-A *et al* 2008 *Europhys. Lett.* **83** 17002

[35] Fujioka M *et al* 2013 *Supercond. Sci. Technol.* **26** 085023

[36] Mazin I I, Singh D J, Johannes M D and Du M H 2008 *Phys. Rev. Lett.* **101** 057003

[37] Wang Q-W, Liu D-Y, Quan Y-M and Zou L-J 2016 *Phys. Lett.* A **380** 2685–92

[38] Martinelli A, Bernardini F and Massidda S 2016 *C. R. Phys.* **17** 5–35

[39] Shibauchi T, Carrington A and Matsuda Y 2014 *Annu. Rev. Condens. Matter Phys.* **5** 113–35

[40] Mazin I I 2010 *Nature* **464** 183–6

[41] Seidel P 2011 *Supercond. Sci. Technol.* **24** 043001

[42] Obradors X and Puig T 2014 *Supercond. Sci. Technol.* **27** 044003

[43] Iida K, Hänisch J and Tarantini C 2018 *Appl. Phys. Rev.* **5** 031304

[44] Gray D E 1972 *American Institute of Physics Handbook* 3rd edn (New York: McGraw-Hill)

[45] Watanabe H, Yamada N and Okaji M 2004 *Int. J. Thermophys.* **25** 221–36

[46] Nakabayashi M, Fujimoto T, Katsuno M and Ohtani N 2006 Precise determination of thermal expansion coefficients observed in 4H-SiC single crystals *Silicon Carbide and Related Materials* 2005 *Materials Science Forum* ed D J Larkin *et al* vol 527–529 (Uetikon-Zuerich: Trans Tech Publications) pp 699–702

[47] Soma T, Satoh J and Matsuo H 1982 *Solid State Commun.* **42** 889–92

[48] Ekinci Y and Toennies J P 2004 *Surf. Sci.* **563** 127–34

[49] Rao A S M and Narender K 2014 *J. Thermodyn.* **2014** 123478

[50] Phillips J M 1996 *J. Appl. Phys.* **79** 1829–48

[51] Smith D K and Leider H R 1968 *J. Appl. Crystallogr.* **1** 246–9

[52] Kapralik I 1969 *Chem. zvesti* **23** 665–70

[53] Roberts R B and White G K 1986 *J. Phys. C: Solid State Phys.* **19** 7167

[54] Hummer D R, Heaney P J and Post J E 2007 *Powder Diffr.* **22** 352–7

[55] Harshavardhan K S *et al* 1994 *Appl. Phys. Lett.* **64** 1570–2

[56] Chaix-Pluchery O, Chenevier B and Robles J J 2005 *Appl. Phys. Lett.* **86** 251911

[57] Biegalski M D, Haeni J H, Trolier-McKinstry S, Schlom D G, Brandle C D and Graitis A V 2005 *J. Mater. Res.* **20** 952–8

[58] White G K 1981 *J. Phys. C: Solid State Phys.* **14** L297

[59] Chakoumakos B C, Schlom D G, Urbanik M and Luine J 1998 *J. Appl. Phys.* **83** 1979–82

[60] Wongmaneerung R, Guo R, Bhalla A, Yimnirun R and Ananta S 2008 *J. Alloys Compd.* **461** 565–9

[61] Goldstein L and Post B 1969 *J. Appl. Phys.* **40** 3056–7

[62] Goodfellow http://goodfellow.com/A/Hastelloy-C276-Heat-Resisting-Alloy-Alloy.html

[63] Pachmayr U, Fehn N and Johrendt D 2016 *Chem. Commun.* **52** 194–7

[64] Margadonna S, Takabayashi Y, McDonald M T, Kasperkiewicz K, Mizuguchi Y, Takano Y, Fitch A N, Suard E and Prassides K 2008 *Chem. Commun.* **43** 5607–9

[65] Hamad R M, Kayed T S, Kunwar S, Elsayed K A, Abu-Ruz E and Ziq K A 2018 *J. Supercond. Nov. Magn.* **31** 1727–32

[66] Tsurkan V V, Deisenhofer J, Günther A, Kant C, Klemm M, Krug von Nidda H-A, Schrettle F and Loidl A 2011 *Eur. Phys. J.* B **79** 289–99

[67] Guo Z, Zhang H, Han B and Yuan W 2015 *Physica* C **509** 29–33

[68] Lee B, Khim S, Kim J S, Stewart G R and Kim K H 2010 *Europhys. Lett.* **91** 67002

[69] Rotter M, Tegel M, Johrendt D, Schellenberg I, Hermes W and Pöttgen R 2008 *Phys. Rev.* B **78** 020503

[70] Delaire O *et al* 2010 *Phys. Rev.* B **81** 094504

[71] Rullier-Albenque F, Colson D, Forget A, Thuéry P and Poissonnet S 2010 *Phys. Rev.* B **81** 224503

[72] Ni N, Thaler A, Yan J-Q, Kracher A, Colombier E, Bud'ko S L, Canfield P C and Hannahs S T 2010 *Phys. Rev.* B **82** 024519

[73] Rotter M, Pangerl M, Tegel M and Johrendt D 2008 *Angew. Chem. Int. Ed.* **47** 7949–52

[74] Sun D L, Xiao J Z and Lin C T 2011 *J. Cryst. Growth* **321** 55–9

[75] Konzen L M N and Sefat A S 2017 *J. Phys.: Condens. Matter* **29** 083001

[76] Kasahara S *et al* 2010 *Phys. Rev.* B **81** 184519

[77] Kim J S, Khim S, Kim H J, Eom M J, Law J M, Kremer R K, Shim J H and Kim K H 2010 *Phys. Rev.* B **82** 024510

[78] Nomura T, Kim S W, Kamihara Y, Hirano M, Sushko P V, Kato K, Takata M, Shluger A L and Hosono H 2008 *Supercond. Sci. Technol.* **21** 125028

[79] Jia Y, Cheng P, Fang L, Luo H, Yang H, Ren C, Shan L, Gu C and Wen H-H 2008 *Appl. Phys. Lett.* **93** 032503

[80] Cui Y J, Chen Y L, Cheng C H, Yang Y, Wang Y Z, Li Y C and Zhao Y 2011 *J. Phys. Chem. Solids* **72** 449–52

[81] Dong X-L *et al* 2015 *J. Am. Chem. Soc.* **137** 66–9

[82] Kauffmann-Weiss S *et al* 2019 Microscopic origin of highly enhanced current carrying capabilities of thin NdFeAs(O,F) films *Nanoscale Adv.* accepted (https://doi.org/10.1039/C9NA00147F)

[83] Hanawa M, Ichinose A, Komiya S, Tsukada I, Akiike T, Imai Y, Hikage T, Kawaguchi T, Ikuta H and Maeda A 2011 *Japan. J. Appl. Phys.* **50** 053101

[84] Imai Y, Akiike T, Hanawa M, Tsukada I, Ichinose A, Maeda A, Hikage T, Kawaguchi T and Ikuta H 2010 *Appl. Phys. Express* **3** 043102

[85] Iida K *et al* 2013 *Phys. Rev.* B **87** 104510

[86] Ozaki T, Wu L, Zhang C, Jaroszynski J, Si W, Zhou J, Zhu Y and Li Q 2016 *Nat. Commun.* **7** 13036

[87] Bellingeri E, Buzio R, Gerbi A, Marrè D, Congiu S, Cimberle M R, Tropeano M, Siri A S, Palenzona A and Ferdeghini C 2009 *Supercond. Sci. Technol.* **22** 105007

[88] Si W, Lin Z-W, Jie Q, Yin W-G, Zhou J, Gu G, Johnson P D and Li Q 2009 *Appl. Phys. Lett.* **95** 052504

[89] Lee S *et al* 2009 *Appl. Phys. Lett.* **95** 212505

[90] Iida K, Hänisch J, Hühne R, Kurth F, Kidszun M, Haindl S, Werner J, Schultz L and Holzapfel B 2009 *Appl. Phys. Lett.* **95** 192501

[91] Lee S *et al* 2010 *Nat. Mater.* **9** 397–402

[92] Yoon S *et al* 2017 *Supercond. Sci. Technol.* **30** 035001

[93] Herranz G *et al* 2007 *Phys. Rev. Lett.* **98** 216803

[94] Ge J-F, Liu Z-L, Liu C, Gao C-L, Qian D, Xue Q-K, Liu Y and Jia J-F 2015 *Nat. Mater.* **14** 285–9

[95] He S *et al* 2013 *Nat. Mater.* **12** 605–10

[96] Tan S *et al* 2013 *Nat. Mater.* **12** 634–40

[97] Adachi S, Shimode T, Murai M, Chikumoto N and Tanabe K 2014 *Physica* C **502** 31–5

[98] Iida K, Hänisch J, Thersleff T, Kurth F, Kidszun M, Haindl S, Hühne R, Schultz L and Holzapfel B 2010 *Phys. Rev.* B **81** 100507R

[99] Hiramatsu H, Sato H, Katase T, Kamiya T and Hosono H 2014 *Appl. Phys. Lett.* **104** 172602

[100] Ichinose A, Tsukada I, Nabeshima F, Imai Y, Maeda A, Kurth F, Holzapfel B, Iida K, Ueda S and Naito M 2014 *Appl. Phys. Lett.* **104** 122603

[101] Kurth F *et al* 2013 *Appl. Phys. Lett.* **102** 142601

[102] Iida K *et al* 2016 *Sci. Rep.* **6** 28390

[103] Uemura H, Kawaguchi T, Ohno T, Tabuchi M, Ujihara T, Takeda Y and Ikuta H 2012 *Solid State Commun.* **152** 735–9

[104] Haindl S, Hanzawa K, Sato H, Hiramatsu H and Hosono H 2016 *Sci. Rep.* **6** 3296

[105] Ueda S, Takeda S, Takano S, Yamamoto A and Naito M 2011 *Appl. Phys. Lett.* **99** 232505

[106] Böhmer A, Hardy F, Eilers F, Ernst D, Adelmann P, Schweiss P, Wolf T and Meingast C 2013 *Phys. Rev.* B **87** 180505R

[107] Bud'ko S L, Ni N, Nandi S, Schmiedeshoff G M and Canfield P C 2009 *Phys. Rev.* B **79** 054525

[108] da Luz M S, Neumeier J J, Bollinger R K, Sefat A S, McGuire M A, Jin R, Sales B C and Mandrus D 2009 *Phys. Rev.* B **79** 214505

[109] Hardy F, Adelmann P, Wolf T, Löhneysen H V and Meingast C 2009 *Phys. Rev. Lett.* **102** 187004

[110] Wang L *et al* 2009 *Phys. Rev.* B **80** 094512

[111] Klingeler R, Wang L, Köhler U, Behr G, Hess C and Büchner B 2010 *J. Phys.: Conf. Ser.* **200** 012088

[112] Jacob M V, Mazierska J, Ledenyov D and Krupka J 2003 *J. Eur. Ceram. Soc.* **23** 2617–22

[113] Thersleff T *et al* 2010 *Appl. Phys. Lett.* **97** 22506

[114] Lee S *et al* 2013 *Nat. Mater.* **12** 392–6

[115] Engelmann J, Iida K, Kurth F, Behler C, Oswald S, Hühne R, Holzapfel B, Schultz L and Haindl S 2013 *Physica* C **494** 185–8

[116] Foltyn S R, Wang H, Civale L, Jia Q X, Arendt P N, Maiorov B, Li Y, Maley M P and MacManus-Driscoll J L 2005 *Appl. Phys. Lett.* **87** 162505

[117] Ichinose A, Nabeshima F, Tsukada I, Hanawa M, Komiya S, Akiike T, Imai Y and Maeda A 2013 *Supercond. Sci. Technol.* **26** 075002

[118] Yuan F *et al* 2017 *AIP Adv.* **7** 065015

[119] Kang J-H *et al* 2018 *Nano Lett.* **18** 6347–52

[120] Sarnelli E, Adamo M, Nappi C, Braccini V, Kawale S, Bellingeri E and Ferdeghini C 2014 *Appl. Phys. Lett.* **104** 162601

[121] Qiu W, Ma Z, Liu Y, Shahriar Al Hossain M, Wang X, Cai C and Dou S X 2016 *ACS Appl. Mater. Interfaces* **8** 7891–6

[122] Qiu W, Ma Z, Patel D, Sang L, Cai C, Shahriar Al Hossain M, Cheng Z, Wang X and Dou S X 2017 *ACS Appl. Mater. Interfaces* **9** 37446–53

[123] Iida K, Sugimoto Y, Hatano T, Urata T, Langer M, Holzapfel B, Hänisch J and Ikuta H 2019 *Appl. Phys. Express* **12** 016503

[124] Li Q, Si W and Dimitrov I K 2011 *Rep. Prog. Phys.* **74** 124510

[125] Mele P 2012 *Sci. Technol. Adv. Mater.* **13** 054301

[126] Imai Y, Nabeshima F and Maeda A 2017 *Condens. Matter* **2** 25

[127] Nabeshima F, Imai Y, Hanawa M, Tsukada I and Maeda A 2013 *Appl. Phys. Lett.* **103** 172602

[128] Feng Z *et al* 2018 *Sci. Rep.* **8** 3296

[129] Feng Z *et al* 2018 High-throughput investigation of tunable superconductivity in FeSe films (arXiv:1807.01273)

[130] Si W, Han S J, Shi X, Ehrlich S N, Jaroszynski J, Goyal A and Li Q 2013 *Nat. Commun.* **4** 1397

[131] Molatta S, Haindl S, Trommler S, Schulze M, Wurmehl S and Hühne R 2015 *Sci. Rep.* **5** 16334

[132] Imai Y, Sawada Y, Nabeshima F and Maeda A 2015 *Proc. Natl Acad. Sci. USA* **112** 1937–40

[133] Seo S *et al* 2017 *Sci. Rep.* **7** 9994

[134] Yuan F *et al* 2018 *New J. Phys.* **20** 093012

[135] Richter S 2018 Neue Schichtarchitekturen Fe-basierter Supraleiter: Epitaktische Ba(Fe$_{1-x}$Ni$_x$)$_2$As$_2$ Dünnschichten und aufgerollte FeSe$_{1-x}$Te$_x$ Mikrostrukturen *PhD Thesis* TU Dresden http://nbn-resolving.de/urn:nbn:de:bsz:14-qucosa-237811

[136] Nabeshima F, Imai Y, Ichinose A, Tsukada I and Maeda A 2017 *Japan. J. Appl. Phys.* **56** 20308

[137] Huang J, Chen L, Li L, Qi Z, Sun X, Zhang X and Wang H 2018 *J. Phys. D: Appl. Phys.* **51** 205301

[138] Huang J, Wang H, Wang L-L, Zhang B, Qian X and Wang H 2018 Superconducting iron chalcogenide thin films integrated on flexible mica substrates *Applied Superconductivity Conf. 2018 (Seattle)*

[139] Bryja H, Hühne R, Iida K, Molatta S, Sala A, Putti M, Schultz L, Nielsch K and Hänisch J 2017 *Supercond. Sci. Technol.* **30** 115008

[140] Mele P, Matsumoto K, Haruyama Y, Mukaida M, Yoshida Y and Kiss T 2009 *Appl. Phys. Express* **2** 073002

[141] Mele P, Matsumoto K, Haruyama Y, Mukaida M, Yoshida Y, Ichino Y, Kiss T and Ichinose A 2010 *Physica* C **470** 1033–7

[142] Mele P, Matsumoto K, Haruyama Y, Mukaida M, Yoshida Y, Ichino Y, Kiss T and Ichinose A 2010 *Supercond. Sci. Technol.* **23** 052001

[143] Fujiwara K, Shiogai J and Tsukazaki A 2017 *Japan. J. Appl. Phys.* **56** 100308

[144] Nabeshima F, Ishikawa T, Oyanagi K-i, Kawai M and Maeda A 2018 *J. Phys. Soc. Japan.* **87** 073704
[145] Kurth F *et al* 2015 *Appl. Phys. Lett.* **106** 072602
[146] Engelmann J *et al* 2013 *Nat. Commun.* **4** 2877
[147] Katase T, Iimura S, Hiramatsu H, Kamiya T and Hosono H 2012 *Phys. Rev.* B **85** 140516
[148] Imai Y, Nabeshima F, Nakamura D, Katase T, Hiramatsu H, Hosono H and Maeda A 2013 *J. Phys. Soc. Japan.* **82** 043709
[149] Katase T, Sato H, Hiramatsu H, Kamiya T and Hosono H 2013 *Phys. Rev.* B **88** 140503
[150] Katase T, Hiramatsu H, Kamiya T and Hosono H 2013 *New J. Phys.* **15** 073019
[151] Lee N H, Jung S-G, Kim D H and Kang W N 2010 *Appl. Phys. Lett.* **96** 202505
[152] Hiramatsu H, Matsuda S, Sato H, Kamiya T and Hosono H 2014 *ACS Appl. Mater. Interfaces* **6** 14293–301
[153] Shipulin I, Richter S, Anna Thomas A, Brandt M, Aswartham S and Hühne R 2018 *Mater. Res. Express* **5** 126001
[154] Richter S *et al* 2017 *Appl. Phys. Lett.* **110** 22601
[155] Richter S, Aswartham S, Pukenas A, Grinenko V, Wurmehl S, Skrotzki W, Büchner B, Nielsch K and Hühne R 2017 *IEEE Trans. Appl. Supercond.* **27** 7300304
[156] Adachi S, Shimode T, Miura M, Chikumoto N, Takemori A, Nakao K, Oshikubo Y and Tanabe K 2012 *Supercond. Sci. Technol.* **25** 105015
[157] Grinenko V *et al* 2017 *Sci. Rep.* **7** 1383
[158] Miura M, Adachi S, Shimode T, Wada K, Takemori A, Chikumoto N, Nakao K and Tanabe K 2013 *Appl. Phys. Express* **6** 093101
[159] Miura M, Maiorov B, Kato T, Shimode T, Wada K, Adachi S and Tanabe K 2013 *Nat. Commun.* **4** 2499
[160] Sato H, Hiramatsu H, Kamiya T and Hosono H 2014 *Appl. Phys. Lett.* **104** 182603
[161] Sato H, Hiramatsu H, Kamiya T and Hosono H 2016 *Sci. Rep.* **6** 36828
[162] Iida K, Sato H, Tarantini C, Hänisch J, Jaroszynski J, Hiramatsu H, Holzapfel B and Hosono H 2017 *Sci. Rep.* **7** 39951
[163] Langer M 2014 Supraleitende Eigenschaften heteroepitaktischer Ba(Fe$_{1-x}$Ru$_x$)$_2$As$_2$-Dünnschichten *Diploma Thesis* TU Dresden
[164] Hiramatsu H, Katase T, Kamiya T, Hirano M and Hosono H 2008 *Appl. Phys. Express* **1** 101702
[165] Choi E-M, Jung S-G, Lee N H, Kwon Y S, Kang W N, Kim D H, Jung M-H, Lee S-I and Sun L 2009 *Appl. Phys. Lett.* **95** 062507
[166] Hiramatsu H, Katase T, Kamiya T and Hosono H 2013 *IEEE Trans. Appl. Supercond.* **23** 7300405
[167] Hiramatsu H, Katase T, Kamiya T, Hirano M and Hosono H 2009 *Phys. Rev.* B **80** 052501
[168] Katase T, Hiramatsu H, Kamiya T and Hosono H 2012 *Supercond. Sci. Technol.* **25** 084015
[169] Sakoda M, Iida K and Naito M 2018 *Supercond. Sci. Technol.* **31** 093001
[170] Katase T, Hiramatsu H, Yanagi H, Kamiya T, Hirano M and Hosono H 2009 *Solid State Commun.* **149** 2121–4
[171] Katase T, Hiramatsu H, Kamiya T and Hosono H 2010 *Appl. Phys. Express* **3** 063101
[172] Lei Q Y *et al* 2014 *Supercond. Sci. Technol.* **27** 115010
[173] Lee S *et al* 2011 *IEEE Trans. Appl. Supercond.* **21** 2882–6
[174] Tarantini C, Lee S, Kametani F, Jiang J, Weiss J D, Jaroszynski J, Folkman C M, Hellstrom E E, Eom C-B and Larbalestier D C 2012 *Phys. Rev.* B **86** 214504
[175] Katase T, Ishimaru Y, Tsukamoto A, Hiramatsu H, Kamiya T, Tanabe K and Hosono H 2011 *Nat. Commun.* **2** 409
[176] Kurth F *et al* 2013 *Supercond. Sci. Technol.* **26** 025014
[177] Tarantini C, Kametani F, Lee S, Jiang J, Weiss J D, Jaroszynski J, Hellstrom E E, Eom C-B and Larbalestier D C 2014 *Sci. Rep.* **4** 7305
[178] Lee J *et al* 2017 *Supercond. Sci. Technol.* **30** 085006
[179] Katase T, Hiramatsu H, Matias V, Sheehan C, Ishimaru Y, Kamiya T, Tanabe K and Hosono H 2011 *Appl. Phys. Lett.* **98** 242510
[180] Iida K *et al* 2011 *Appl. Phys. Express* **4** 013103
[181] Trommler S, Hänisch J, Matias V, Hühne R, Reich E, Iida K, Haindl S, Schultz L and Holzapfel B 2012 *Supercond. Sci. Technol.* **25** 084019
[182] Xu Z, Yuan P, Fan F, Chen Y and Ma Y 2018 *Supercond. Sci. Technol.* **31** 055001
[183] Hiramatsu H, Kamiya T, Hirano M and Hosono H 2009 *Physica* C **469** 657–66
[184] Maiorov B, Baily S A, Kohama Y, Hiramatsu H, Civale L, Hirano M and Hosono H 2009 *Supercond. Sci. Technol.* **22** 125011
[185] Trommler S, Hühne R, Hänisch J, Reich E, Iida K, Haindl S, Matias V, Schultz L and Holzapfel B 2012 *Appl. Phys. Lett.* **100** 122602
[186] Langer M, Grinenko V, Hänisch J, Yuan F, Iida K, Holzapfel B, Schultz L and Hühne R 2015 Superconductivity in Ru-substituted BaFe$_2$As$_2$ epitaxial thin films *EUCAS (Lyon)*
[187] Qi Y, Wang L, Gao Z, Wang D, Zhang X, Yao C, Wang C, Wang C and Ma Y 2011 *Europhys. Lett.* **96** 17007
[188] Lv B, Deng L, Gooch M, Wei F, Sun Y, Meen J K, Xue Y-Y, Lorenz B and Chu C-W 2011 *Proc. Natl Acad. Sci. USA* **108** 15705–9
[189] Saha S R, Butch N P, Drye T, Magill J, Ziemak S, Kirshenbaum K, Zavalij P Y, Lynn J W and Paglione J 2012 *Phys. Rev.* B **85** 024525
[190] Kudo K, Iba K, Takasuga M, Kitahama Y, Matsumura J-I, Danura M, Nogami Y and Nohara M 2013 *Sci. Rep.* **3** 1478
[191] Katase T, Hiramatsu H, Kamiya T and Hosono H 2014 *Proc. Natl Acad. Sci.* USA **111** 3979–83
[192] Engelmann J, Müller K H, Nenkov K, Schultz L, Holzapfel B and Haindl S 2012 *Eur. Phys. J.* B **85** 020503
[193] Xiao Z, Ran F-Y, Hiramatsu H, Matsuishi S, Hosono H and Kamiya T 2014 *Thin Solid Films* **559** 100–4
[194] Backen E, Haindl S, Niemeier T, Hühne R, Freudenberg T, Werner J, Behr G, Schultz L and Holzapfel B 2008 *Supercond. Sci. Technol.* **21** 122001
[195] Kidszun M, Haindl S, Thersleff T, Werner J, Langer M, Hänisch J, Iida K, Reich E, Schultz L and Holzapfel B 2010 *Europhys. Lett.* **90** 57005
[196] Kidszun M, Haindl S, Reich E, Hänisch J, Schultz L and Holzapfel B 2010 *Supercond. Sci. Technol.* **23** 022002
[197] Kidszun M, Haindl S, Thersleff T, Hänisch J, Kauffmann A, Iida K, Freudenberger J, Schultz L and Holzapfel B 2011 *Phys. Rev. Lett.* **106** 137001
[198] Naidyuk Y G, Kvitnitskaya O E, Yanson I K, Fuchs G, Haindl S, Kidszun M, Schultz L and Holzapfel B 2011 *Supercond. Sci. Technol.* **24** 065010
[199] Haindl S, Kidszun M and Kampert E 2017 *Phys. Status Solidi* (B) **254** 1600341
[200] Hiramatsu H, Katase T, Kamiya T, Hirano M and Hosono H 2008 *Appl. Phys. Lett.* **93** 162504
[201] Haindl S, Kinjo H, Hanzawa K, Hiramatsu H and Hosono H 2018 *Appl. Surf. Sci.* **437** 418–28
[202] Hiramatsu H, Kamihara Y, Yanagi H, Ueda K, Kamiya T, Hirano M and Hosono H 2009 *J. Eur. Ceram. Soc.* **29** 245–53
[203] Takeda S, Ueda S, Takano S, Yamamoto A and Naito M 2012 *Supercond. Sci. Technol.* **25** 035007
[204] Jourdan M and ten Haaf S 2010 *J. Appl. Phys.* **108** 023913
[205] Agatsuma S, Yamagishi T, Takeda S and Naito M 2010 *Physica* C **470** 1468–72

[206] Wang Q-Y *et al* 2012 *Chin. Phys. Lett.* **29** 37402
[207] McQueen T M *et al* 2009 *Phys. Rev.* B **79** 014522
[208] Song C-L, Wang Y-L, Jiang Y-P, Li Z, Wang L-L, He K, Chen X, Ma X-C and Xue Q-K 2011 *Phys. Rev.* B **84** 020503
[209] Lee J J *et al* 2014 *Nature* **515** 245–8
[210] Chang K *et al* 2015 *Europhys. Lett.* **109** 28003
[211] Yamagishi T, Ueda S, Takeda S, Takano S, Mitsuda A and Naito M 2011 *Physica* C **471** 1177–80
[212] Hatano T, Fujimoto R, Nakamura I, Mori Y and Ikuta H 2014 Thin film growth of CaFe$_2$As$_2$-based superconductors by MBE *(ISS2014)* http://www.istec.or.jp/ISS2014/FD/FD2.pdf#FD-8
[213] Li W *et al* 2012 *Nat. Phys.* **8** 126–30
[214] Sakagami A, Kawaguchi T, Tabuchi M, Ujihara T, Takeda Y and Ikuta H 2013 *Physica* C **494** 181–4
[215] Kawaguchi T, Sakagami A, Mori Y, Tabuchi M, Ujihara T, Takeda Y and Ikuta H 2014 *Supercond. Sci. Technol.* **27** 065005
[216] Ueda S, Yamagishi T, Takeda S, Agatsuma S, Takano S, Mitsuda A and Naito M 2011 *Physica* C **471** 1167–73
[217] Naito M, Ueda S, Takeda S, Takano S and Mitsuda A 2012 *MRS Proc.* **1434** Mrss12-1434-i09-04
[218] Ueda S, Takeda S, Takano S, Mitsuda A and Naito M 2012 *Japan. J. Appl. Phys.* **51** 10103
[219] Takeda S, Ueda S, Yamagishi T, Agatsuma S, Takano S, Mitsuda A and Naito M 2010 *Appl. Phys. Express* **3** 093101
[220] Hatano T, Kawaguchi T, Fujimoto R, Nakamura I, Mori Y, Harada S, Ujihara T and Ikuta H 2016 *Supercond. Sci. Technol.* **29** 015013
[221] Xiao H *et al* 2012 *Phys. Rev.* B **85** 024530
[222] Dung D D, Feng W and Cho S 2011 *J. Vac. Sci. Technol.* B **29** 031210
[223] Kawaguchi T, Uemura H, Ohno T, Watanabe R, Tabuchi M, Ujihara T, Takenaka K, Takeda Y and Ikuta H 2009 *Appl. Phys. Express* **2** 093002
[224] Kawaguchi T, Uemura H, Ohno T, Tabuchi M, Ujihara T, Takenaka K, Takeda Y and Ikuta H 2010 *Appl. Phys. Lett.* **97** 042509
[225] Kawaguchi T, Uemura H, Ohno T, Tabuchi M, Ujihara T, Takeda Y and Ikuta H 2011 *Appl. Phys. Express* **4** 083102
[226] Kawaguchi T, Uemura H, Ohno T, Tabuchi M, Ujihara T, Takenaka K, Takeda Y and Ikuta H 2011 *Physica* C **471** 1174–6
[227] Takano S, Ueda S, Takeda S, Sugawara H and Naito M 2012 *Physica* C **475** 10–13
[228] Sugawara H, Tsuneki T, Watanabe D, Yamamoto A, Sakoda M and Naito M 2015 *Supercond. Sci. Technol.* **28** 015005
[229] Chihara M, Sumiya N, Arai K, Ichinose A, Tsukada I, Hatano T, Iida K and Ikuta H 2015 *Physica* C **518** 69–72
[230] Srivastava M M and Srivastava O N 1975 *Thin Solid Films* **29** 275–84
[231] Liu K W, Zhang J Y, Shen D Z, Shan C X, Li B H, Lu Y M and Fan X W 2007 *Appl. Phys. Lett.* **90** 262503
[232] Wu X J, Zhang Z Z, Zhang J Y, Ju Z G, Li B H, Li B S, Shan C X, Zhao D X, Yao B and Shen D Z 2008 *Thin Solid Films* **516** 6116–9
[233] Hussain R A, Badshah A, Younis A, Khan M D and Akhtar J 2014 *Thin Solid Films* **567** 58–63
[234] Hussain R A, Badshah A, Yasmin F, Khan M D and Tahir M N 2015 *Aust. J. Chem.* **68** 298–306
[235] Ubale A U, Sakhare Y S and Bombatkar S M 2013 *Mater. Res. Bull.* **48** 3564–71
[236] Speller S C, Aksoy C, Saydam M, Taylor H, Burnell G, Boothroyd A T and Grovenor C R M 2011 *Supercond. Sci. Technol.* **24** 075023
[237] Mousavi T, Grovenor C and Speller S 2015 *J. Mater. Sci.* **50** 6970–8
[238] Mousavi T, Grovenor C and Speller S 2015 *IEEE Trans. Appl. Supercond.* **25** 7500604
[239] Huang J, Chen L, Jian J, Khatkhatay F, Jacob C and Wang H 2015 *J. Alloys Compd.* **647** 380–5
[240] Chen L, Tsai C-F, Lee J H, Zhang X and Wang H 2013 *Japan. J. Appl. Phys.* **52** 020201
[241] Schneider R, Zaitsev A G, Fuchs D and v Löhneysen H 2012 *Phys. Rev. Lett.* **108** 257003
[242] Schneider R, Zaitsev A G, Fuchs D and Fromknecht R 2013 *Supercond. Sci. Technol.* **26** 055014
[243] Zaitsev A G, Schneider R, Fuchs D, Beck A and Hott R 2014 *J. Phys.: Conf. Ser.* **507** 012054
[244] Schneider R, Zaitsev A G, Fuchs D and Löhneysen H von 2014 *J. Phys.: Condens. Matter* **26** 455701
[245] Schneider R, Zaitsev A G, Fuchs D and Hott R 2019 *Supercond. Sci. Technol.* **32** 025001
[246] Chai Q-L, Tu H-L, Hua Z-Q, Wang L and Qu F 2011 *Physica* C **471** 428–31
[247] Qi X, Wang J-Y, Kuo J-C, Yates K A and Cohen L F 2011 *J. Alloys Compd.* **509** 6350–3
[248] Qi X, Wang J-Y, Hung C-J, Kuo J-C, Yates K and Cohen L F 2010 *J. Am. Ceram. Soc.* **93** 3195–200
[249] Chen P Y, Hu S F, Liu R S and Huang C Y 2011 *Thin Solid Films* **519** 8397–400
[250] Yamashita A, Tanaka M, Takeya H and Takano Y 2017 *J. Phys. Soc. Japan.* **86** 75001
[251] Demura S *et al* 2012 *J. Phys. Soc. Japan.* **81** 043702
[252] Demura S *et al* 2013 *Solid State Commun.* **154** 40–2
[253] Demura S *et al* 2016 *J. Phys. Soc. Japan.* **85** 015001
[254] Yamashita A, Matsumoto R, Tanaka M, Hara H, Iida K, Holzapfel B, Takeya H and Takano Y 2018 *Solid State Commun.* **270** 72–5
[255] Li L, Yang Z R, Sun Y P, Zhang J Y, Shen D Z and Zhang Y H 2011 *Supercond. Sci. Technol.* **24** 015010
[256] Feng J Q, Zhang S N, Liu J X, Hao Q B, Li C S and Zhang P X 2017 *J. Phys.: Conf. Ser.* **871** 012063
[257] Yoshimoto T, Fujii Y, Teranishi R, Kurumi K, Yoshida K, Yoshida Y, Ichino Y, Nishiyama T, Munetoh S and Kaneko K 2012 *Supercond. Sci. Technol.* **25** 105013
[258] Corrales-Mendoza I, Conde-Gallardo A and Sánchez-Reséndiz V M 2011 *IEEE Trans. Appl. Supercond.* **21** 2849–52
[259] Corrales-Mendoza I and Conde-Gallardo A 2014 *IEEE Trans. Appl. Supercond.* **24** 7300106
[260] Corrales-Mendoza I, Bartolo-Pèrez P, Sánchez-Reséndiz V M, Gallardo-Hernández S and Conde-Gallardo A 2015 *Europhys. Lett.* **109** 17007
[261] Corrales-Menoza I *et al* 2019 *Supercond. Sci. Technol.* **32** 055005
[262] Zhao L *et al* 2016 *Nat. Commun.* **7** 10608
[263] Huang Y *et al* Matrix-assisted fabrication and exotic charge mobility of (Li,Fe)OHFeSe superconductor films (arXiv:1711.02920)
[264] Hänisch J, Huang Y, Tian J P, Yuan J, Zhou F, Jin K, Dong X-L, Holzapfel B and Zhao Z 2018 Flux pinning and critical current densities in (Li,Fe)OHFeSe thin films *Applied Superconductivity Conf. 2018 (Seattle)*
[265] Hosono H, Tanabe K, Takayama-Muromachi E, Kageyama H, Yamanaka S, Kumakura H, Nohara M, Hiramatsu H and Fujitsu S 2015 *Sci. Technol. Adv. Mater.* **16** 033503
[266] Lee C-H, Iyo A, Eisaki H, Kito H, Teresa Fernandez-Diaz M, Ito T, Kihou K, Matsuhata H, Braden M and Yamada K 2008 *J. Phys. Soc. Japan.* **77** 083704
[267] Kuroki K, Usui H, Onari S, Arita R and Aoki H 2009 *Phys. Rev.* B **79** 224511
[268] Mizuguchi Y, Hara Y, Deguchi K, Tsuda S, Yamaguchi T, Takeda K, Kotegawa H, Tou H and Takano Y 2010 *Supercond. Sci. Technol.* **23** 054013

[269] Shein I R and Ivanovskii A L 2011 *Solid State Commun.* **151** 671–3

[270] Ballatino A 1995 *Poisson's Ratio for Tetragonal Crystals (ARL-TR-423)* (Fort Monmouth, NJ: US Army Research Laboratory)

[271] Hanzawa K, Yamaguchi Y, Obata Y, Matsuishi S, Hiramatsu H, Kamiya T and Hosono H 2019 *Phys. Rev.* B **99** 35148

[272] Chandra S and Islam A K M A 2010 *Physica C* **470** 2072–5

[273] Chowdhury U K, Rahman M A, Rahman M A and Bhuiyan M T H 2016 *Cogent Phys.* **3** 1265779

[274] Kawai M, Nabeshima F and Maeda A 2018 *J. Phys.: Conf. Ser.* **1054** 012023

[275] Imai Y, Sawada Y, Nabeshima F, Asami D, Kawai M and Maeda A 2017 *Sci. Rep.* **7** 46653

[276] Hu Z, Xu W, Chen C, Wen Y and Liu L 2018 *Adv. Mater. Sci. Eng.* **2018** 3219685

[277] Shein I R and Ivanovskii A L 2009 *Tech. Phys. Lett.* **35** 961–3

[278] Aftabuzzaman M and Islam A K M A 2010 *Physica C* **470** 202–5

[279] Kawale S, Bellingeri E, Braccini V, Pallecchi I, Putti M, Grimaldi G, Leo A, Guarino A, Nigro A and Ferdeghini C 2013 *IEEE Trans. Appl. Supercond.* **23** 7500704

[280] Bellingeri E *et al* 2012 *Supercond. Sci. Technol.* **25** 084022

[281] Iida K, Hänisch J, Trommler S, Haindl S, Kurth F, Hühne R, Schultz L and Holzapfel B 2011 *Supercond. Sci. Technol.* **24** 125009

[282] Chekhonin P, Engelmann J, Langer M, Oertel C-G, Holzapfel B and Skrotzki W 2015 *Cryst. Res. Technol.* **50** 891–902

[283] Pukenas A *et al* 2019 *Micron* **119** 1–7

[284] Yamagiwa K, Matsumoto K and Hirabayashi I 2000 *J. Mater. Res.* **15** 2547–57

[285] Haindl S *et al* 2014 *Rep. Prog. Phys.* **77** 046502

[286] Langer M, Meyer S, Ackermann K, Grünewald L, Kauffmann-Weiss S, Aswartham S, Wurmehl S, Hänisch J and Holzapfel B 2019 On the growth of Co-doped BaFe$_2$As$_2$ thin films on CaF$_2$ *J. Phys.: Conf. Ser.* accepted

[287] Maeda A, Nabeshima F, Takahashi H, Okada T, Imai Y, Tsukada I, Hanawa M, Komiya S and Ichinose A 2014 *Appl. Surf. Sci.* **312** 43–9

[288] Tsukada I, Ichinose A, Nabeshima F, Imai Y and Maeda A 2016 *AIP Adv.* **6** 95314

[289] Trommler S, Hühne R, Iida K, Pahlke P, Haindl S, Schultz L and Holzapfel B 2010 *New J. Phys.* **12** 103030

[290] Trommler S, Molatta S, Hänisch J, Iida K, Schultz L and Hühne R 2015 *IEEE Trans. Appl. Supercond.* **25** 8400404

[291] Tropeano M, Pallecchi I, Cimberle M R, Ferdeghini C, Lamura G, Vignolo M, Martinelli A, Palenzona A and Putti M 2010 *Supercond. Sci. Technol.* **23** 054001

[292] Kogan V G 2009 *Phys. Rev.* B **80** 214532

[293] Liu Y, Tanatar M A, Straszheim W E, Jensen B, Dennis K W, McCallum R W, Kogan V G, Prozorov R and Lograsso T A 2014 *Phys. Rev.* B **89** 134504

[294] Salamon M B, Cornell N, Jaime M, Balakirev F F, Zakhidov A, Huang J and Wang H 2016 *Sci. Rep.* **6** 241

[295] Chen L *et al* 2013 *Supercond. Sci. Technol.* **26** 112001

[296] Tarantini C, Gurevich A, Jaroszynski J, Balakirev F F, Bellingeri E, Pallecchi I, Ferdeghini C, Shen B, Wen H-H and Larbalestier D C 2011 *Phys. Rev.* B **84** 184522

[297] Fang M, Yang J, Balakirev F F, Kohama Y, Singleton J, Qian B, Mao Z Q, Wang H-D and Yuan H Q 2010 *Phys. Rev.* B **81** 020509R

[298] Her J L, Kohama Y, Matsuda Y H, Kindo K, Yang W-H, Chareev D A, Mitrofanova E S, Volkova O S, Vasiliev A N and Lin J-Y 2015 *Supercond. Sci. Technol.* **28** 045013

[299] Khim S, Kim J W, Choi E S, Bang Y, Nohara M, Takagi H and Kim K H 2010 *Phys. Rev.* B **81** 184511

[300] Lei H, Hu R, Choi E S, Warren J B and Petrovic C 2010 *Phys. Rev.* B **81** 094518

[301] Kida T, Matsunaga T, Hagiwara M, Mizuguchi Y, Takano Y and Kindo K 2009 *J. Phys. Soc. Japan.* **78** 113701

[302] Hühne R, Trommler S, Pahlke P and Schultz L 2014 Low temperature performance of Pb(Mg$_{1/3}$Nb$_{2/3}$)$_{0.72}$Ti$_{0.28}$O$_3$ single crystals mapped by metallic and superconducting thin films *Joint IEEE Int. Symp. on the Applications of Ferroelectric, International Workshop on Acoustic Transduction Materials and Devices & Workshop on Piezoresponse Force Microscopy* pp 1–4

[303] Trommler S 2014 Einfluss von reversibler epitaktischer Verspannung auf die elektronischen Eigenschaften supraleitender Dünnschichten *PhD Thesis* TU Dresden http://nbn-resolving.de/urn:nbn:de:bsz:14-qucosa-149690

[304] Hicks C W, Barber M E, Edkins S D, Brodsky D O and Mackenzie A P 2014 *Rev. Sci. Instrum.* **85** 065003

[305] Gooch M, Lorenz B, Huang S X, Chien C L and Chu C W 2012 *J. Appl. Phys.* **111** 112610

[306] Ueno K, Nakamura S, Shimotani H, Yuan H T, Kimura N, Nojima T, Aoki H, Iwasa Y and Kawasaki M 2011 *Nat. Nanotechnol.* **6** 408–12

[307] Ye J T, Zhang Y J, Akashi R, Bahramy M S, Arita R and Iwasa Y 2012 *Science* **338** 1193–6

[308] Yuan H, Shimotani H, Tsukazaki A, Ohtomo A, Kawasaki M and Iwasa Y 2009 *Adv. Funct. Mater.* **19** 1046–53

[309] Eguchi R, Senda M, Uesugi E, Goto H, Kambe T, Noji T, Koike Y, Fujiwara A and Kubozono Y 2013 *Appl. Phys. Lett.* **102** 103506

[310] Geim A K 2011 *Rev. Mod. Phys.* **83** 851–62

[311] Hanzawa K, Sato H, Hiramatsu H, Kamiya T and Hosono H 2016 *Proc. Natl Acad. Sci.* **113** 3986–90

[312] Shiogai J, Ito Y, Mitsuhashi T, Nojima T and Tsukazaki A 2016 *Nat. Phys.* **12** 42–6

[313] Lei B, Cui J H, Xiang Z J, Shang C, Wang N Z, Ye G J, Luo X G, Wu T, Sun Z and Chen X H 2016 *Phys. Rev. Lett.* **116** 077002

[314] Shiogai J, Miyakawa T, Ito Y, Nojima T and Tsukazaki A 2017 *Phys. Rev.* B **95** 115101

[315] Shimizu S, Shiogai J, Takemori N, Sakai S, Ikeda H, Arita R, Nojima T, Tsukazaki A and Iwasa Y 2019 *Nat. Commun.* **10** 825

[316] Kouno S, Sato Y, Katayama Y, Ichinose A, Asami D, Nabeshima F, Imai Y, Maeda A and Ueno K 2018 *Sci. Rep.* **8** 14731

[317] Liu D *et al* 2012 *Nat. Commun.* **3** 931

[318] Miyakawa T *et al* 2018 *Phys. Rev. Mater.* **2** 031801(R)

[319] Harada T, Shiogai J, Miyakawa T, Nojima T and Tsukazaki A 2018 *Supercond. Sci. Technol.* **31** 055003

[320] Lei B *et al* 2016 *Phys. Rev.* B **93** 060501

[321] Lei B *et al* 2017 *Phys. Rev.* B **95** 020503

[322] Zhu C S *et al* 2017 *Phys. Rev.* B **95** 174513

[323] Piatti E *et al* 2018 *Phys. Rev. Mater.* **3** 044801

[324] Eisterer M, Raunicher R, Weber H W, Bellingeri E, Cimberle M R, Pallecchi I, Putti M and Ferdeghini C 2011 *Supercond. Sci. Technol.* **24** 065016

[325] Tsukada I *et al* 2011 *Appl. Phys. Express* **4** 53101

[326] Si W, Zhou J, Jie Q, Dimitrov I K, Solovyov V, Johnson P D, Jaroszynski J, Matias V, Sheehan C and Li Q 2011 *Appl. Phys. Lett.* **98** 262509

[327] Iida K, Hänisch J, Schulze M, Aswartham S, Wurmehl S, Büchner B, Schultz L and Holzapfel B 2011 *Appl. Phys. Lett.* **99** 202503

[328] Braccini V *et al* 2013 *Appl. Phys. Lett.* **103** 172601

[329] Bellingeri E *et al* 2014 *Supercond. Sci. Technol.* **27** 044007

[330] Yuan F *et al* 2015 *Supercond. Sci. Technol.* **28** 065005

[331] Yuan P, Xu Z, Zhang H, Wang D, Ma Y, Zhang M and Li J 2015 *Supercond. Sci. Technol.* **28** 065009

[332] Yuan P, Xu Z, Ma Y, Sun Y and Tamegai T 2016 *Supercond. Sci. Technol.* **29** 035013

[333] Seo S *et al* 2018 Artificially engineered nanostrain in iron chalcogenide superconductor thin film for enhancing supercurrent (arXiv:1812.02380v1)

[334] Han Y, Li W Y, Cao L X, Wang X Y, Xu B, Zhao B R, Guo Y Q and Yang J L 2010 *Phys. Rev. Lett.* **104** 017003

[335] Zhang W-H *et al* 2014 *Chin. Phys. Lett.* **31** 017401

[336] Bellingeri E, Pallecchi I, Buzio R, Gerbi A, Marrè D, Cimberle M R, Tropeano M, Putti M, Palenzona A and Ferdeghini C 2010 *Appl. Phys. Lett.* **96** 102512

[337] Bellingeri E *et al* 2011 *J. Supercond. Nov. Magn.* **24** 35–41

[338] Bellingeri E *et al* 2012 *Appl. Phys. Lett.* **100** 082601

[339] Mele P, Matsumoto K, Fujita K, Yoshida Y, Kiss T, Ichinose A and Mukaida M 2012 *Supercond. Sci. Technol.* **25** 084021

[340] Grimaldi G, Leo A, Nigro A, Pace S, Braccini V, Bellingeri E and Ferdeghini C 2018 *Sci. Rep.* **8** 4150

[341] Iida K *et al* 2010 *Appl. Phys. Lett.* **97** 172507

[342] Katase T, Ishimaru Y, Tsukamoto A, Hiramatsu H, Kamiya T, Tanabe K and Hosono H 2010 *Appl. Phys. Lett.* **96** 142507

[343] Maiorov B, Katase T, Baily S A, Hiramatsu H, Holesinger T G, Hosono H and Civale L 2011 *Supercond. Sci. Technol.* **24** 055007

[344] Yuan P, Xu Z, Wang D, Zhang M, Li J and Ma Y 2017 *Supercond. Sci. Technol.* **30** 025001

[345] Hänisch J, Iida K, Kurth F, Thersleff T, Trommler S, Reich E, Hühne R, Schultz L and Holzapfel B 2014 *AIP Conf. Proc.* **1574** 260–7

[346] Hänisch J *et al* 2015 *Sci. Rep.* **5** 17363

[347] Talantsev E F and Mataira R C 2018 *AIP Adv.* **8** 75213

[348] Haindl S *et al* 2010 *Phys. Rev. Lett.* **104** 077001

[349] Iida K *et al* 2013 *Sci. Rep.* **3** 2139

[350] Tarantini C *et al* 2016 *Sci. Rep.* **6** 36047

[351] Tarantini C, Iida K, Sumiya N, Chihara M, Hatano T, Ikuta H, Singh R K, Newman N and Larbalestier D C 2018 *Supercond. Sci. Technol.* **31** 034002

[352] Zhang C, Si W and Li Q 2016 *Appl. Phys. Lett.* **109** 202601

[353] Lee S *et al* 2010 *Nat. Mater.* **9** 397–402

[354] Zhang Y *et al* 2011 *Appl. Phys. Lett.* **98** 42509

[355] Tarantini C *et al* 2010 *Appl. Phys. Lett.* **96** 142510

[356] Sylva G *et al* 2018 *Supercond. Sci. Technol.* **31** 054001

[357] Ozaki T, Wu L, Zhang C, Si W, Jie Q and Li Q 2018 *Supercond. Sci. Technol.* **31** 024002

[358] Maiorov B, Katase T, Usov I O, Weigand M, Civale L, Hiramatsu H and Hosono H 2012 *Phys. Rev. B* **86** 094513